



UNIVERSITÀ  
DEGLI STUDI  
DI PADOVA

UNIVERSITA' DEGLI STUDI DI PADOVA

**Dipartimento di Ingegneria Industriale DII**

Corso di Laurea Magistrale in Ingegneria dei Materiali

**DEVELOPMENT OF COMPOSITE AEROGELS BASED  
ON AMMONIUM ALGINATE**

Relatore: *Prof. Alessandro Martucci*

Relatore estero: *Prof. Tobias Abt*

Giovanni Lutman 2013250

Anno Accademico 2021/2022



# Abstract

Aerogels were discovered by Steven Kistler in 1931, who defined them as “*gels in which the liquid has been replaced by air, with very moderate shrinkage of the solid network*”. They are therefore porous materials with a very low density (approx.  $0.1 \text{ g/cm}^3$ ). Due to their low weight, low thermal conductivity and high specific surface, they have great potential in many technological fields such as selective absorption of pollutants, catalysis, energy storage or thermal insulation to mention a few. Inorganic aerogels tend to be brittle which has led to the generation of polymer-based aerogels which are materials that can exhibit properties similar to polymeric foams. Incorporation of polymers into aerogels increases, however, the flammability of those materials, potentially restricting their use in applications requiring fire safety, such as thermal insulation materials in building construction. A significant effort has targeted to the enhancement of the flame retardancy of aerogels, including the use of intrinsically flame-retardant polymers, polymer crosslinking, addition of flame retardants, and post-treatment of the resulting aerogels. Another possibility consists in adding fillers that can simultaneously increase the mechanical and thermal resistance of these materials.

Furthermore, in this historical period there is a focus on the environmental impact of industrial products, which is why there is also a strong development in the world of aerogels on the creation of bio-based products. Several studies have been conducted on the use of polysaccharides such as cellulose, starch, chitosan, alginate, carrageenan or pectin as precursors for aerogels in order to find viable alternatives to petroleum-based foams on the market, such as polystyrene or polyurethane foams.

Thus, the objective of this project is the creation and characterisation of eco-friendly composite aerogels made of bio-based materials: Ammonium alginate, a polysaccharide from seaweed, serves as a biopolymer, tannic acid, extracted from certain trees, was used as an additive due to its flame retardant and crosslinker characteristics. Finally, montmorillonite clay was used to significantly increase fire resistance and modify the mechanical properties. This inorganic material, found in abundance in the earth, allows the residue to increase considerably if the material is thermally degraded. The solvent used was deionised water and a sol-gel process followed by freeze-drying was performed, which allowed aerogels to be obtained with a moderate environmental impact.

The different compositions were characterised using: Compression test, thermal conductivity analyser, thermogravimetric analysis, cone calorimeter, moisture analyser, Fourier transform infrared spectroscopy. In this way, it was possible to evaluate the

influence of the additives on the material properties, noting that the samples with the best thermo-mechanical performance are those containing all chemical species, in particular as they increase, the properties improve. Only bulk density and thermal conductivity improve as the number of components in the aerogels decreases, as they are both also a function of the amount of solid phase present in a micro- and mesoporous material.

# Riassunto

Gli aerogels sono stati scoperti da Steven Kistler nel 1931 che gli ha attribuito questa definizione “*gels in which the liquid has been replaced by air, with very moderate shrinkage of the solid network*” dunque sono materiali ricchi di porosità aventi una densità bassissima (approssimata a  $0.1 \text{ g/cm}^3$ ). Grazie al loro peso ridotto, alla bassa conducibilità termica e all'elevata superficie specifica, hanno un grande potenziale in molti campi tecnologici, come l'assorbimento selettivo degli inquinanti, la catalisi, l'accumulo di energia o l'isolamento termico. Gli aerogel inorganici tendono a essere fragili, il che ha portato alla generazione di aerogel polimerici, che sono materiali in grado di esibire proprietà simili alle schiume polimeriche. L'incorporazione di polimeri negli aerogel aumenterebbe, tuttavia, l'infiammabilità di questi materiali, limitandone potenzialmente l'uso in applicazioni che richiedono una maggiore sicurezza, come i materiali per l'isolamento termico nell'edilizia. Un notevole sforzo è stato rivolto al miglioramento della resistenza di fiamma degli aerogel, compreso l'uso di polimeri intrinsecamente ritardanti di fiamma, la reticolazione dei polimeri, l'aggiunta di ritardanti di fiamma e il post-trattamento degli aerogel. Un'altra possibilità consiste nell'aggiunta di cariche che possono aumentare contemporaneamente la resistenza meccanica e termica di questi materiali.

Inoltre in questo periodo storico c'è un focus sull'impatto ambientale dei prodotti industriali ecco perché anche nel mondo degli aerogel si stanno sviluppando prodotti bio-basati. Sono stati condotti diversi studi sull'uso di polisaccaridi come la cellulosa, l'amido, il chitosano, l'alginato, la carragenina o la pectina come precursori per gli aerogel, al fine di trovare valide alternative alle schiume di origine petrolifera disponibili in commercio, come il polistirene o il poliuretano.

Dunque l'obiettivo di questo progetto è la creazione e la caratterizzazione di *Eco-Friendly* aerogel compositi formati da materiali bio-basati: l'alginato d'ammonio ovvero un polisaccaride proveniente dalle alghe del mare funge da biopolimero, l'acido tannico, estratto da determinati alberi, è stato utilizzato come additivo grazie alle sue caratteristiche di ritardante di fiamma e *crosslinker*. Infine, per incrementare notevolmente la resistenza al fuoco e modificare le proprietà meccaniche è stata utilizzata la montmorillonite: materiale inorganico, presente in abbondanza nella terra, consente di aumentare notevolmente il residuo se il materiale viene degradato termicamente. Il solvente utilizzato è stato l'acqua deionizzata e si è eseguito il processo sol-gel seguito dal *Freeze-drying*, che permette di ottenere gli aerogel con un impatto ambientale moderato.

Le diverse composizioni sono state caratterizzate utilizzando: *Compression test, thermal conductivity analyser, thermogravimetric analysis, cone calorimeter, moisture analyser, Fourier transform infrared spectroscopy*. In questo modo è stato possibile valutare l'influenza degli additivi sulle proprietà del materiale notando che i provini più performanti termo-meccanicamente sono quelli contenenti tutte le specie chimiche, in particolare all'aumentare di esse migliorano le proprietà. Solo la densità apparente e la conducibilità termica migliorano al diminuire degli elementi presenti nell'aerogel poiché sono entrambe funzione anche della quantità di fase solida presente in un materiale micro e mesoporoso.

# Acknowledgements

Questa tesi mi permette di completare la laurea magistrale in ingegneria dei materiali iniziata a settembre 2020. Voglio ringraziare l'Università degli Studi di Padova e i professori che mi hanno insegnato tutte le conoscenze fondamentali per poter diventare un dottore in ingegneria dei materiali. In particolare un ringraziamento speciale va al Prof. Alessandro Martucci che oltre ad essere il relatore della tesi mi ha permesso di eseguire il progetto finale all'estero mostrandosi sempre interessato e disponibile nei miei confronti.

Ringrazio l'Universidad Politècnica de Catalunya ed in particolare il Prof. Tobias Abt che mi ha insegnato molte cose e dato la possibilità di lavorare nel gruppo di ricerca CCP in cui ho passato mesi felici e motivanti assieme a professori e dottorandi che mi hanno accompagnato in questo progetto trattandomi come collega/amico.

Inoltre ci tengo a ringraziare i miei compagni di corso Abdul e Francesca con cui ho sempre studiato per gli esami universitari. Anche Francesca ha svolto il progetto all'Universidad Politècnica de Catalunya rafforzando il nostro rapporto di amicizia e motivante collaborazione in ambito lavorativo.

Infine e non per importanza, ci tengo a ringraziare la mia famiglia che mi ha sempre motivato in questo percorso universitario e dato i mezzi necessari per poter studiare all'Università, la mia fidanzata Alice e tutti i miei amici che mi sono sempre stati vicini.

# Table of contents

<b>ABSTRACT</b>	<b>I</b>
<b>RIASSUNTO</b>	<b>III</b>
<b>ACKNOWLEDGEMENTS</b>	<b>V</b>
<b>INTRODUCTION</b>	<b>3</b>
Prologue.....	3
Objectives .....	4
<b>CHAPTER 1: STATE OF THE ART</b>	<b>5</b>
1.1 Aerogel.....	5
1.1.1 Definition .....	5
1.1.2 Origin .....	6
1.1.3 Properties .....	7
1.2 Sol-Gel Process.....	8
1.3 Drying Methods .....	9
1.4 Classification of aerogels .....	11
1.5 Biodegradable polymers.....	13
1.5.1 Fossil-based and biodegradable aerogels .....	14
1.5.2 Bio-based and biodegradable aerogels .....	14
1.6 Aerogel composites .....	15
1.7 Eco-friendly aerogels as a flame retardance system .....	17
<b>CHAPTER 2: MATERIALS &amp; METHODS</b>	<b>21</b>
2.1 Polymers .....	21
2.1.1 Ammonium Alginate.....	21
2.2 Additives .....	23
2.2.1 Tannic Acid .....	23
2.3 Fillers .....	24
2.3.1 Montmorillonite.....	24
2.4 Solvent .....	26
2.4.1 Deionised water .....	26
2.5 Aerogels Preparation .....	28
2.5.1 Sample nomenclature.....	28
2.5.2 Technologies employed for the sol-gel process .....	29
2.5.3 Sol-Gel process.....	32



2.6	Chemical and physical reactions.....	35
2.7	Freeze-drying (lyophilization) .....	37
2.8	Characterization .....	40
2.8.1	Intrinsic viscosity.....	40
2.8.2	Fourier transform infrared spectroscopy (FTIR) .....	43
2.8.3	Thermal conductivity .....	44
2.8.4	Stabilisation .....	46
2.8.5	Density.....	47
2.8.6	Compressive strength.....	47
2.8.7	Moisture content.....	49
2.8.8	Thermogravimetric analysis (TGA).....	50
2.8.9	Cone calorimetry .....	51
<b>CHAPTER 3: RESULTS</b> .....		<b>53</b>
3.1	Intrinsic viscosity .....	53
3.2	FTIR.....	55
3.3	Thermal conductivity .....	57
3.4	Stabilisation .....	58
3.5	Density.....	59
3.6	Compressive strength .....	60
3.7	Moisture content .....	63
3.8	TGA.....	64
3.9	Cone calorimetry.....	66
<b>ENVIRONMENTAL IMPACT</b> .....		<b>71</b>
<b>CONCLUSION</b> .....		<b>73</b>
<b>ECONOMIC ANALYSIS</b> .....		<b>75</b>
<b>GLOSSARY</b> .....		<b>77</b>
<b>REFERENCES</b> .....		<b>81</b>

# List of figures

Figure 1. <i>Phase diagram of supercritical fluids [7].</i>	6
Figure 2. <i>Open-cell structure [10].</i>	7
Figure 3. <i>Steps of the process.</i>	8
Figure 4. <i>Sol-Gel process [14].</i>	9
Figure 5. <i>The phase diagram: a) Vacuum drying b) Oven drying; c) Freeze-drying; d) Supercritical drying [15].</i>	10
Figure 6. <i>Freeze-Drying [18].</i>	11
Figure 7. <i>Classification of Aerogels [19].</i>	12
Figure 8. <i>Inorganic and Organic Aerogels [20]</i>	13
Figure 9. <i>Classification of polymers.</i>	13
Figure 10. <i>Classification of composites [27].</i>	16
Figure 11. <i>a) Interphase Models for Nanoparticle-Polymer Composites [29] b) Strong interphase in polymer nanocomposites [30].</i>	16
Figure 12. <i>a) Interpenetrating inorganic and organic networks; b) Incorporation of organic molecules; c) Modification of oxidic materials with organic substituents; d) Dual networks [31].</i>	17
Figure 13. <i>Fire triangle [32].</i>	18
Figure 14. <i>Combustion process self-sustained.</i>	18
Figure 15. <i>a) Alginic acid structure b) Example of random alternation of blocks [39].</i>	21
Figure 16. <i>From alginic acid to ammonium alginate.</i>	22
Figure 17. <i>Structure of tannic acid [42].</i>	24
Figure 18. <i>Phyllosilicate structure [46].</i>	25
Figure 19. <i>Hydrated alumina oxide's structure [45].</i>	25

Figure 20. <i>Montmorillonite's structure [45].</i>	26
Figure 21. <i>Highly acidic cationic + highly basic anionic resin systems [51].</i>	27
Figure 22. <i>Highly acidic cationic + weakly basic anion + highly basic anion resin systems [51].</i>	28
Figure 23. <i>a) Overhead stirrer RZR 1, manufactured by Heidolph [53] b) Axial flow [55].</i>	30
Figure 24. <i>a) Magnetic stirrer 7002431 [59] b) Vortex flow generated by a magnetic stirrer [58].</i>	30
Figure 25. <i>a) T 25 digital ULTRA-TURRAX®, IKA [63] b) Operating mechanism of Ultra Turrax [60].</i>	31
Figure 26. <i>Temperature detector Raynger ST, Raytek [64].</i>	31
Figure 27. <i>Preparation process of A5.</i>	32
Figure 28. <i>Preparation process of A5T1.</i>	32
Figure 29. <i>Preparation process of A5C5.</i>	33
Figure 30. <i>Process for preparing A5C5T1 and A5C5T2.</i>	34
Figure 31. <i>Process for preparing A5T1C5 and A5T2C5.</i>	34
Figure 32. <i>Interaction between ammonium alginate and water.</i>	35
Figure 33. <i>Possible interaction between ammonium alginate and tannic acid.</i>	36
Figure 34. <i>Possible interaction between ammonium alginate and montmorillonite.</i>	37
Figure 35. <i>Examples of processes and microstructures [79].</i>	38
Figure 36. <i>a) b) c) and d) Creation of the cooling bath in an EPS container by monitoring the temperature; e) Insertion of the specimens.</i>	38
Figure 37. <i>a) Direction of water solidification. b) Bottom surface of A5C5T2 after freezing.</i>	39
Figure 38. <i>Freeze-drying process in the water T-P phase diagram [80].</i>	39
Figure 39. <i>CRYODOS, Teslar® (1. - Condenser with 8 cocks 2.- LCD alphanumeric viewer 3.- Operation panel 4.- Draining pipe 5.- Electrical connection 6.- Main switch 7.- Vacuum pump) [81].</i>	40

Figure 40. a) <i>Viscosimeter Ubbelohde [85]</i> b) <i>VISCOSIMETER PRECISION BATH VB-1423, PSELECTA [86].</i>	42
Figure 41. <i>FTIR operation.</i>	44
Figure 42. a) <i>Scheme of TCi equipment [91].</i> b) <i>C-Therm TCi Thermal conductivity Analyzer which employs the Modified Transient Plane Source (MTPS).</i>	45
Figure 43. <i>Stabilisation process.</i>	46
Figure 44. A) <i>Stabilised samples</i> B) <i>Cutting of samples</i> C) <i>Surface finish</i> D) <i>Measurement</i> E) <i>Compression Test.</i>	48
Figure 45. <i>ZwickRoell 10 kN RetroLine [97].</i>	49
Figure 46. <i>Steps to evaluate moisture content.</i>	49
Figure 47. <i>TGA Mettler Toledo, Columbus, Ohio.</i>	50
Figure 48. <i>Cone calorimeter test on A5C5 sample.</i>	52
Figure 49. <i>Reduced and inherent viscosity of ammonium alginate solutions.</i>	54
Figure 50. <i>Absorption spectrum obtained with FTIR.</i>	55
Figure 51. <i>Moisture adsorption (%).</i>	58
Figure 52. <i>Stress-strain curves.</i>	60
Figure 53. <i>Specific stress-strain curves.</i>	61
Figure 54. a) <i>Microstructure in this project</i> b) <i>Microstructure in the article [25].</i>	63
Figure 55. <i>Mass loss as a function of temperature.</i>	65
Figure 56. <i>Derivate mass loss of aerogels as a function of temperature.</i>	65
Figure 57. <i>Representative graph of HRR evolution as a function of time.</i>	68

## List of tables

Table 1. <i>Chemical/physical specifications; * measured at 20°C on a Brookfield RV viscosimeter, 20 rpm</i>	23
Table 2. <i>Sample Nomenclature</i>	29
Table 3. <i>Quantity of powders used and volume of water in which they were dissolved to obtain 300ml of product</i>	35
Table 4. <i>Solutions tested</i>	42
Table 5. <i>Testing conditions for thermal conductivity</i>	45
Table 6. <i>Set parameters</i>	49
Table 7. <i>Test execution parameters</i>	50
Table 8. <i>Capillary travel times from solvent</i>	53
Table 9. <i>Capillary travel times from solutions</i>	53
Table 10. <i>Relative viscosity, specific viscosity, reduced viscosity, inherent viscosity</i>	53
Table 11. <i>Detected peaks</i>	57
Table 12. <i>Thermal conductivities detected</i>	57
Table 13. <i>Measurements taken to calculate bulk density</i>	59
Table 14. <i>Calculated mechanical properties</i>	62
Table 15. <i>Humidity values in aerogels</i>	63
Table 16. <i>Data obtained from analysis of TGA graphs</i>	64
Table 17. <i>Data obtained from the calorimetric cone test</i>	66
Table 18. <i>Residue and type of burning</i>	69
Table 19. <i>Electrical energy consumed</i>	71
Table 20. <i>Costs of materials</i>	75

Table 21. *Costs of the equipments* \_\_\_\_\_ 75

Table 22. *Labour costs* \_\_\_\_\_ 76







# INTRODUCTION

## Prologue

Aerogels were discovered by Steven Kistler in 1931 that attributed them this definition “*gels in which the liquid has been replaced by air, with very moderate shrinkage of the solid network*” [1]. In fact, they are foam-like materials rich in micro- and mesoporosity, which implies a very high specific area and low density. Over the years, different types of aerogels have been created as well as increasingly high-performance technologies have been used to synthesise them.

The common properties of aerogels are, in general, low thermal conductivity due to the high amount of air in them, low electrical conductivity, good specific properties due to the low density. Furthermore, it is possible to improve characteristics such as fire resistance and thermal degradation through the use of additives in order to create hybrid aerogels.

In this historic period, the environmental impact of industrial products is fundamental, which is why it is necessary to find Eco-Friendly alternatives to petroleum-based foams such as, for example, expanded polystyrene (EPS) that is used in packing, insulation, cushioning and floating.

There is a lot of research concerning bio-based aerogels, i.e. made of raw materials from biological sources such as alginate, gelatine, cellulose and chitosan.

In this project, aerogels were created using ammonium alginate as the main component, which is obtained from certain seaweeds and is a linear anionic copolymer consisting of  $\alpha$ -L-guluronic (G) and  $\beta$ -D-mannuronic (M) acid units joined with 1-4 glycosidic bonds arranged in an irregular structure. For safety issues, fire resistance is paramount and is also the weak point of petroleum-based foams since they are by definition rich in fuels, which is why hybrid aerogels were created improving several properties including thermal stability. As an additive, tannic acid was used, an inexpensive polyphenolic organic component obtained from various plants, which acts as both a crosslinker and flame retardant.

In addition, montmorillonite was used as a filler, which is an inorganic component that modifies both mechanical properties and improves fire resistance by acting as a flame retardant.

In order to produce the aerogels, the sol-gel method is typically used, and there are various techniques for drying the wet gel: vacuum drying, oven drying, freeze-drying and supercritical drying. Since this project is based on the creation of the least polluting products possible, the Freeze-drying process was adopted, which, of those listed, is

certainly the most eco-friendly because water can be used as a solvent in the production process. Once the different aerogels were created, they were characterised by testing them with different technologies: FTIR, Compression test, TGA, calorimetric cone, TCi and Moisture Analyzer.

## Objectives

In this project, different types of biobased aerogels were created, consisting of a matrix of ammonium alginate additivated with montmorillonite and tannic acid in different compositions. The raw materials all come from renewable sources except montmorillonite, but the earth's crust is predominantly made up of aluminium silicates or magnesium silicates, therefore it is easily available.

The main objective is to evaluate the influence of additives on the different material properties by trying to identify the composition with the most relevant characteristics. Various aerogels characterisation techniques were carried out, which allowed many material properties to be analysed:

- Identification of functional groups using Fourier transform infrared spectroscopy (FTIR)
- Evaluation of bulk density
- Evaluation of thermal conductivity using the thermal conductivity analyser (TCi)
- Evaluating the mechanical properties of the material by means of a compression test
- Evaluation of the hygroscopicity of aerogels using the moisture analyzer
- Evaluate the thermal degradation mechanism using thermogravimetric analysis (TGA)
- Evaluate fire resistance using the calorimetric cone

This project has been divided into three parts:

- Chapter 1: The state of the art of aerogels is explained, i.e. all the information required to carry out this project
- Chapter 2: Explanation of the raw materials used, the aerogels production process adopted and the technologies used to assess material properties
- Chapter 3: Analysis of the results obtained, identification of the material with the best compromise between thermal and mechanical stability; the influence of the components present in the various aerogels tested was also studied.

# CHAPTER 1: STATE OF THE ART

## 1.1 Aerogel

In the following subsections, the definition of aerogels, their origin and properties will be defined.

### 1.1.1 Definition

Steven Kistler, an American scientist, discovered aerogels in 1931: the least dense solid material known to date, giving the following definition: "*gels in which the liquid has been replaced by air, with very moderate shrinkage of the solid network*" [1]. This definition is certainly more appropriate than the IUPAC definition, i.e. "*gels comprised of a microporous solid in which the dispersed phase is a gas*" [2], since this explanation does not take into account the presence of mesoporosity, i.e. the presence of pores with a width of 2-50 nm; in fact, the size of the pores is closely linked to the production process.

A definition very similar to Kistler's was given by Hüsing and Schubert, "*materials in which the typical pore structure and network are largely maintained when the pore liquid of a gel is replaced by air*" [3].

Two other very accurate and recent definitions cite:

- "*aerogel is an open non-fluid colloidal network or polymer network that is expanded throughout its whole volume by a gas, and is formed by the removal of all swelling agents from a gel without substantial volume reduction or network compaction*" Nicholas Leventis [4].
- "*an aerogel is a solid with meso- and macropores with diameters up to a few hundred nanometers and a porosity of more than 95% in which the dispersed phase is a gas*" [5].

Therefore, compared to other classes of materials, it does not have an unambiguous and specific definition because aerogels have been discovered relatively recently and because depending on the production process, constituent chemical species change both their structure from the point of view of porosity and their physical properties.

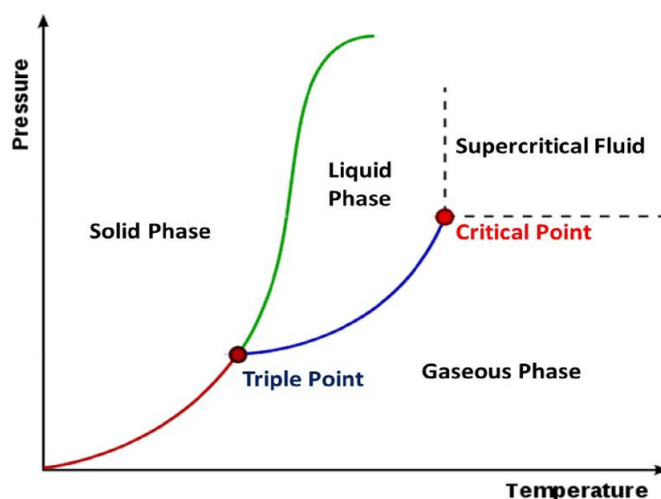
In any case, in all the definitions mentioned, the presence of two phases is made explicit: the solid phase and the gas phase, which is predominant, and it is precisely the control of porosity that makes it possible to obtain relevant peculiarities and properties.

### 1.1.2 Origin

As already explained in § 1.1.1, Kistler discovered aerogels in 1931 by means of a special drying mechanism for wet gels.

The term gel refers to a two-phase system in which there is a chemically or physically interconnected three-dimensional solid phase and a liquid phase [6]. Depending on its origin, it may be organic or inorganic. Furthermore, depending on the solvent present, it changes its name i.e. hydrogel: “*is a Gel in which the swelling agent is water*” [2].

Until 1932, gels were dried by evaporation, but this did not allow the original three-dimensional solid lattice to be retained. Kistler had the intuition to remove the liquid by placing the wet gel in an autoclave at a temperature and pressure that transformed the liquid trapped in the pores into a supercritical fluid: “*defined state of a compound, mixture or element above its critical pressure ( $P_C$ ) and critical temperature ( $T_C$ )*” [2], as shown in Figure 1.



**Figure 1.** Phase diagram of supercritical fluids [7].

Thanks to this procedure, the mechanical stresses to which the pore walls are subjected are greatly reduced as the formation of liquid-vapour menisci at the exit of the gel pores is prevented.

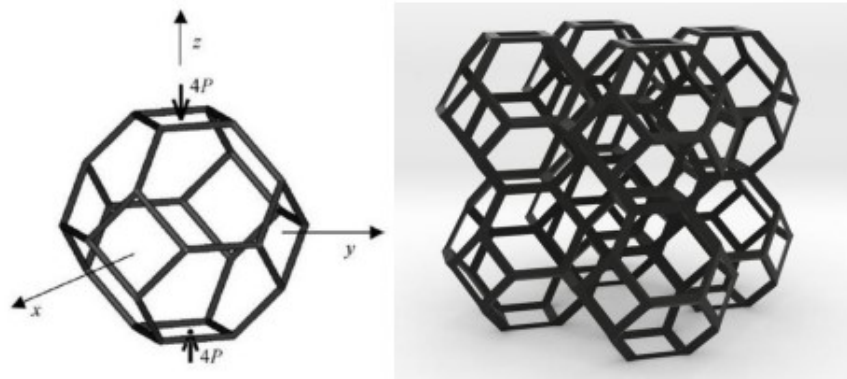
The supercritical fluid can be easily removed so that the dry solid skeleton remains, which is virtually identical to the initial skeleton in the wet gel. In this way, materials with a very high porosity and, therefore, a much lower density than the monolithic solid can be obtained [8].

During his lifetime, Kistler synthesized different types of aerogels, initially based on silica and later on those based on alumina, tungstic, ferric or stannic oxide and nickel tartrate. He also succeeded in creating organic aerogels made of cellulose, nitrocellulose, gelatine, agar or egg albumin [8].

In 1990, the first carbon-based aerogels were developed and patents were acquired by aerospace companies. In fact, NASA made a major contribution to the development of this class of materials by using them as super thermal insulation for space clothing. In addition, the high specific surface area was used to trap stardust particles in the Stardust expedition on 2 January 2004 [9].

### 1.1.3 Properties

**Density and Porosity:** Aerogels are materials consisting of at least 95% air, so they are solids with a very low density in the range of 0.0011 to  $\sim 0.5 \text{ g/cm}^3$ . The porosity present in them is open-cell, i.e. the solid phase is distributed along the edges of empty polyhedral structures ("cells"), and not closed-cell in which the solid phase is also positioned along the faces, as illustrated in Figure 2 [10].



**Figure 2.** *Open-cell structure [10].*

The pore diameters in aerogels range from 1nm to 100nm, in particular microporosity is defined as being smaller than 2nm and mesoporosity as having cavities in the 2-50nm range.

The high porosity gives a very high specific surface area of 10-2000  $\text{m}^2/\text{g}$ , which is important for certain aerospace applications [11].

Regarding the thermal conductivity, the high amount of air in the structure can be seen as an obstacle to the propagation of heat transfer, in fact, being located in very small cavities, it has little freedom of movement which inhibits both convection and conduction in the gas phase.

The low conductivity allows aerogels to be used as a high-performance thermal insulator [11].

Different mechanical behaviours can be found in the literature; depending on the constituent elements, aerogels can exhibit ductile or brittle behaviour. The bulk density, i.e. the volume of the pores, also modifies the mechanical properties of the material [12].

Moreover, aerogels can be surface functionalised either through chemical reactions or by surface deposition. This allows the functional groups of the polymer chains to be modified. Functionalisation can also be carried out on the internal part of the material by embedding of particles inside or by interpenetrating hybrid aerogel networks [11].

The optical properties of aerogels are strongly influenced by the starting chemical species. In fact there are both transparent and opaque aerogels.

## 1.2 Sol-Gel Process

Before describing how the process works, it is important to define:

- Sol: A very fine colloidal suspension dispersed in a liquid, so the physical and chemical properties are different to a solution. Solid particles have diameters between 1 nm and 1  $\mu\text{m}$ .
- Gel: “*Non-fluid colloidal network or polymer network that is expanded throughout its whole volume by a fluid*” [2]. So the gel is a viscous semi-solid phase, because the particles form a three-dimensional structure due to their aggregation.

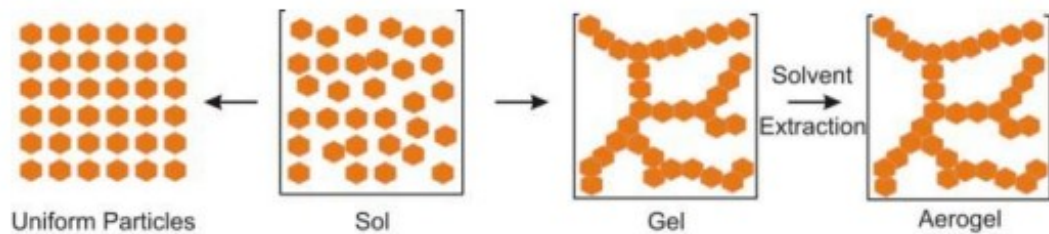
The Sol-Gel process is used in the production of aerogels; the different steps are:

- 1) Preparation of the Sol: Powders are dissolved in a dispersing medium so that nanometric particles are formed.
- 2) Transition from Sol to Gel: An interconnected structure is formed thanks to the bonds between the particles. A catalyst can be added to increase the bonds between the polymer chains, acting as a crosslinker.
- 3) Aging: To increase the mechanical characteristics of the final product, the gel can be aged for a set time.
- 4) Drying of the gel: The solvent is removed using different techniques [13].



Figure 3. Steps of the process.

Therefore, an easily removable liquid solvent is used to create cross-linking of the colloidal suspension, as explained in the following Figure 4.



**Figure 4.** *Sol-Gel process [14].*

This process allows a high degree of control over the nanoarchitecture; in fact, by modifying various process parameters such as pH, concentration, additives, temperature, etc., it is possible to vary the lattice formed and thus the final aerogel.

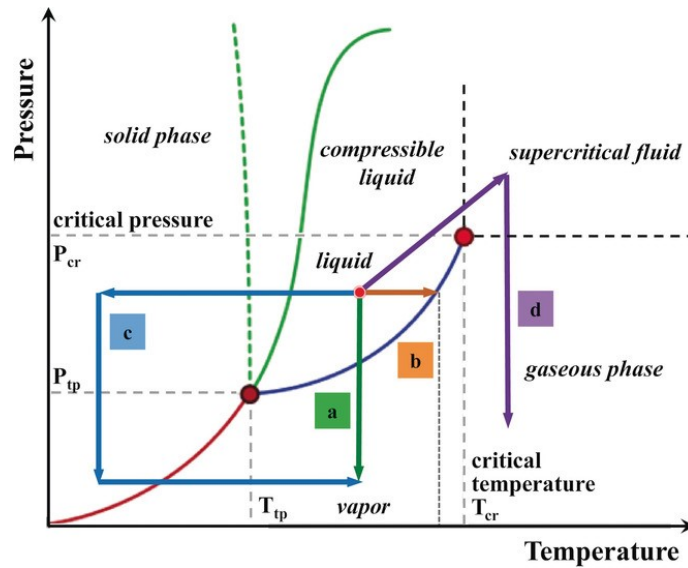
The properties of a material are also a function of its structure, so the possibility of modulating the process makes it possible to synthesise a product with the desired characteristics.

### 1.3 Drying Methods

Drying allows the solvent to be removed in order to create a solid rich in porosity. However, this operation is not easy because one must try to maintain the solid micro architecture formed during the sol-gel process.

Therefore, the main objective is to remove the solvent without damaging the structure created by the particles, which is the most critical step in the entire production process.

There are several methods, the main ones being: vacuum drying, oven drying, freeze-drying and supercritical drying. These methods are represented in the following temperature-pressure phase diagram.



**Figure 5.** The phase diagram: a) Vacuum drying b) Oven drying; c) Freeze-drying; d) Supercritical drying [15].

In 1931, Kistler used Supercritical drying (SCD) to synthesise the first aerogel: this technique is still the most common for creating these materials and, of course, over the years it has been improved by various research groups to increase productivity while reducing costs so that it can also be used on an industrial scale [16].

The process is based on the transformation of the liquid phase into a supercritical fluid at high temperature and pressure, i.e. above their respective critical points. In this way, high surface tension and capillary forces are avoided and shrinkage is significantly reduced, namely the decrease in volume of a network, gel or solid associated with the exudation of a fluid [2] and the nanoarchitecture is not damaged while keeping the porosity unaltered [17].

Once the fluid enters the supercritical zone it is easily removed in the form of gases such as:  $\text{CO}_2$ , Xe and  $\text{N}_2\text{O}$ . With this method of drying, waste gases are produced, so care must be taken about the environmental impact [15].

The supercritical drying process (referred to as SCD) is divided into 2 subgroups:

- HTSCD (high temperature supercritical drying): The solvent becomes a supercritical fluid in an autoclave at high temperature and pressure.
- LTSCD (low temperature supercritical drying): A supercritical fluid is used to extract the organic solvent present in the sample [17].

The second most frequently used process is freeze-drying (FD). This method is also used in this project because the environmental impact in terms of the solvent, water, is lower as compared to other technologies.



FD, as can be seen from the phase diagram (Figure 5) and in Figure 6, is based on sublimation, i.e. the change of state from solid to gas. Initially, the gel has to be frozen so that the solvent,  $H_2O$ , becomes solid. But the solidification of it, due to the fact that the density of ice is lower than that of liquid water, leads to an increase in volume and therefore, since the solvent is located in the cavities, an increase in the size of the pores or damage to them can occur [17].

In order to sublimate the water, a lyophilizer is used: A technology that exploits the decrease in pressure at a constant temperature so that steam is formed and the final solid structure is obtained.

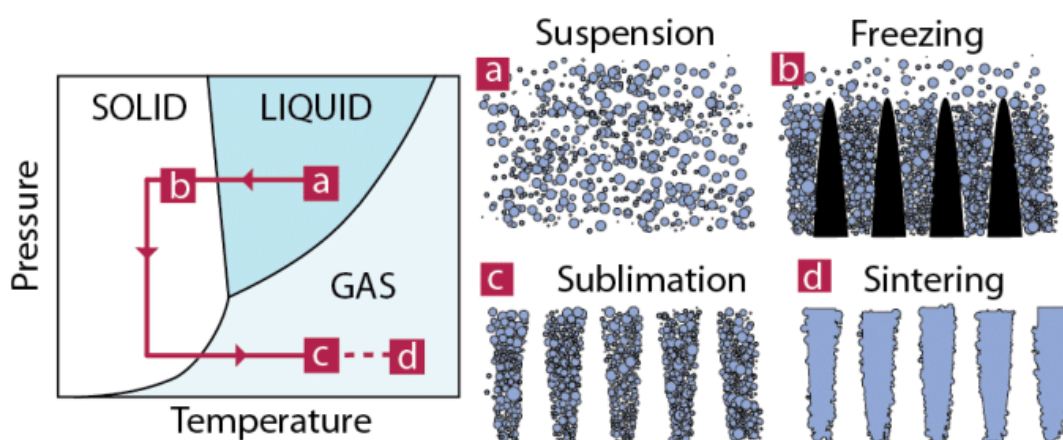


Figure 6. Freeze-Drying [18].

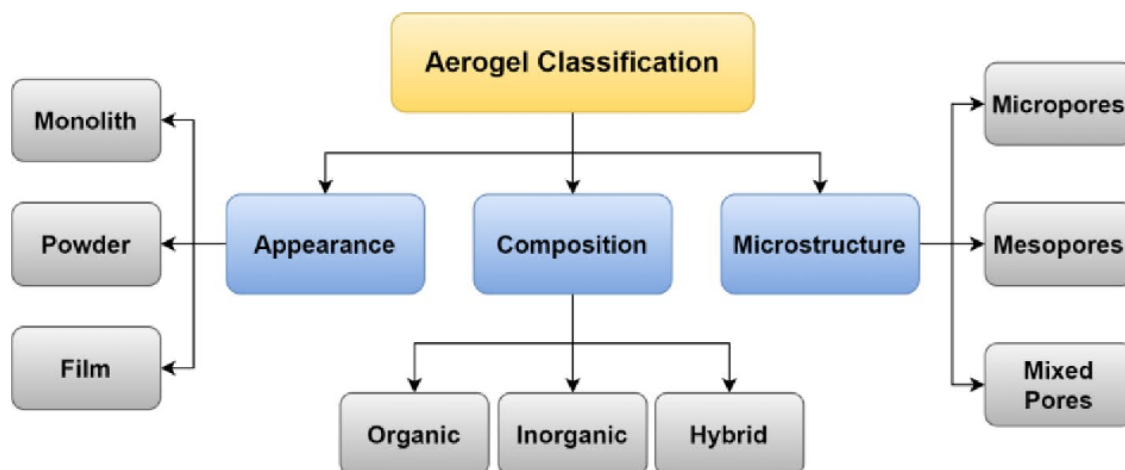
In the freezing stage, if the cooling is not homogeneous throughout the volume, the growth of the ice crystals is directional, resulting in an anisotropic material, which may be advantageous in certain applications.

Vacuum drying and oven drying are two techniques that exploit the evaporation of the solvent, but they are little used because the capillary forces created at the liquid-gas interface are high, so the nanostructure formed by the solute network is subjected to high tensions that damage it [15].

The choice of the appropriate drying process depends on multiple factors such as: Productivity, product reproducibility, speed of execution, costs, environmental impact, etc.

## 1.4 Classification of aerogels

Aerogels can be classified according to: Appearance, Composition or Microstructure (Figure 7).



**Figure 7.** Classification of Aerogels [19].

The first classification is based on appearance then size which depends on the end use of them, there are 3 subgroups: Monolith, Powder and Film [11].

The second classification places a focus on the type of porosity that is present in the material. Again, aerogels are divided into three groups:

- Micropores: If only pores with a maximum diameter of 2 nm are present
- Mesopores: If the pores have a diameter of between 2 and 50 nm.
- Mixed pores: If the material has both types of pores.

The third classification is the most commonly used because it divides aerogels into three categories according to their composition:

- Organic: They are divided into 2 subcategories as shown in Figure 8: i) Carbon-based aerogels and ii) Polymer-based Aerogels. The latter are split according to the origin of the raw materials, i.e. they can be synthetic or bio-based.
- Inorganic: These are divided into 5 sub-categories (Figure 8) based on the nature of the materials used to produce the aerogel: Fluoride, Silica, Metal, Oxides and Chalcogens.
- Hybrid: Mix of the 2 previous categories in fact it is possible to create composite aerogels in order to modulate the physical and chemical properties [11].

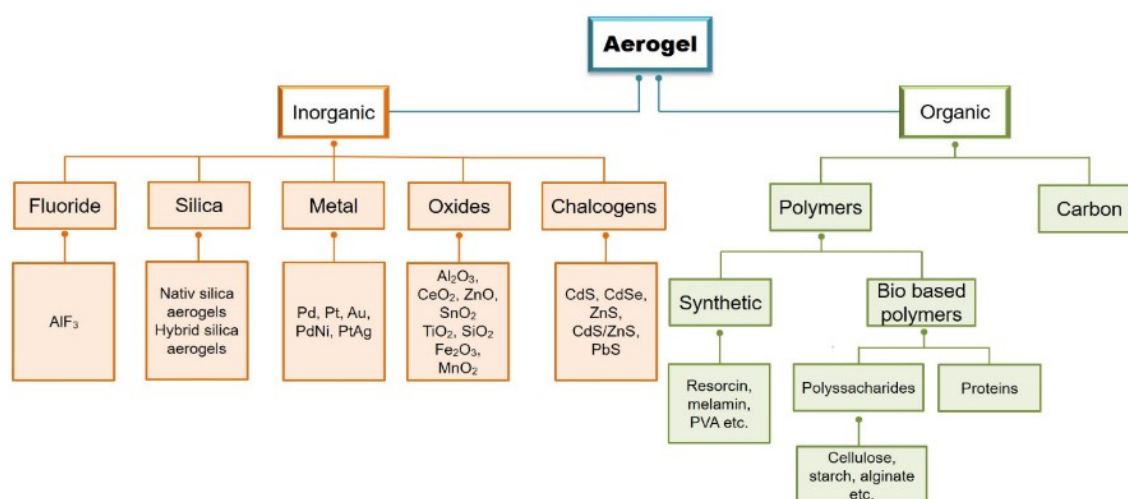


Figure 8. Inorganic and Organic Aerogels [20]

## 1.5 Biodegradable polymers

IUPAC defines biodegradable polymers as follows: "*Polymer susceptible to degradation by biological activity, with the degradation accompanied by a lowering of its molar mass*" [2]. However, the term biodegradable is ambiguous, since the time of degradation and the environmental conditions under which it occurs should be specified.

Polymers can be divided into two classes of materials: Fossil based, i.e. derived from fossil resources and biobased which are synthesised from biological products [21]. In both cases they can be biodegradable or not as shown in Figure 9.

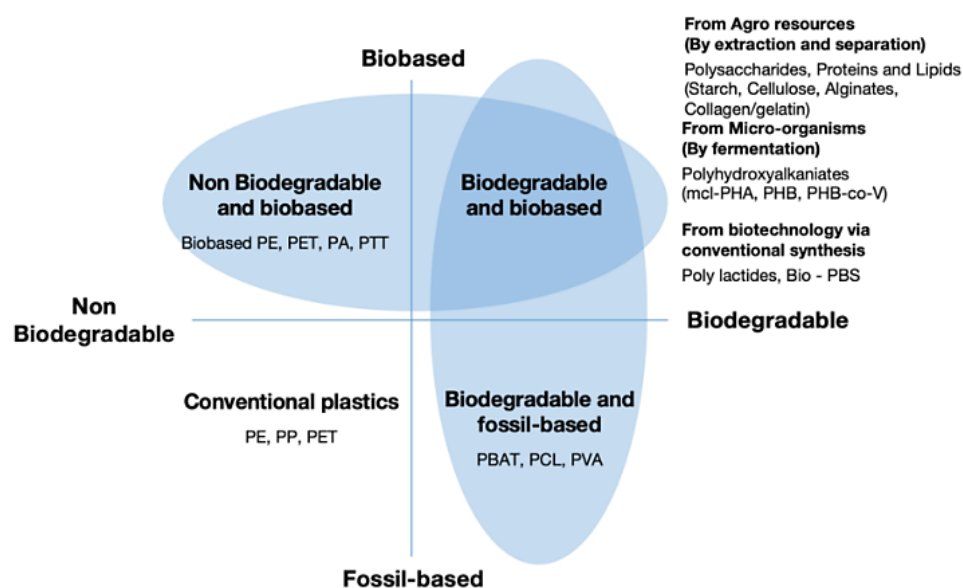


Figure 9. Classification of polymers.

### 1.5.1 Fossil-based and biodegradable aerogels

Fossil-based polymers come from fossil fuels or derivatives. For example, they are produced from petrol and therefore from non-renewable sources, but they can still be biodegradable.

An example of a fossil-based but biodegradable polymer used to produce aerogels is PVOH or PVA or polyvinyl alcohol: it is readily soluble in water, which means that water can be used as a solvent and the freeze drying process can be employed.

PVA has very good biocompatibility properties due to its low toxicity; it is also not expensive and has good chemical stability [22]. In addition, PVOH has good chemical compatibility with clay, which allows a composite aerogel to be created to improve several properties, including fire resistance in order to increase its competitiveness with traditional foams [23].

### 1.5.2 Bio-based and biodegradable aerogels

In this historical period, due to high pollution, there is a focus on products from renewable sources. For this reason, the research and development of bio-based and biodegradable aerogels is growing rapidly. Many of them are insoluble in CO<sub>2</sub> but soluble in water, which makes it possible to perform the freeze-drying process, which is the most eco-friendly process [20].

Two families of biobased and biodegradable aerogels can be distinguished:

- Polysaccharides: Originating from the plant world, they have several interesting properties such as: biocompatibility, very porous aerogels are obtained and therefore very light and with high specific surface area, good chemical affinity with many cross-linking agents due to their many functional groups, they are non-toxic and the production process is inexpensive [20].

There are several polysaccharides used to produce aerogels such as:

- Cellulose-based aerogels: Cellulose is the most common biopolymer on earth, which is the reason why it was the first material used in the production of aerogels. Cellulose is a linear biopolymer made of two repeating anhydroglucose units (b-glucopyranose) connected through 1,4-glucosidic bonds [24]. The aerogels produced can be used in a variety of applications such as biomedical applications due to their high biocompatibility or as thermal insulation.
- Alginate-based aerogels: Alginate derives from seaweed and is a bio-based copolymer with an unordered structure of alternating M blocks (mannuronic

acid) and G blocks (guluronic acid), forming an irregular structure. In addition to the characteristics common to polysaccharides (biocompatibility, high porosity, non-toxicity, water affinity, etc.), aerogels produced from alginate have high fire resistance properties [25].

- Other polysaccharides suitable for producing aerogels are: Lignin, starch and chitosan. Lignin makes it possible to create aerogels with good sound insulation [20].

Starch, on the other hand, produces a three-dimensional network useful in the pharmaceutical field.

- Protein-based aerogels are obtained from both plant and animal sources, the second deriving biopolymers from food production waste. Protein-based aerogels have several interesting properties such as biocompatibility, high interconnected porosity, high specific surface area and good cytocompatibility, which is essential for use in the biomedical field [20].

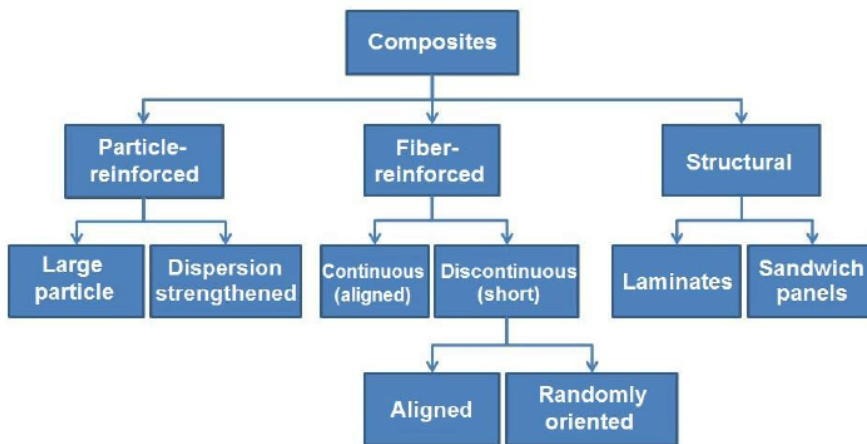
There are several Protein-based aerogels such as:

- Gelatin aerogels: Gelatin is produced from collagen and has a triple helix structure with high contents of glycine, alanine, pro line, and hydroxyproline [26]. Due to their excellent biocompatibility and non-immunogenicity, the aerogels produced can be used in the pharmaceutical field [20].
- Casein-based aerogels: Casein is a protein found in milk that can be crosslinked either chemically or enzymatically while remaining biodegradable. The aerogels produced from it have both good mechanical properties and low densities (0.07-0.12 g/cm<sup>3</sup>) [20].

## 1.6 Aerogel composites

A composite material is defined by IUPAC as follows: "*Multicomponent material comprising multiple, different (non-gaseous) phase domains in which at least one type of phase domain is a continuous phase.*"[2]. Thus, composites are materials having at least two phases with different physicochemical properties. The aim of creating heterogeneous materials is to obtain a product with better properties than the individual constituents.

Composite materials can be classified in different ways, e.g. they are divided into three groups: Particle-reinforced, Fibre-reinforced and Structural composite as shown in Figure 10.



**Figure 10.** Classification of composites [27].

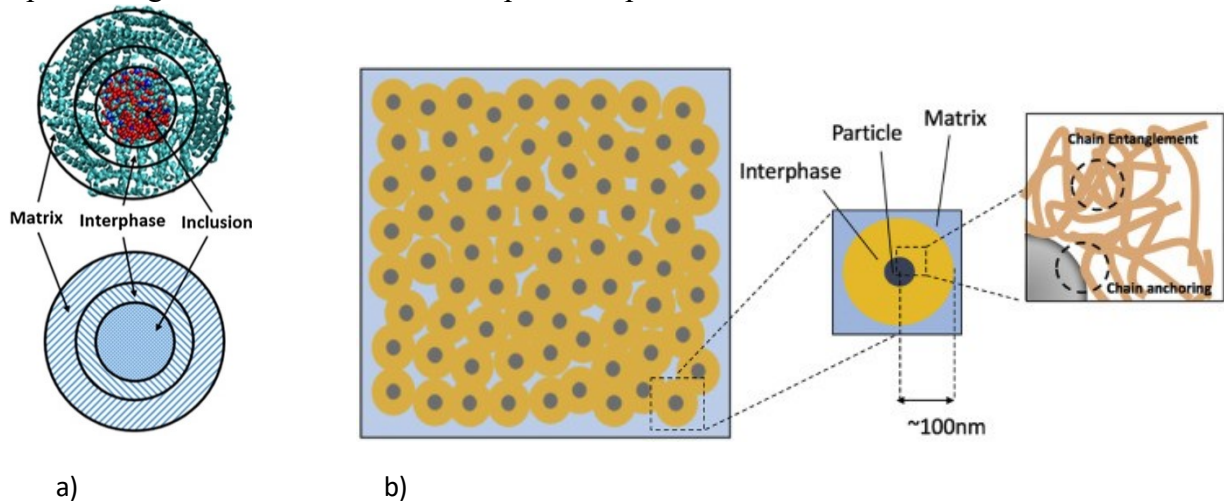
However, each type of classification is arbitrary and imperfect, in any case, in both particle-reinforced and fibre-reinforced composites, there is a continuous phase, i.e. the matrix that embeds a dispersed phase [27].

The matrix, from a mechanical point of view, has two 2 main tasks:

- Transferring stresses to the dispersed phase
- Enclosing and protecting the dispersed phase from the external environment

Furthermore, strong interphase is also important, the matrix in the vicinity of the reinforcement has different properties and morphology because it has to bond to it, as shown in Figure 11 [28].

It is crucial to study the interphase because the properties also depend on them, for example the presence of a very dense interphase gives better mechanical properties [29] as well as preventing, in the case of fibres, the "pull-out" phenomenon.

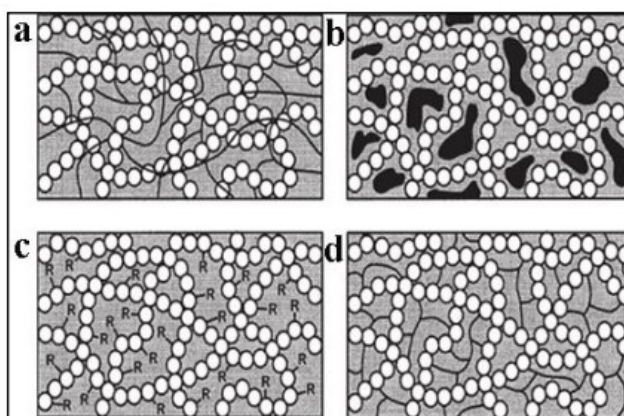


**Figure 11.** a) Interphase Models for Nanoparticle-Polymer Composites [29] b) Strong interphase in polymer nanocomposites [30].

Analogously, in the field of aerogels, properties can be tailored by creating hybrid aerogels. Depending on the fillers used, there can be an increase in both physical properties such as Young modulus, toughness, thermal conductivity, and chemical properties such as the material's behaviour when in contact with a solvent [19].

In this project, bio-based/inorganic hybrid aerogels are created, in fact, montmorillonite and tannic acid are added to ammonium alginate to create an aerogel consisting of organic building blocks combined with ceramic structural elements [31]. Solid montmorillonite is brittle but has high thermal and fire resistance properties, particularly as it is an inorganic material, a large amount of residue remains after burning, which is essential for safety reasons in structural applications. Conversely, ammonium alginate, being organic, has little residue after fire tests but is more ductile than clay. Tannic acid, an organic additive, acts as a crosslinker as explained in § 2.2.1.

In bio-based hybrid aerogels, additives and fillers can be incorporated in different ways as shown in Figure 12.



**Figure 12.** a) Interpenetrating inorganic and organic networks; b) Incorporation of organic molecules; c) Modification of oxidic materials with organic substituents; d) Dual networks [31].

## 1.7 Eco-friendly aerogels as a flame retardance system

The combustion process is divided into 3 steps:

1. Initially, the polymer heats up, releasing gases and vapours as degradation begins
2. Ignition of the vapour phase
3. Combustion and propagation

Three elements are required for combustion to occur: Combustible, heat and an oxidising elements (such as oxygen in the air) as shown in Figure 13.

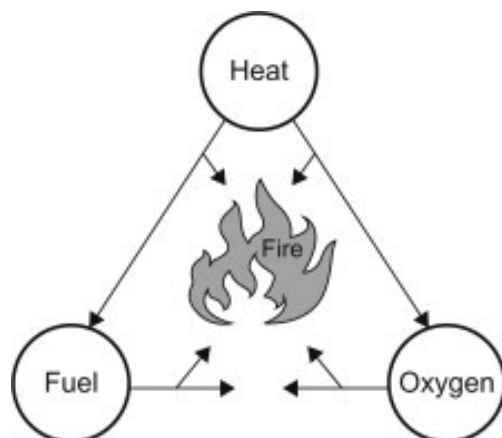
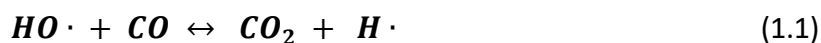


Figure 13. Fire triangle [32].

The substances that burn are the vapour-phase degradation products. From a chemical point of view, the reactions occurring in the propagation phase are radical and, of course, strongly exothermic [33]:



It is important to know the degradation mechanism of a polymer and the toxicity of the gaseous products, so it is possible to add additives or modify the polymer structure in order to improve the fire behaviour of the material. Furthermore, it is essential to know the flammability limits of polymers because self-sustained combustion can occur as shown in Figure 14.

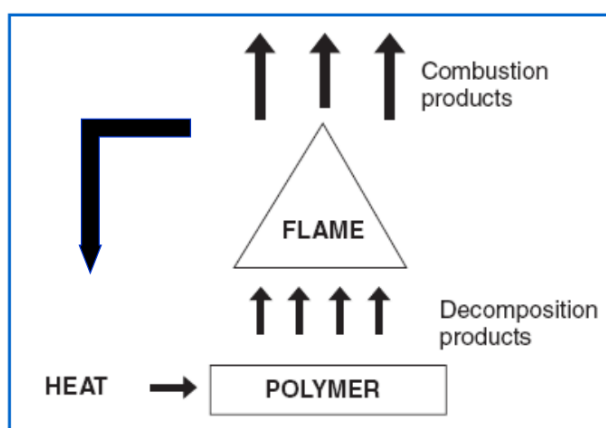


Figure 14. Combustion process self-sustained.



Various tests can be performed in order to study the fire behaviour of a material: LOI (Limited Oxygen Index), UL94 (which can have a horizontal or vertical configuration), the calorimetric cone and finally the S.B.I. test (Single Burning Item) [34]. In this project, the calorimetric cone was used for characterisation, which will be explained further in § 2.8.9. Biobased aerogels are excellent thermal insulators but their fire resistance is generally moderate as they are made of many combustible substances. However, it is possible to create hybrid biobased aerogels or to use additives that can significantly improve fire resistance.

Flame retardants are used to retard or inhibit combustion, depending on the mechanism of action they can be divided into 2 groups:

- Physical interaction: E.g. there exist flame retardants that cool the system through the development of endothermic reactions, or there are also surface layers that have the task of both preventing the propagation of decomposition products and creating a protective barrier between material and flame [34].
- Chemical reactions: In this case, it is possible to divide flame retardants into two sub-groups: those that act in the gas phase by developing reactants capable of inhibiting radical reactions or those that react in the solid phase by forming intumescent or char systems (two different protective barriers) [34].

In the literature, it is possible to find many examples of Bio-based Aerogels composites that exhibit considerable fire resistance compared to the base material such as:

- The use of montmorillonite and ammonium polyphosphate significantly improves the fire properties of aerogels made from recycled cellulose fibres and sodium carboxymethyl cellulose [35].
- The combined action of sodium alginate and tannic acid also enhances the fire properties of aerogels based on polyvinyl alcohol [36].



# CHAPTER 2: MATERIALS & METHODS

## 2.1 Polymers

### 2.1.1 Ammonium Alginate

Alginate, also called alginic acid, is a linear anionic copolymer consisting of  $\alpha$ -L-guluronic (G) and  $\beta$ -D-mannuronic (M) acid units joined with 1-4 glycosidic bonds arranged in an irregular structure (Figure 15) [37]. Alginate is a polysaccharide that is mainly obtained from brown algae/seaweed such as: *Ascophyllum*, *Macrocystis*, and *Laminaria*; but it can also be synthesised from two bacteria: *Pseudomonas*, *Azotobacter*. Thus, it is a biobased polymer from renewable sources [38].

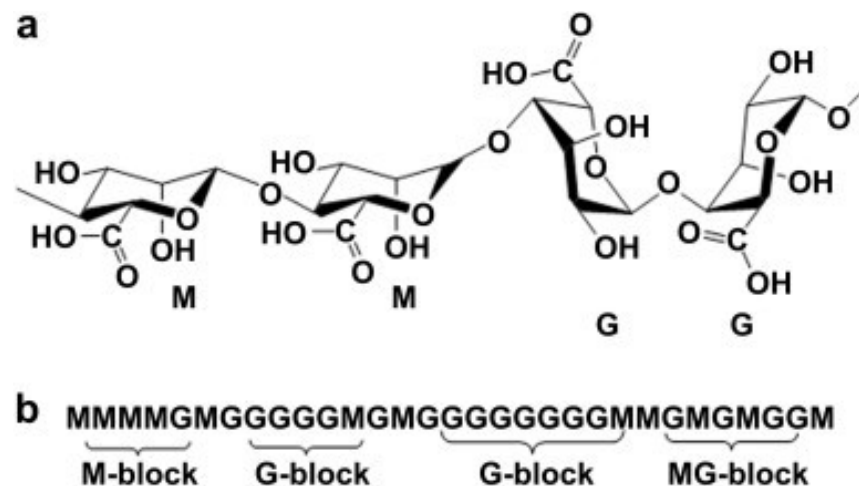


Figure 15. a) Alginic acid structure b) Example of random alternation of blocks [39].

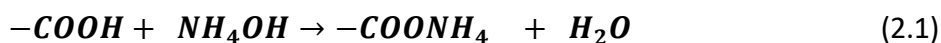
The alternation of the two blocks present in the chain depends on the seaweed used, but it is possible to state that the stiffness and strength are proportional to the quantity of G-Blocks present.

In order to obtain alginic acid from seaweed, it has to be treated with HCl, which separates the alginate from the unwanted components, i.e. the residue which is filtered out [38].

Alginic acid contains several functional groups including the carboxyl group which is very reactive and can be used to produce different types of alginate.

Ammonium alginate was used in this thesis project because several studies have shown the high fire resistance of aerogels made of it [25].

Ammonium alginate is obtained by reacting alginic acid with a solution containing ammonium hydroxide ( $NH_4OH$ ) [37] which is present in aqueous ammonia solutions, thus creating  $-COONH_4$  groups in the chain:



Thus, the structure of macromolecules changes as follows:

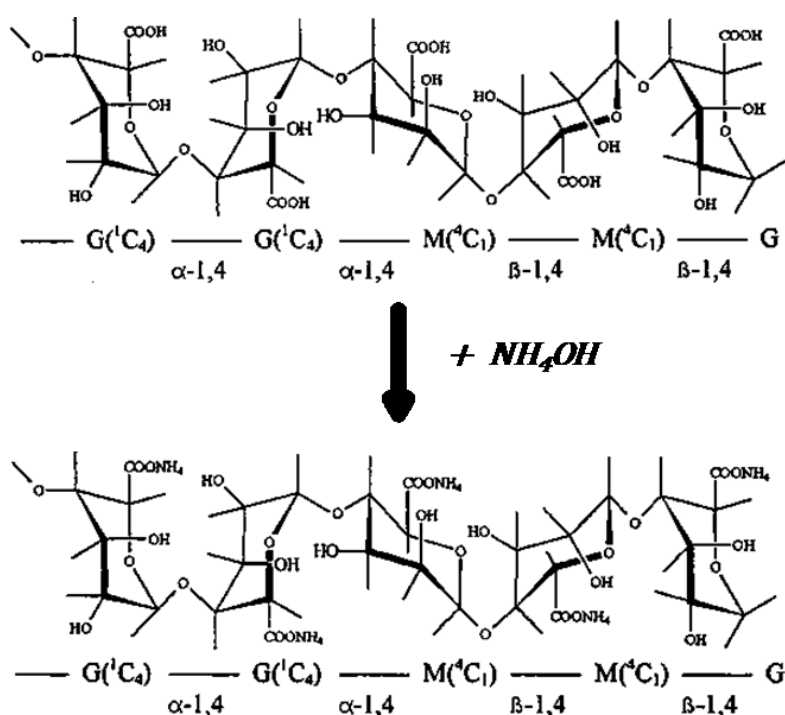


Figure 16. From alginic acid to ammonium alginate.

Alginate is a hydrophilic biopolymer, bio-based, biodegradable, it is very abundant in the earth and the production process is simple, it is nontoxic, has a low density, mechanical flexibility, chemical/structural modifiability and inherent flame retardancy [38]. In addition, crosslinking (increasing the degree of reticulation of the biopolymer) can be easily performed due to its chemical inertness in order to increase the mechanical properties and fire resistance. In particular, different strategies can be used for crosslinking, which can be either ionic or covalent depending on the intramolecular bonds that are formed [38].

Thanks to these characteristics and the need to find eco-friendly alternatives to non-biodegradable industrial products, it is used in various production sectors:

- Thermal insulation and flame retardant: Ammonium alginate can be used to create aerogels with very low thermal conductivity compared to traditional fossil-based foams, and fire resistance is also fundamental for thermal insulation in buildings [25].
- Biomedical: Thanks to its non-toxicity, biocompatibility and biodegradability, it can be used for drug delivery, as a substrate in cell cultures and as medical textiles.
- Food industry: Alginate could be used in food packaging because, in addition to being biodegradable, it can protect food by acting as a barrier and increasing shelf life.
- Textiles and paper: It is possible to create fibres that are usable in the clothing industry. Alginate could also be added to the paper production process to modify its viscosity and adhesive properties [38].

Ammonium alginate produced by ALGAIA with the following characteristics (found in the data sheet) was used in this project :

**Table 1.** Chemical/physical specifications; \* measured at 20°C on a Brookfield RV viscosimeter, 20 rpm

<b>Viscosity*</b>	1% sol.	350 – 450 mPa.s
<b>pH</b>	1% sol.	5.0-6.0
<b>Loss on drying</b>		Max 20%
<b>Granulometry</b>	< 500 µm (US 35#)	Mini 98%

## 2.2 Additives

### 2.2.1 Tannic Acid

Tannic acid, referred to as TA, is an inexpensive organic polyphenolic additive derived from several plants: oak, walnut and mahogany [40].

Its structure (Figure 17) is rich in benzene rings, in particular there is a high density of pyrogallol, *Benzene-1,2,3-triolo*, and catechol, *1,2 diidrossibenzene*, groups [41].

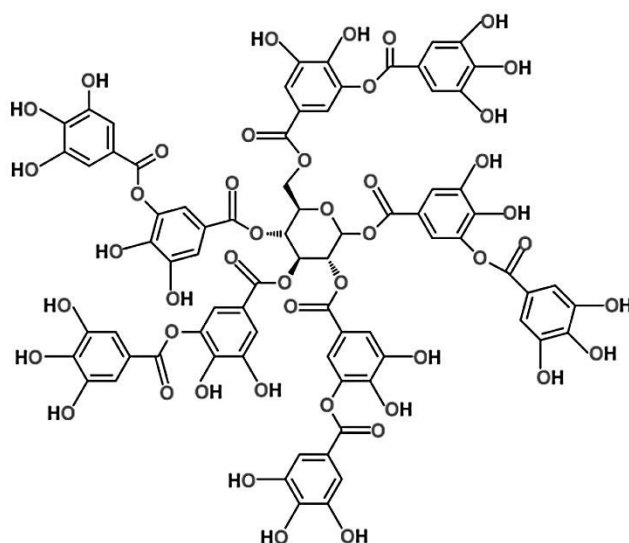


Figure 17. Structure of tannic acid [42].

Tannic acid is a crosslinker, operating under acidic conditions through various crosslinking mechanisms: hydrogen bonding, ionic bonding, coordination bonding to several metal ions (Fe, V, Cu, Ni, Mg, Zn), and hydrophobic interactions between the catechol and gallol groups.

Thus, the degree of cross-linking of the alginate increases, allowing an improvement in the mechanical properties [40]. In addition, the fire resistance characteristics are also modified by using TA, since it has thermal stability and is able to reduce and inhibit the free radicals present in the combustion process.

Since TA is rich in hydroxyl groups and soluble in water, it is used in the form of a yellow powder. To conduct this research, TA,  $C_{76}H_{52}O_{46}$  with a molecular weight of 1701.20 g/mol was used; the melting temperature is  $218^{\circ}C$  and the density is  $2.12 \text{ g/cm}^3$  [43].

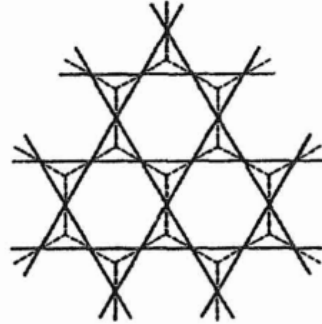
## 2.3 Fillers

### 2.3.1 Montmorillonite

Clay, a very fine sediment ( $<2\mu\text{m}$ ), consists mainly of aluminium silicates or magnesium silicates [44].

Silicon is a very common component in the earth's crust, in fact 26% of it is made up of silicon, and it combines with oxygen to generate various tetrahedral structures. Depending on the  $\frac{O}{Si}$  ratio, where  $O$  indicates the number of oxygen atoms and  $Si$  the number of silicon atoms, there are various structures composed of tetrahedra in which the central silicon is bound to oxygen atoms: orthosilicates, pyrosilicates, metasilicates and layered structures [45].

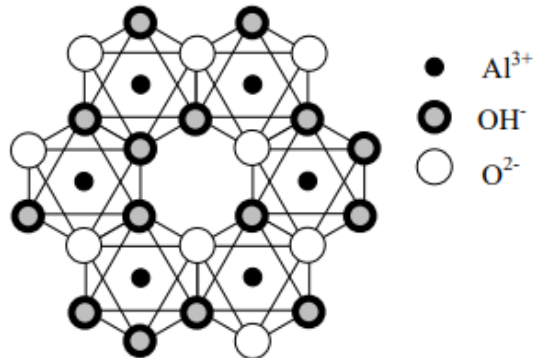
Clay minerals are composed of layered structures,  $(Si_2O_5)_n^{2n-}$ , so the  $\frac{O}{Si}$  ratio is 2.5. The tetrahedra are bonded together through bridged oxygens, generating a two-dimensional hexagonal mesh as shown in Figure 18.



**Figure 18.** Phyllosilicate structure [46].

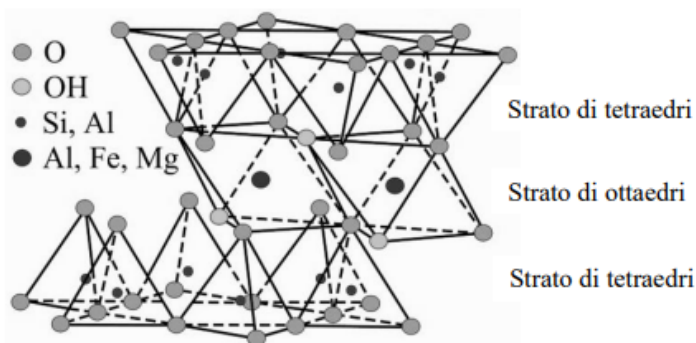
The earth's crust is composed of 8% aluminium, so this chemical species is also readily available.

Like silicates, the hydrated alumina oxide  $AlO(OH)_2$ , can have a hexagonal lattice with two-dimensional development but in this case it is composed of octahedra linked together thanks to the sharing of an edge as shown in Figure 19 [45].



**Figure 19.** Hydrated alumina oxide's structure [45].

Depending on the arrangement of these layers, different clay compounds can be created. Montmorillonite is a trimorphic structure [46] so the ratio between Si and Al layers is 2:1, creating a structure called a "sandwich" in which the bond between the two layers is made by water, through the intermolecular Van de Waals forces, and the distance between them is 15 Å.



**Figure 20.** *Montmorillonite's structure [45].*

The nomenclature used to denote montmorillonite is  $Al_2(Si_2O_5)_2(OH)_2 \cdot nH_2O$ . As can be seen in the Figure 20, aluminium, whose valence is +3, can be replaced by other atoms such as magnesium, valence +2, but since the valence electrons are not the same in the two chemical species, a charge imbalance will be created which can be "neutralised" by alkaline ions [45], and silicon atoms can be replaced by aluminium ones.

Regarding the physical properties, montmorillonite is hydrophilic so it is easy to dissolve in water, and has low cytotoxicity both in vivo and in vitro [47]. Due to its hydroxyl groups, it is easily functionalised, its layered structure, high surface area and electrostatic forces allow easy exchange and intercalation of cations such as  $Na^+$  and  $K^+$ , modifying their properties [48] [49].

Montmorillonite is also used as a filler in polymer matrices as it improves the thermal properties: the silicate layers create a barrier effect allowing the degradation temperature of the polymer to be increased [48].

Mechanical properties and fire resistance are also modified in the presence of montmorillonite.

The montmorillonite used in this project is: Sodium montmorillonite ( $Na^+Mt$ ), PGW from Nanocor Inc, with cation exchange capacity of 145 meq/100g ( $\pm 10\%$ ) and aspect ratio of 200–400.

## 2.4 Solvent

### 2.4.1 Deionised water

In this project, deionised water, also known as demineralised water, was used as a solvent. Very often, the terms deionised and distilled are in fact confused: in the first case, it is water from which all the mineral salts have been removed but there may be dissolved gases and bacteria; in the second case, on the other hand, the distillation process also allows gases and microorganisms to be removed in addition to the salts dissolved in it [50].



In order to obtain demineralised water, ion-exchange processes are used that are able to replace the mineral salts present with ions capable of joining and forming water such as, for example:



Production processes that lead to the removal of dissolved ions are: Highly acidic cationic + highly basic anionic resin systems; Highly acidic cationic + weakly basic anion + highly basic anion resin systems; mixed bed deionisation. The first two are illustrated in Figure 21 and Figure 22 while mixed bed deionisation presents the combined action of anion and cation exchange resins [51].

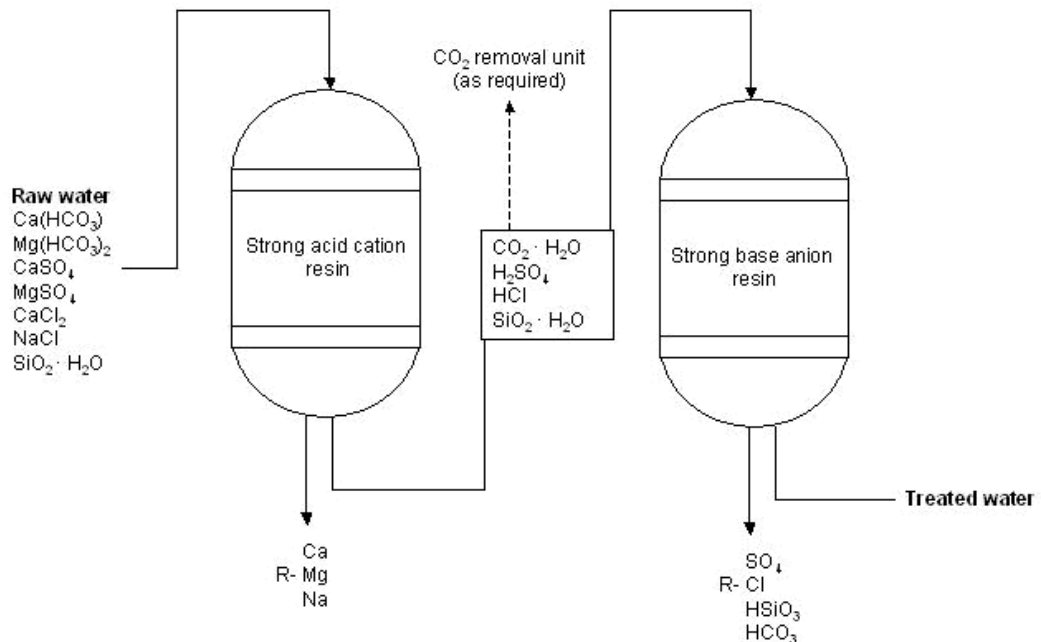
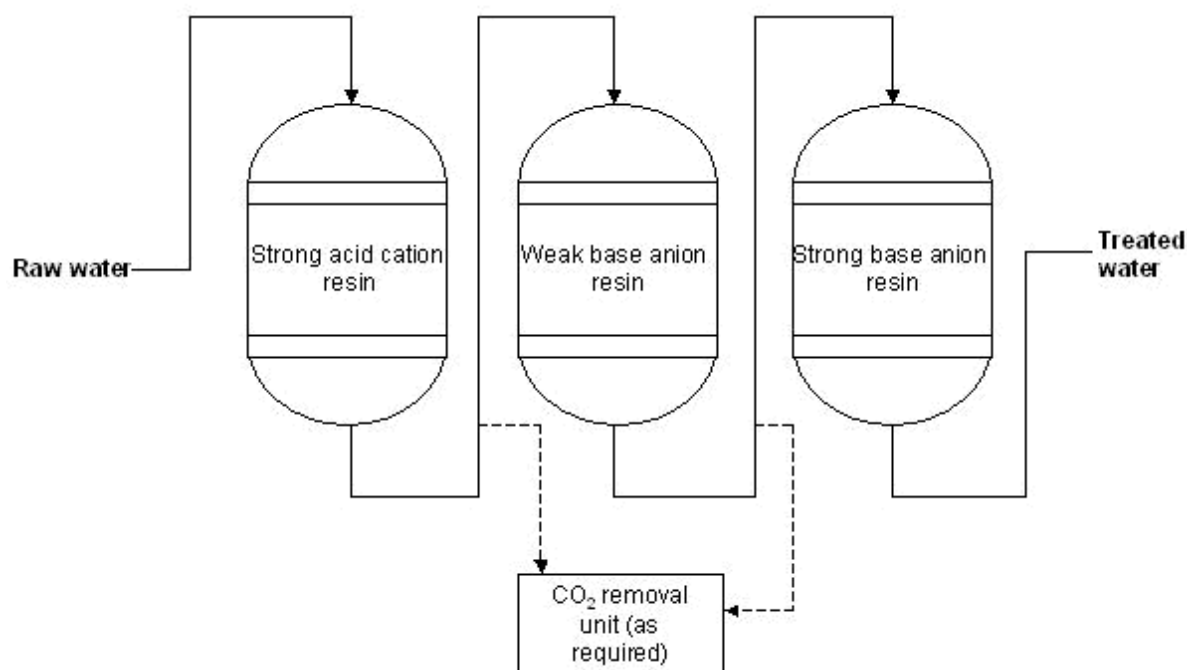


Figure 21. Highly acidic cationic + highly basic anionic resin systems [51].



**Figure 22.** *Highly acidic cationic + weakly basic anion + highly basic anion resin systems [51].*

Lastly, the reverse osmosis process can be adopted to produce deionised water [51].

## 2.5 Aerogels Preparation

The following subsections will define the nomenclature used to identify the different compositions, the technologies used to perform the sol-gel process and the steps in the production procedure.

### 2.5.1 Sample nomenclature

Before explaining the specimen preparation in detail, it is appropriate to define the nomenclature used in Table 2.

The letter A identifies ammonium alginate, C identifies montmorillonite and, T identifies tannic acid. After each letter in the name, there is a number indicating the weight in grams of the chemical species dissolved in the total volume of 100 ml of water.

**Table 2.** *Sample Nomenclature*

<b>Name</b>	<b>Amm. Alginate (g)</b>	<b>Montmorillonite (g)</b>	<b>Tannic Acid (g)</b>	<b>Water (ml)</b>
<b>A5</b>	5	-	-	100
<b>A5T1</b>	5	-	1	100
<b>A5C5</b>	5	5	-	100
<b>A5C5T1</b>	5	5	1	100
<b>A5T1C5</b>	5	5	1	100
<b>A5C5T2</b>	5	5	2	100
<b>A5T2C5</b>	5	5	2	100

### 2.5.2 Technologies employed for the sol-gel process

In order to facilitate the explanation of the process adopted to produce the aerogels, it is important to describe the instruments used.

The powders were weighed using a PB303DR balance, Metter Toledo, Switzerland with a sensitivity of 0.01g.

The volume of deionised water used to disperse the particles was also measured in a graduated cylinder with a maximum volume of 100mL.

The main step in the sol-gel process is the mixing and homogenisation of the solutions; three different mixers were used:

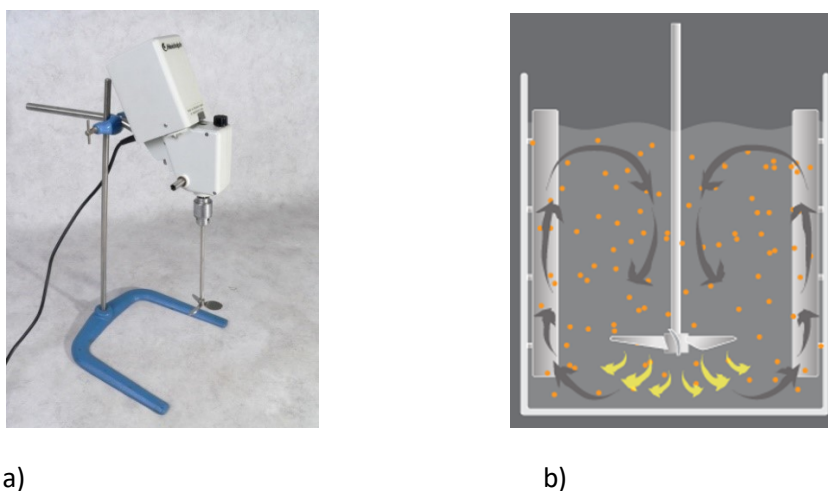
- **Mechanical propeller stirrers:** These are widely used stirrers that allow solutions with a higher viscosity than water to be mixed.

It consists of a motor that allows the rod, which is the fundamental element enabling mixing, to rotate at the desired speed. There are different types and models of mixing rods such as, for example, floating blade, propeller, turbo-propeller and blade with holes [52].

In this project, a mechanical stirrer with a helical mixing rod was used. Specifically, the model used was the overhead stirrer RZR 1, shown in Figure 23a, manufactured by Heidolph with the following technical specifications: Number of revolutions range I: 35 - 250 rpm. Number of revolutions range II: 280 x 2200 rpm. Maximum stirring capacity: 20000 ml of water [53].

The mechanical propeller stirrer allows the liquid to move according to an axial flow, which also enables the mixing of solid suspensions [54].

As can be seen in Figure 23b the mixing is not homogeneous so, after a certain time it is necessary to switch off the machinery in order to move the more heterogeneous areas manually.

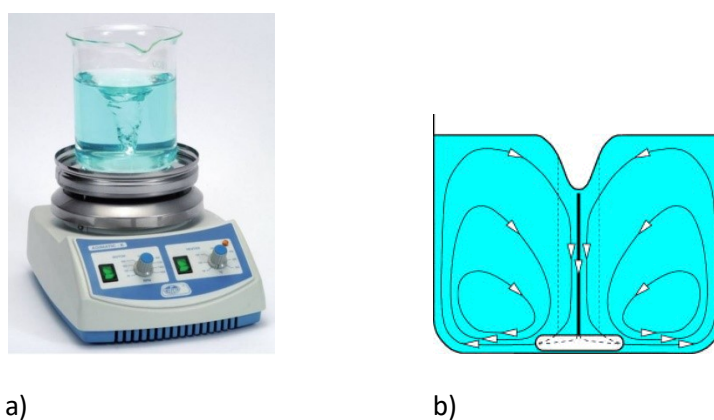


**Figure 23.** a) Overhead stirrer RZR 1, manufactured by Heidolph [53] b) Axial flow [55].

- Magnetic stirrers: These are magnetic stirrers that use rotating magnetic fields to move the stir bar inserted in the liquid to be stirred [56].

The variations of these devices vary depending on the application, and they can also be equipped with a heating plate in order to increase the temperature of the liquid to be mixed. In this project, a magnetic stirrer 7002431 (Figure 24a) manufactured by J.P Selecta, Spain, with an rpm range of 60-1600 [57] was used.

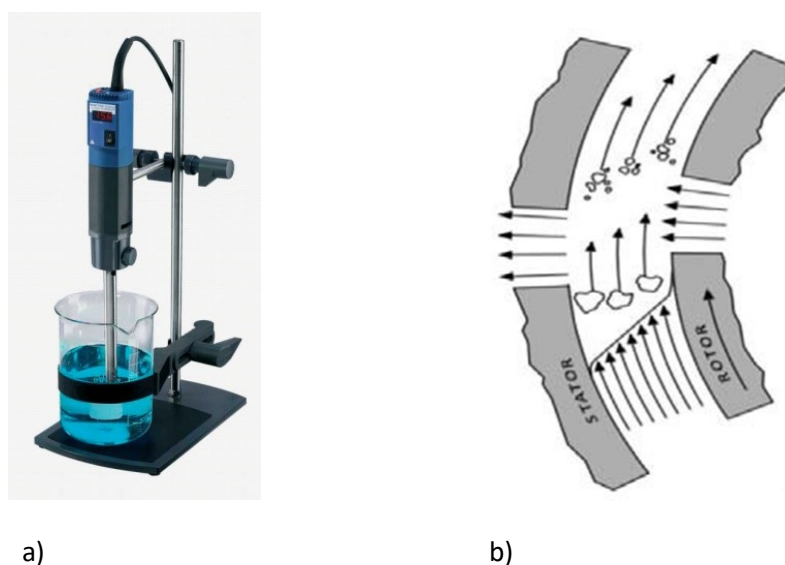
When the stir bar is set into rotation, a vortex is created, shown in Figure 24b, which increases in size as the speed of rotation of the magnet increases, allowing the mixing and dispersion of particles [58].



**Figure 24.** a) Magnetic stirrer 7002431 [59] b) Vortex flow generated by a magnetic stirrer [58].

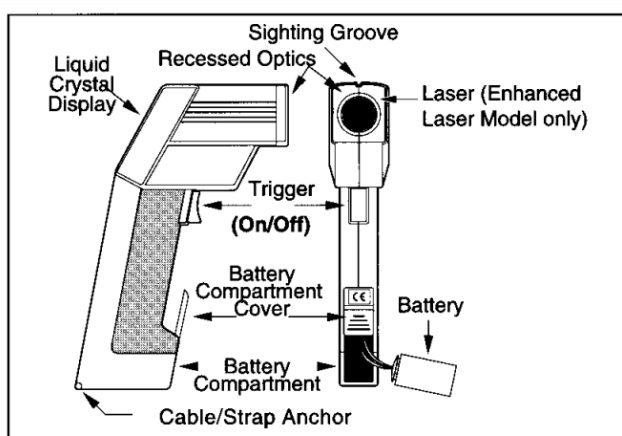
- Ultra Turrax: This is a mixer consisting of a rotor and stator separated by a gap (Figure 25b) [60] in such a way that this device sucks up the fluid by means of the high rotor speed and then expels it radially. That shear forces are achieved which enable the suspension to be mixed [61].

The model of Ultra Turrax used in this project was T 25 digital ULTRA-TURRAX® (Figure 25a), IKA, with a maximum rotation of 25000 rpm and a maximum stirring capacity of 2000 ml. [62].



**Figure 25.** a) T 25 digital ULTRA-TURRAX®, IKA [63] b) Operating mechanism of Ultra Turrax [60].

Finally, the temperature was monitored during the process using the Raynger ST laser detector, manufactured by Raytek shown in Figure 26.



**Figure 26.** Temperature detector Raynger ST, Raytek [64].

### 2.5.3 Sol-Gel process

To prepare the aerogels, the sol-gel process was followed in order to obtain homogeneous and repeatable products, which were poured into moulds in order to freeze them and create specimens for both the compression test and the calorimetric cone.

After weighing the raw materials and measuring the amount of deionised water to obtain the desired compositions, seven different aerogels were created and tested:

- 1) A5: Ammonium alginate was dissolved in a beaker containing deionised water, and a mechanical propeller stirrer was used, gradually increasing the speed. Figure 27 shows the steps performed during the process.

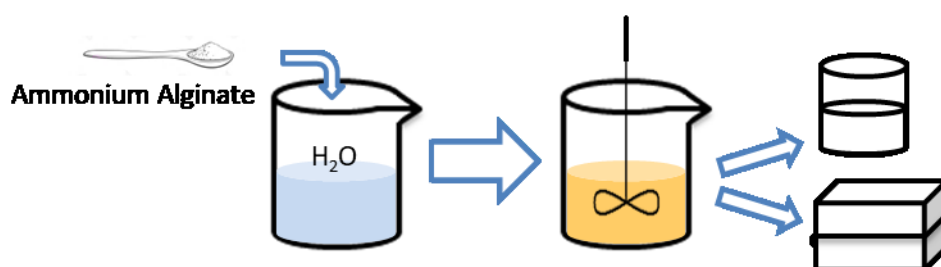


Figure 27. Preparation process of A5.

- 2) A5T1: In this case, there are two components in the mixture, therefore it is first necessary to dissolve them separately in deionised water and then to combine the two solutions by continuing mixing in order to obtain a homogeneous product. For the dissolution of ammonium alginate, the procedure explained in A5 was followed. Instead, the tannic acid was poured into another vessel and mixed using a magnetic stirrer. Once homogenisation was achieved, both solutions were combined and mixing continued in the mechanical propeller stirrer as can be seen in Figure 28.

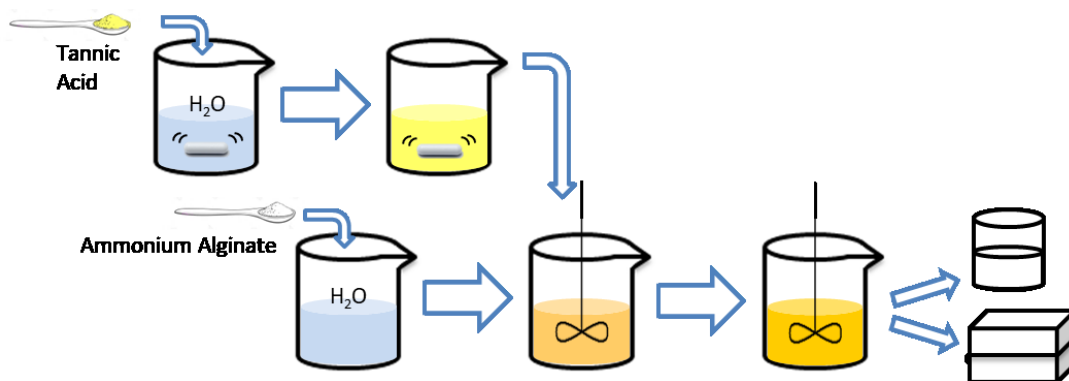


Figure 28. Preparation process of A5T1.

- 3) A5C5: Also in this case there are two components and therefore they are first homogenised separately. For ammonium alginate, the process of A5 is always followed, but the solution containing montmorillonite is first dispersed manually and then, as homogenisation is difficult to achieve, the Ultra Turrax is used.

Once both solutions were homogenised, the one containing the clay was poured into the beaker in which ammonium alginate was present. As can be seen in Figure 29, an initial mixing was carried out using the mechanical propeller stirrer but, in order to speed up the process by optimising it, the Ultra Turrax was also used. However, as it is not a fast process, the speed of the Ultra Turrax is gradually increased, but this causes energy dissipation in the form of heat; in fact, a maximum temperature of 35°C was measured with a laser temperature detector *Raytek*.

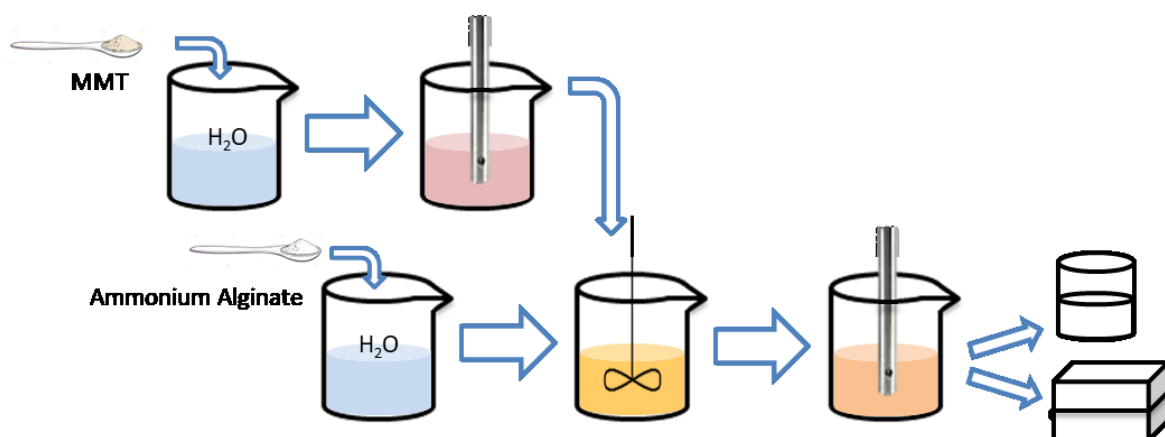
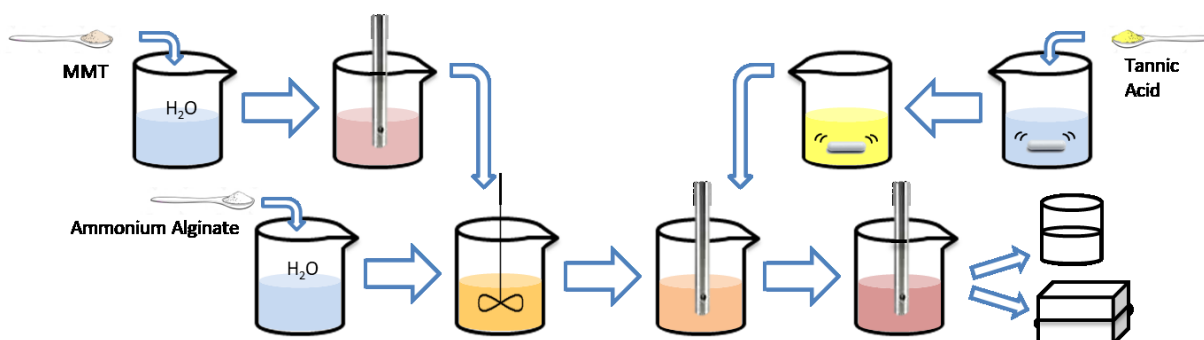


Figure 29. Preparation process of A5C5.

- 4) A5C5T1 and A5C5T2: The most difficult processes were those with all three chemical species, in fact, it was always necessary to dissolve them separately and then combine two of them, homogenise them, and then add the third chemical species and continue mixing until the heterogeneities disappear, as can be seen in Figure 30.

Following the preparation described in A5C5, a homogeneous solution of ammonium alginate and montmorillonite was obtained. Meanwhile, the tannic acid was also dissolved in water using the magnetic stirrer and then combined with the mixture having the other two chemical species.

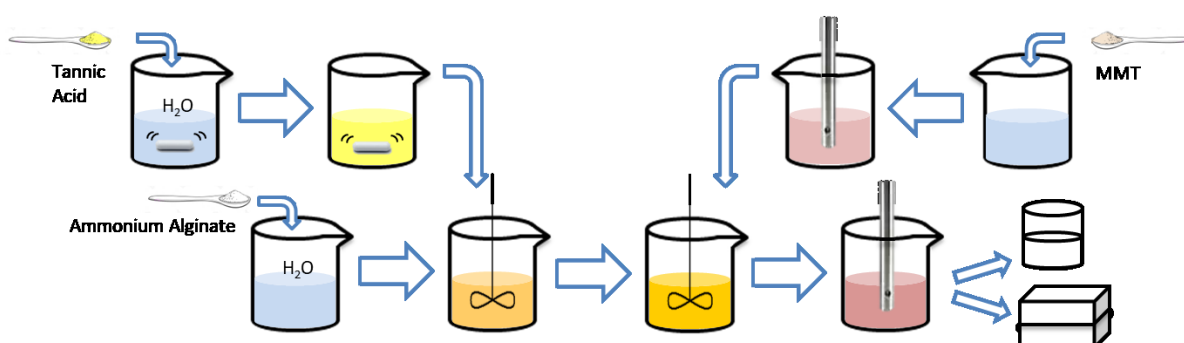
The final mixing to obtain the desired product was performed with the Ultra Turrax and, as explained in A5C5, the temperature was increased to a maximum of 34.5°C for A5C5T1 and 37.2°C for A5C5T2.



**Figure 30.** Process for preparing A5C5T1 and A5C5T2.

- 5) A5T1C5 and A5T2C5: In order to observe whether the production process changes the properties of the material, it was decided, in the case where all three components are present, to reverse the order in which the additives are combined with the solution containing ammonium alginate; Figure 31 shows the process followed. This variation is referred to as a “step change”.

In this case, tannic acid dissolved in deionised water was first combined with the solution containing ammonium alginate following the process of A5T1. In the meantime, montmorillonite was also mixed using Ultra Turrax, and once homogenisation was achieved, it was combined with the solution containing the other two chemical species. Once again given the high number of elements present in the mixture, it was difficult to remove the heterogeneities, which is why after an initial period in the mechanical propeller stirrer it was mixed with Ultra Turrax. Precisely as with A5C5, the temperature increased to 35.9°C for A5T1C5 instead of 39.1°C for A5T2C5.



**Figure 31.** Process for preparing A5T1C5 and A5T2C5.

Table 3 shows the quantities of powders used and the volume of water in which they were dissolved in order to obtain a 300 ml volume of solution.



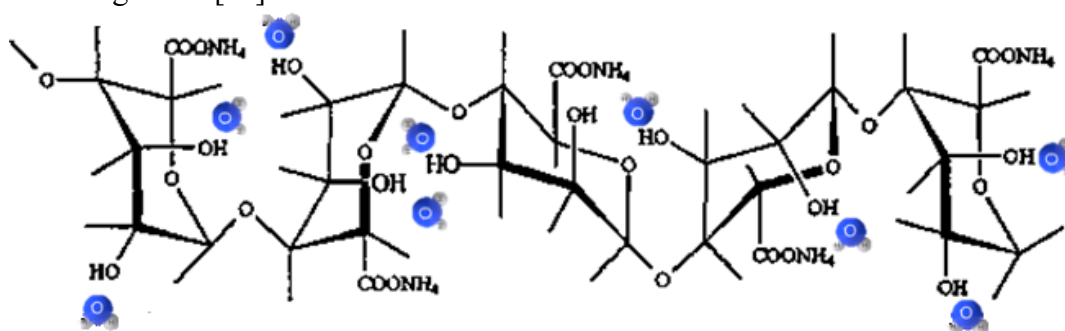
**Table 3.** Quantity of powders used and volume of water in which they were dissolved to obtain 300ml of product

Composition		Ammonium alginate	MMT	Tannic acid
A5	Weight (g)	15	-	-
	H <sub>2</sub> O (ml)	300	-	-
A5T1	Weight (g)	15	-	3
	H <sub>2</sub> O (ml)	240	-	60
A5C5	Weight (g)	15	15	-
	H <sub>2</sub> O (ml)	150	150	-
A5C5T1 A5T1C5	Weight (g)	15	15	3
	H <sub>2</sub> O (ml)	120	120	60
A5C5T2 A5T2C5	Weight (g)	15	15	6
	H <sub>2</sub> O (ml)	120	120	60

## 2.6 Chemical and physical reactions

It is important to determine the chemical interactions between the molecules in the mixture, in particular the interactions of ammonium alginate with the different elements are analysed:

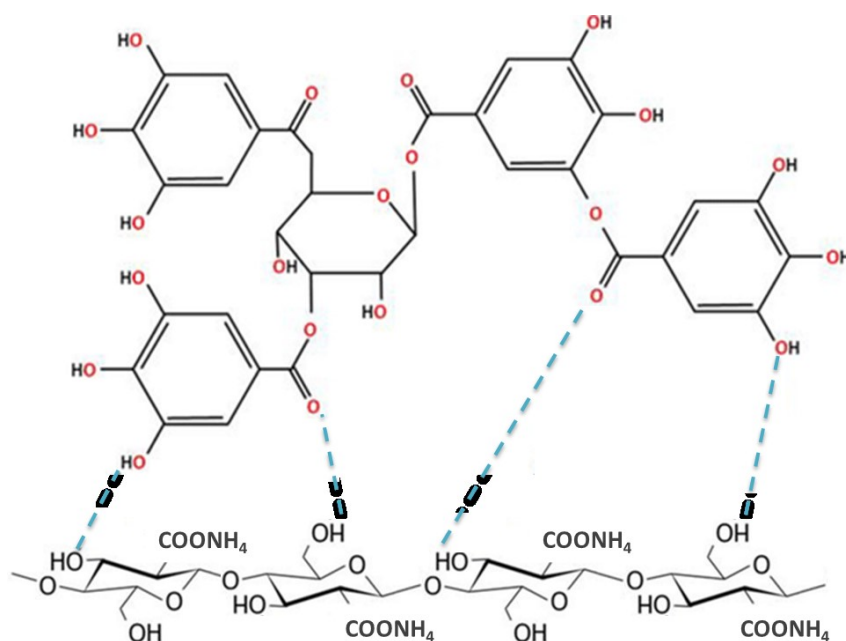
- Ammonium alginate + deionised water: It was easy to dissolve ammonium alginate powder in deionised water to obtain a very viscous solution. Alginate is hydrophilic due to the presence of many polar groups such as hydroxyl groups (-OH) which interact with H<sub>2</sub>O molecules. In fact, dipole-dipole interactions are created between the functional groups present in the polysaccharide macromolecules and water as seen in Figure 32 [65].

**Figure 32.** Interaction between ammonium alginate and water.

- Ammonium alginate + tannic acid: Tannic acid is added to polymer materials to act as a crosslinker in order to obtain a cross-linked structure with covalent bonds. Depending on the operating conditions and the polymer to which it is added, it can act according to different crosslinking mechanisms: Hydrogen bonding,  $\pi$ - $\pi$  stacking, metal phenol network, phenol-amine Michael and Schiff base reaction, phenol-thiol Michael addition, phenol-epoxy ring opening reaction, silanol-phenol condensation, boronate-phenolic network, phenol-alcohol Mitsunobu reaction, phenol-aldehyde reaction, acylation of polyphenols, polyphenol-thiyl radical oxidation reaction [66].

Hydrogen bonding is a dipole-dipole bond, depending on the electronegativity of the atom to which the hydrogen is bonded, different bond energies ranging between 2 and 15 kcal/mol can occur [67].

Tannic acid has many hydroxyl groups capable of forming hydrogen bonds, and ammonium alginate also has these functional groups. However, it is possible to make a prediction as to what happens when phytic acid, which contains a high amount of pendant -OH, reacts with ammonium alginate to form hydrogen bonds, so it is possible that ammonium alginate forms the same bonds with tannic acid as observed in Figure 33 [68].



**Figure 33.** Possible interaction between ammonium alginate and tannic acid.

- Ammonium alginate + montmorillonite: Montmorillonite is rich in positive charges in the edges that can interact electrostatically with the negative charges in the alginate

[69]. The clay has a high surface area so electrostatic interactions are facilitated and, in addition, hydrogen bonds can develop that help to create an ordered network [70]. Figure 34 shows the possible structure formed between montmorillonite and ammonium alginate.

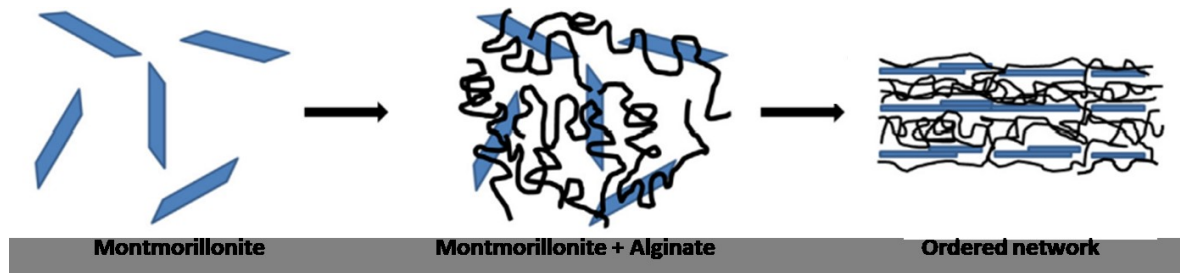
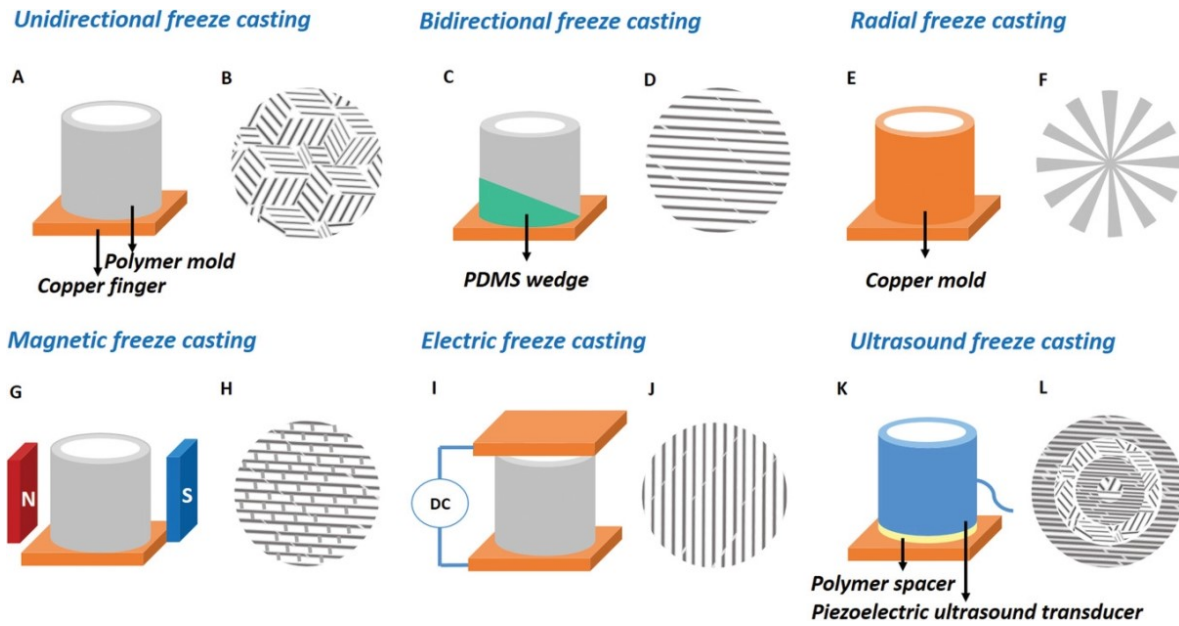


Figure 34. Possible interaction between ammonium alginate and montmorillonite.

## 2.7 Freeze-drying (lyophilization)

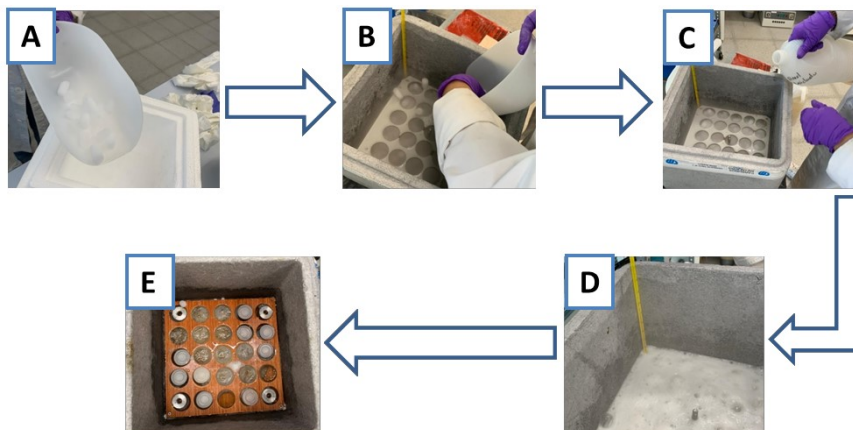
In order to obtain the final product, it was decided to use the freeze drying process because it is a technique that allows different materials to be manufactured with a high degree of porosity control. The process is also called ice-templating and is based on the physical principle of sublimation, i.e. "The direct transition of a solid to a vapour without passing through a liquid phase" [2], and is divided into two main and fundamental steps: solidification and sublimation.

The solidification process is fundamental for obtaining the desired microstructure and it varies depending on the temperature, speed and direction of growth of the solid phase. Temperature is very important because the greater the degree of sub-cooling, the faster the solidification process. There are different solidification techniques (Figure 35): Unidirectional freezing, bidirectional freezing [71], radial freezing [72] [73], radial-concentric freezing [74], freezing under flow [75], dynamic freezing [76], random freezing [77], or freeze-thawing [78]. Depending on the temperature gradients present in the process, different architectures are obtained [79] as can be seen in the following figure:



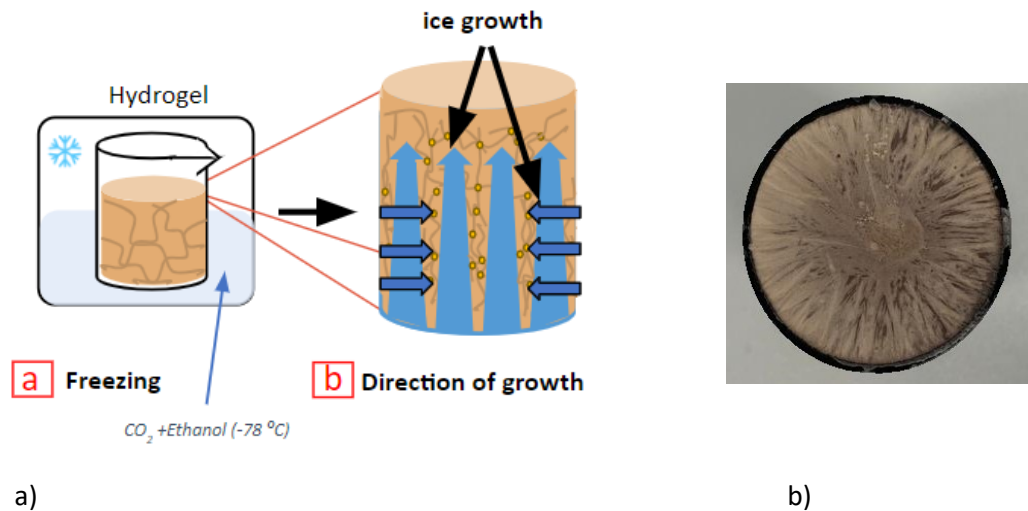
**Figure 35.** Examples of processes and microstructures [79].

In this project, after filling moulds with the products obtained from the sol-gel process, as can be seen in Figure 36, it was decided to solidify them using a cryogenic bath, i.e. “*Low temperature processes, apparatus, etc.. usually applied to systems operated at the temperature of liquid nitrogen, helium or other condensed gas which boils at a very low temperature (at atmospheric pressure)*” [2] of  $\text{CO}_2$  solid and ethanol, in this way it was possible to reach a temperature of  $-70/-80^\circ\text{C}$ , which allowed the specimens to solidify in a maximum of 30 minutes (times are dependent on size).



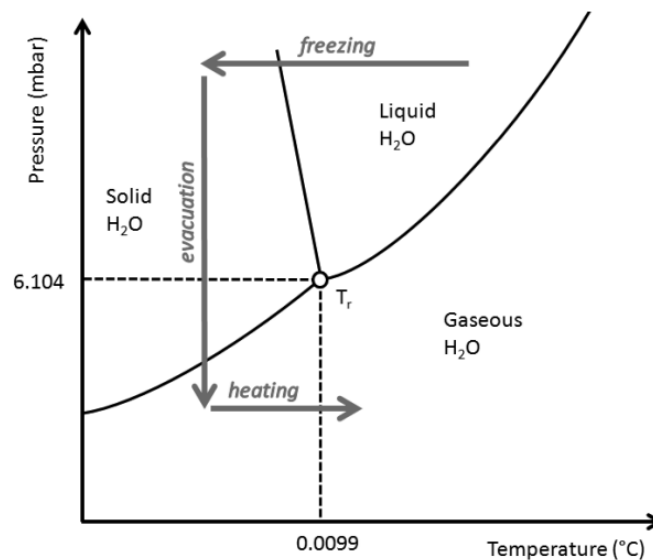
**Figure 36.** a) b) c) and d) Creation of the cooling bath in an EPS container by monitoring the temperature; e) Insertion of the specimens.

By using a cryogenic liquid, only the top surface is not in close contact with the cooling medium, so there is bidirectional solid phase growth: both radially and longitudinally from bottom to top as well as from outside to inside, as can be seen in Figure 37.

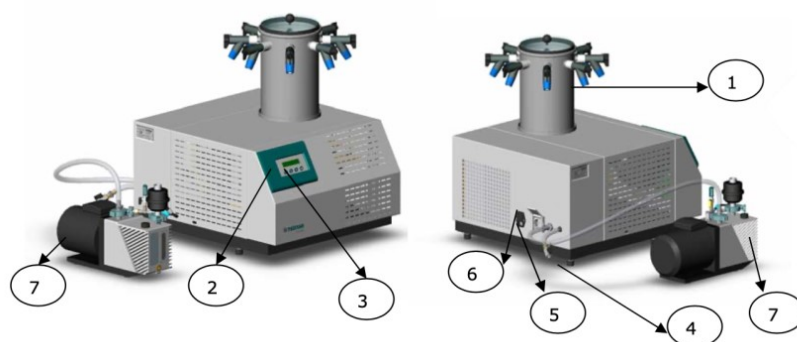


**Figure 37.** a) Direction of water solidification. b) Bottom surface of A5C5T2 after freezing.

The second step in the freeze drying process is sublimation, so in order to obtain the final product it is necessary to place it in the lyophiliser, in this project the *Telstar Cryodos* was used (Figure 39) that operated at  $-80^{\circ}\text{C}$  and 0,08 mbar. It is possible to observe in the pressure-temperature phase diagram, Figure 38, the sublimation process to which the water in the specimens is subjected.



**Figure 38.** Freeze-drying process in the water T-P phase diagram [80].



**Figure 39.** CRYODOS, Teslar® (1. - Condenser with 8 cocks 2.- LCD alphanumeric viewer 3.- Operation panel 4.- Draining pipe 5.- Electrical connection 6.- Main switch 7.- Vacuum pump) [81].

The freeze dryer operates in 2 steps:

- Primary drying: Takes place at very low temperature and pressure and lower than the triple point, in this way through the three heat exchange mechanisms (conduction, convection and radiation) it is possible to remove up to 95% of the total water, in particular all the ice crystals present in the structure are removed [82].
- Secondary drying: This takes place later at a higher temperature than primary drying and results in a product with 0.5-3% moisture content. Water molecules bound to the compound are also removed at this stage [82].

The freeze-drying process is slow and is a function of the size of the specimens; to obtain the aerogels in this paper, it was necessary to place the specimens in the lyophiliser for a week, but of all the practicable technologies for producing aerogels, it is the most eco-friendly.

## 2.8 Characterization

### 2.8.1 Intrinsic viscosity

In order to calculate the average molecular weight,  $M_w$ , of ammonium alginate, it was decided to use the Mark-Houwink-Sakurada equation [83]:

$$[\eta] = k(M_w)^a \quad (2.3)$$

Where  $[\eta]$  is the intrinsic viscosity i.e. “The limiting value of the *reduced viscosity*,  $\eta_i/c$  or the *inherent viscosity*,  $\eta_{inh}$ , at infinite dilution of the polymer, i.e.  $[\eta] = \lim_{c \rightarrow 0} \eta_i/c = \lim_{c \rightarrow 0} \eta_{inh}$ ” [2],  $k$  and  $a$  are two constants depending on the polymer used and the

conditions under which the test was carried out, i.e. temperature, instrument and solvent. The value of  $a$ , which is non-dimensional, depends on the geometry of the polymer and is between the extremes 0.5 and 2. The units of measurement of  $k$  and  $[\eta]$  are  $cm^3/g$  [83].

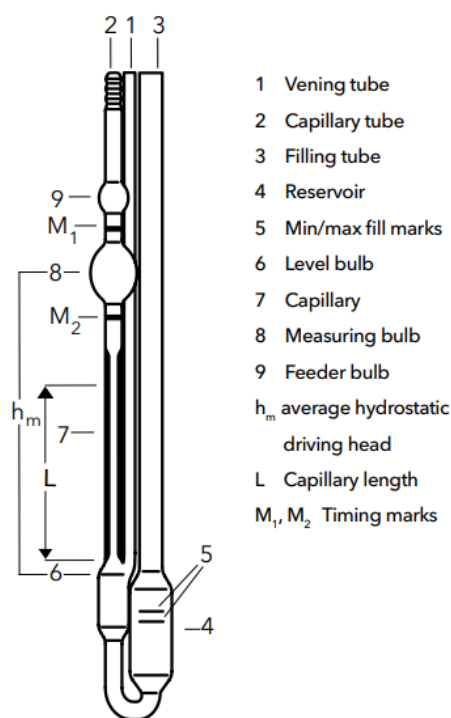
In order to be able to use (2.3), it is necessary to calculate the intrinsic viscosity experimentally. To do this, an Ubbelohde 1B viscometer from COMECTA was used: it is a capillary viscometer in which the time it takes for a solution to flow through a capillary due to the force of gravity is measured. Capillary viscometers are based on the Hagen-Poiseuille equation, which relates flow time to viscosity [84]:

$$\eta = \pi Pr^4 t / 8Ql \quad (2.4)$$

Where  $P$  is the pressure drop along the capillary which has length  $l$  and radius  $r$  from which a volume  $Q$  of liquid exits in time  $t$ .

The structure of the Ubbelohde is shown in the Figure 40a.

Given the strong dependence of intrinsic viscosity on temperature, it is necessary to perform the tests with a high degree of control over it. In fact, the viscometer was fitted with VISCOSIMETER PRECISION BATH VB-1423 manufactured by PSELECTA (Figure 40). This technology allows the viscometer to be kept perfectly vertical in a temperature-controlled water bath so that optimum test repeatability is achieved by reducing experimental errors.



a)



b)

**Figure 40.** a) *Viscosimeter Ubbhelode* [85] b) *VISCOSIMETER PRECISION BATH VB-1423, PSELECTA* [86].

In this project, the ASTM D2857 standard was followed to assess intrinsic viscosity, initially evaluating the capillary flow time of the solvent, deionised water, and then of the solutions, In particular, three solutions with different concentrations were created using a magnetic stirrer set at 600 rpm for 45 minutes, with a solute concentration: ammonium alginate of 0.025 g/dL; 0.055 g/dL; 0.09 g/dL. It is required by normative that at least 4 times are taken for each chemical species tested having a standard deviation of less than 0.02. The test temperature was set at 25°C, also monitored using a thermometer, because many tests performed on alginates have been conducted at the operating condition shown in Table 4 [83].

**Table 4.** *Solutions tested*

Concentration (g/dL)	RPM	Time (min)
0.025	600	45
0.055	600	45
0.09	600	45



As explained, it is necessary to calculate the travel time of the graduated capillary because from these values, it is possible to derive the relative viscosity ( $\eta_r$ ) and specific viscosity ( $\eta_{sp}$ ). Being very dilute solutions, the following relationships are valid [87]:

$$\eta_r = \frac{\eta}{\eta_o} \approx \frac{t}{t_o} \quad (2.5)$$

$$\eta_{sp} = \eta_r - 1 \quad (2.6)$$

Where  $\eta$  and  $t$  are the viscosity and capillary travel time of a solution and  $\eta_o$  and  $t_o$  are the viscosity and travel time of the solvent.

The inherent viscosity is a function of  $\eta_r$  [87]:

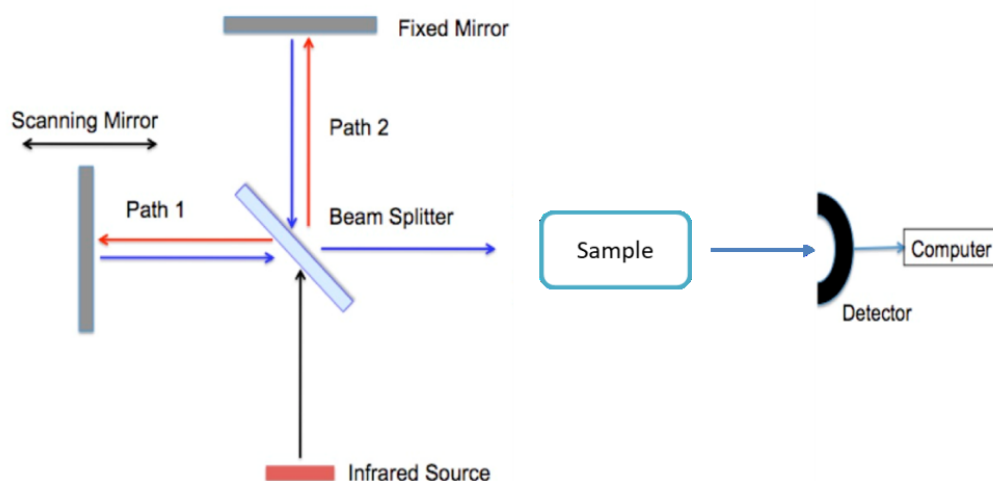
$$\eta_{inh} = \frac{\ln \eta_r}{c_i} \quad (2.7)$$

Where  $c_i$  is the concentration of the  $i$ -th solution; furthermore, the reduced viscosity is the ratio between  $\eta_{sp}$  and  $c_i$ .

When these quantities have been calculated for each composition, it is possible to obtain a graph in which reduced viscosity and inherent viscosity are a function of concentration. By interpolating the experimental points obtained, it is possible to draw two straight lines that intersect at  $c_i = 0$  therefore on the  $y$ -axis, which, by definition, is the inherent viscosity  $[\eta]$  from which the average molecular weight can be derived using (2.3).

### 2.8.2 Fourier transform infrared spectroscopy (FTIR)

The FTIR or Fourier transform infrared spectrophotometer can be used to identify the functional groups in materials. With this instrument, an emission, absorption or photoconductivity spectrum of a material can be obtained [88]. Specifically it consists of the Michelson interferometer: consisting of 3 mirrors, a beam splitter, fixed mirror and scanning mirror.



**Figure 41.** FTIR operation.

As can be seen in Figure 41, the source emits radiation which, once it reaches the beam splitter, splits to reach both the fixed and moving mirrors that reflect it. The two radiations therefore meet again in the beam splitter and, due to the different optical paths, there is both constructive and destructive interference [89]. The radiation coming out of the beam splitter passes through the sample interfering with the transmittance of the material and producing the interferogram, which thanks to an algebraic model, the Fourier transformation, is converted into a spectrum of easier interpretation.

Nicolet 6700 spectrophotometer, WI, USA was used in this project. Mode: Attenuated total reflectance (ATR), the instrument performs 30 scans with a resolution of  $1 \text{ cm}^{-1}$  and wavenumber interval:  $4000 - 400 \text{ cm}^{-1}$ .

### 2.8.3 Thermal conductivity

Thermal conductivity,  $\lambda$ , is a physical property that expresses the ability of a material to transfer heat by conduction. Knowledge of this property is crucial in determining the applicability of an industrial product in a given production sector.

Aerogels in general are excellent thermal insulators due to their very low  $\lambda$  which is linked to their structure: They are open cell foams with a very high number of pores. Thus, the high amount of cavities present in them act as a 'barrier' for heat transfer [90].

The value of  $\lambda$  in porous materials is the sum of several components:

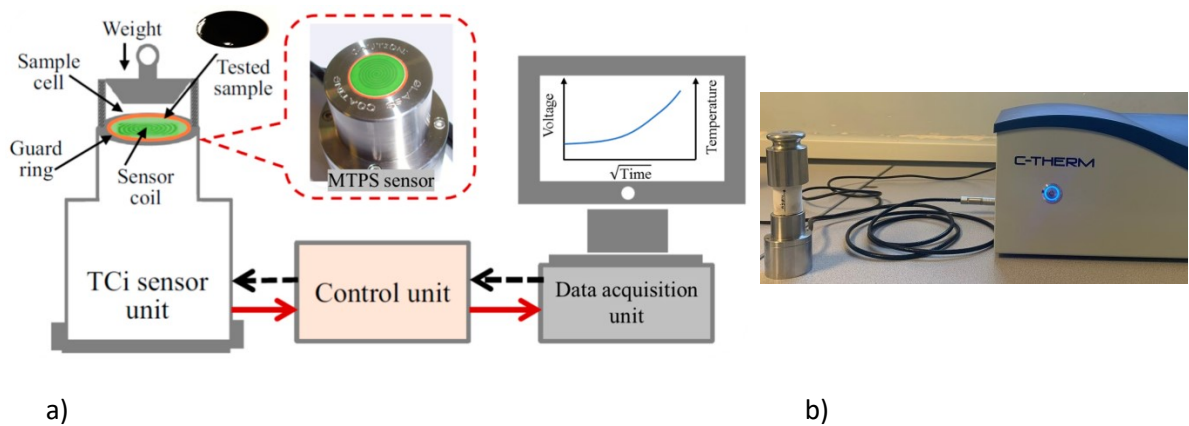
$$\lambda = \lambda_s + \lambda_g + \lambda_c + \lambda_r \quad (2.8)$$

Where  $\lambda_s$  and  $\lambda_g$  are the thermal conductivity of the solid and gas phase;  $\lambda_c$  is a term related to convection of the gas phase and, finally,  $\lambda_r$  is the contribution of radiation through the pores. [34]

In order to be able to define the thermal conductivity of the material, a TCi thermal conductivity analyser was used: This instrument operates by means of a modified transient plane source (MTPS) where a defined amount of heat is transmitted to the sample, which is placed on top of it and held in place by a weight. The heating element operates by passing electrical current through it and, by monitoring the voltage variation linked to the temperature increase at the sensor-sample interface, the instrument obtains the thermal properties of the material being analysed and, thanks to Fourier's law:

$$q = -\lambda \frac{dT}{dx} \quad (2.9)$$

The thermal conductivity is calculated [91].



**Figure 42.** a) Scheme of TCi equipment [91]. b) C-Therm TCi Thermal conductivity Analyzer which employs the Modified Transient Plane Source (MTPS).

In this project, as shown in Figure 42, the TCi Thermal conductivity Analyser which employs the Modified Transient Plane Source (MTPS) from C-Therm was used under the following conditions:

**Table 5.** Testing conditions for thermal conductivity

Radius of sensor (mm)	Power level (mW)	Test time (s)	Cooling time (s)
3.189	60	2.7	90

The test specimens used have a cylindrical shape with a diameter of 25 mm and a height of 25 mm, it is important to have flat surfaces so they were prepared using a polishing machine.

### 2.8.4 Stabilisation

Since aerogels made of alginate are hygroscopic [92] it is important to evaluate the amount of moisture absorbed by the macromolecules from the environment because it could influence the results of the mechanical tests.

This is why it is only after stabilisation that all specimens are at the same operating conditions, so that they can be mechanically tested. Once the freeze drying process was finished, the materials were dried in an oven P-SELECTA: VACIOTEM-TV [93] at a temperature of 60°C and a pressure of 70 mbar for 16 hours.

After drying, the specimens were weighed in a Shimadzu:AUW120D balance and placed in controlled atmosphere containers with a solution of Sulfuric Acid (37 ml) in  $H_2O$  (100 ml) (placed at a distance from the materials so as not to interact with them).

The amount of moisture absorbed is not constant over time, when a dry material is placed in a humid environment it initially absorbs a lot of moisture but over time this phenomenon decreases until it reaches a plateau, meaning stabilisation. For this reason, the samples were weighed every hour for the first 6 hours and thereafter measurements were taken every 24 hours. The process is shown in Figure 43.

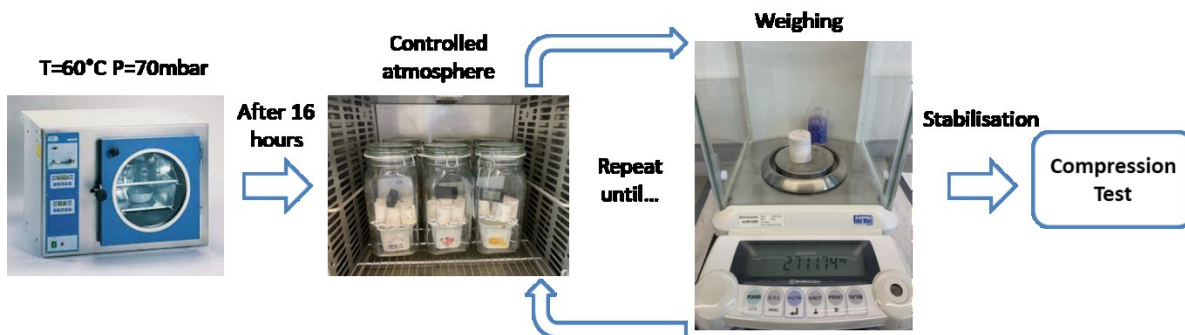


Figure 43. Stabilisation process.

To assess the amount of moisture absorbed, it was decided to use a weighted approach using the following equation (ASTM D 5229):

$$M. \% = \frac{W_i - W_o}{W_o} \cdot 100 \quad (2.10)$$

Where  $W_i$  is the wet mass,  $W_o$  is the dry mass leaving the oven and  $M. \%$  is the mass moisture content.

### 2.8.5 Density

In this project, the bulk density was calculated, which is the ratio between the mass of a material and the external volume including pores and defects [94]:

$$\rho_{bulk} = \frac{\text{Total mass}}{\text{Apparent volume including solids and internal pores}} \quad (2.11)$$

In order to determinate the values of this quantity, samples were used at the end of stabilisation by evaluating their mass and apparent volume using a balance and a calibre. For each composition, the bulk density of 3 specimens was determined: the volume of each was calculated by referring to the perfect cylindrical geometry by measuring three heights and three diameters and averaging them.

### 2.8.6 Compressive strength

Before explaining the specifications of a compression test and the machinery used, it is important to define how the preparation of the samples was carried out.

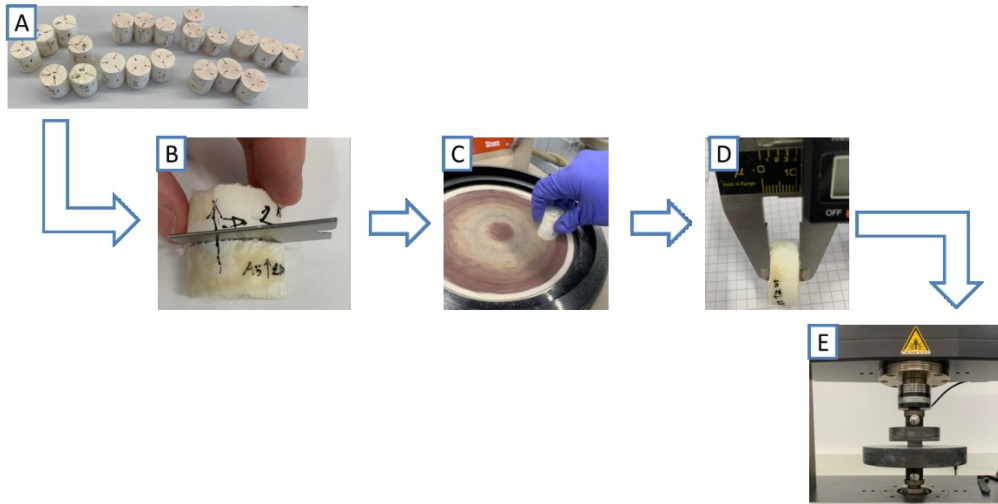
According to ISO 604, the following relationship must be fulfilled:

$$\varepsilon_c^* \leq 0.4 \frac{x^2}{l^2} \quad (2.12)$$

Where  $\varepsilon_c^*$  is the maximum nominal deformation of the compression test,  $x$  is the diameter in the case of a cylindrical specimen and  $l$  is the height.

In this design, it was desired to see the mechanical behaviour of the materials up to a nominal deformation percentage of 50 per cent of the initial height. In addition, the circular sample surfaces must be as flat and parallel as possible. For these reasons, as can be seen in Figure 44, the specimens that finished the stabilisation cycle were first cut and then levelled using a DAP-7 polishing machine, Struers at 125 rpm.

Finally, the diameters and heights were evaluated in order to verify (2.12) and to be able to insert the data into the software of the compression test.



**Figure 44.** A) Stabilised samples B) Cutting of samples C) Surface finish D) Measurement E) Compression Test.

In compression machines, the strain rate, maximum nominal strain and preload have to be defined. Using sensors, such as dynamometers, the instrument is able to evaluate the applied force so that the stress-strain diagram can be viewed on the computer.

The engineering stress  $\sigma$  is defined as the ratio between the instantaneous force applied and the initial area of the specimen, which is why it is important to have flat surfaces in order to transmit the force uniformly over them. One has to be careful about the phenomenon of barreling which consists of heterogeneous deformation [95], precisely to avoid this, it is important to respect (2.12).

Porous solids, including aerogels, exhibit a compressive stress-strain curve in which 3 zones can be recognised [96]:

- Linear elastic region: In which there is recoverable strain associated with bending edges in open cell structures, in this zone the Young's modulus can be derived from the slope of the stress-strain curve
- Constant region: In which the structure is collapsing, the angular coefficient, therefore, changes in comparison to the first region and by evaluating the intersection of two straight lines tangent to the first and second regions, it is possible to derive the yield stress
- Densification region: In the last zone, the stress increases again because the walls of the cavities initially present in the material touch, which increases the force required to deform the specimen.

The machine used in this project was ZwickRoell 10 kN RetroLine (Figure 45) and the parameters set before the test were performed are shown in Table 6.

**Table 6.** *Set parameters*

Preload (N)	Crosshead rate (mm/min)	$\epsilon_c^*$ (mm/mm)
0.5	1	0.5

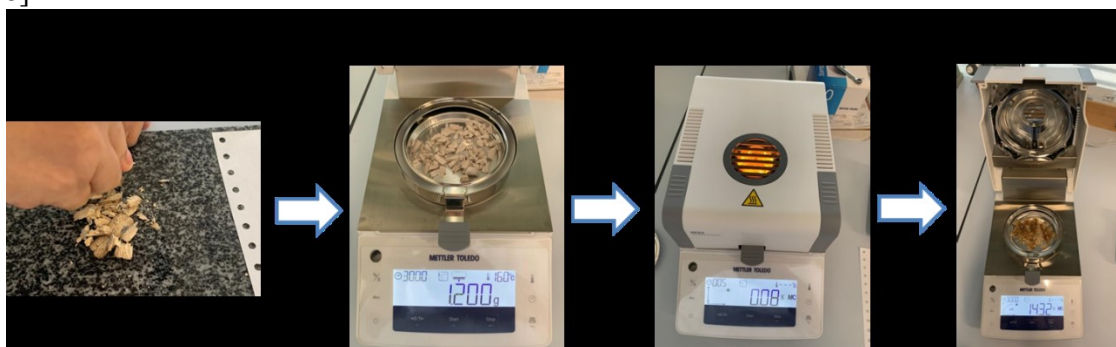
**Figure 45.** *ZwickRoell 10 kN RetroLine [97].*

### 2.8.7 Moisture content

As explained in § 2.8.4, alginate-based aerogels due to their hygroscopicity and high porosity absorb water present in the atmosphere [92]. It is important to know the percentage of moisture absorbed in detail as it influences material properties including mechanical properties.

Precisely for this reason, the specimens, after being mechanically tested, were cut and placed in the Moisture Analyzer HE53, By Mettler Toledo Greifensee, Switzerland at a temperature of 160°C for 30 minutes.

The operating principle of this instrument is based on the LOD or "loss on drying" in fact it is a precision balance that measures the initial weight of the moist material and then increases the temperature and monitors the change in weight because the moisture is evaporating. Finally, as can be seen in Figure 46, when all the water is removed, from the difference of the final and initial weights it is able to define the initial moisture percentage [98].

**Figure 46.** *Steps to evaluate moisture content.*

### 2.8.8 Thermogravimetric analysis (TGA)

To evaluate the thermal properties of a polymer compound, there are various techniques: DSC, TGA, DMA, and TMA.

In this project, thermogravimetric analysis (TGA) was used, this machine makes it possible to evaluate the weight variation of a material as the temperature increases in a controlled atmosphere, in this way it is possible to detect the thermal degradation of the components of a material because different chemical species have different thermal stabilities [99].

The machinery is a thermobalance consisting of an analytical balance capable of evaluating weight variations, a sample crucible, a furnace that gradually increases the temperature, a gas flushing system and a computer capable of analysing the data obtained in the test [100]. To perform the test it is necessary to choose the crucible, which can be, for example, aluminium (if  $T_{\max}=600^{\circ}\text{C}$ ) or alumina for higher temperatures. After calibrating the instrument with the weight of the crucible, setting the maximum temperature, the heating rate rise and the type of inert gas, a defined quantity of material is inserted into the crucible, which is then fed into the TGA and the test is performed.

In this project, the test was performed TGA/DSC 1 instrument (Mettler Toledo, Columbus, Ohio) shown in Figure 47 and under the conditions shown in Table 7.

**Table 7.** Test execution parameters

Type of crucible	Heating rate ( $^{\circ}\text{C}/\text{min}$ )	Temperature range ( $^{\circ}\text{C}$ )	Atmosphere	Sample weight (mg)
Alumina 100 $\mu\text{l}$	10	30-600	$\text{N}_2$	~8



**Figure 47.** TGA Mettler Toledo, Columbus, Ohio.

Two fundamental graphs are obtained from the TGA in order to be able to analyse the thermal stability of materials, namely: mass loss as a function of temperature and derivate mass loss as a function of temperature. From which it is possible to obtain:



- $T_{d5\%}$ : The onset decomposition temperature is a parameter indicating the temperature at which there is a 5% decrease in mass [68].
- $T_{dmax}$ : The maximum degradation temperature, i.e. the temperature at which the maximum peak is present in the graph of the weight derivative corresponding to the inflection point of the primitive function.
- $dW/dT_{dmax}$ : The degradation rate at  $T_{dmax}$
- Residue: Expressed in % represents the ratio between the final mass and the initial mass

### 2.8.9 Cone calorimetry

As explained in § 1.7, there are various tests that can be performed on materials to assess their fire behaviour.

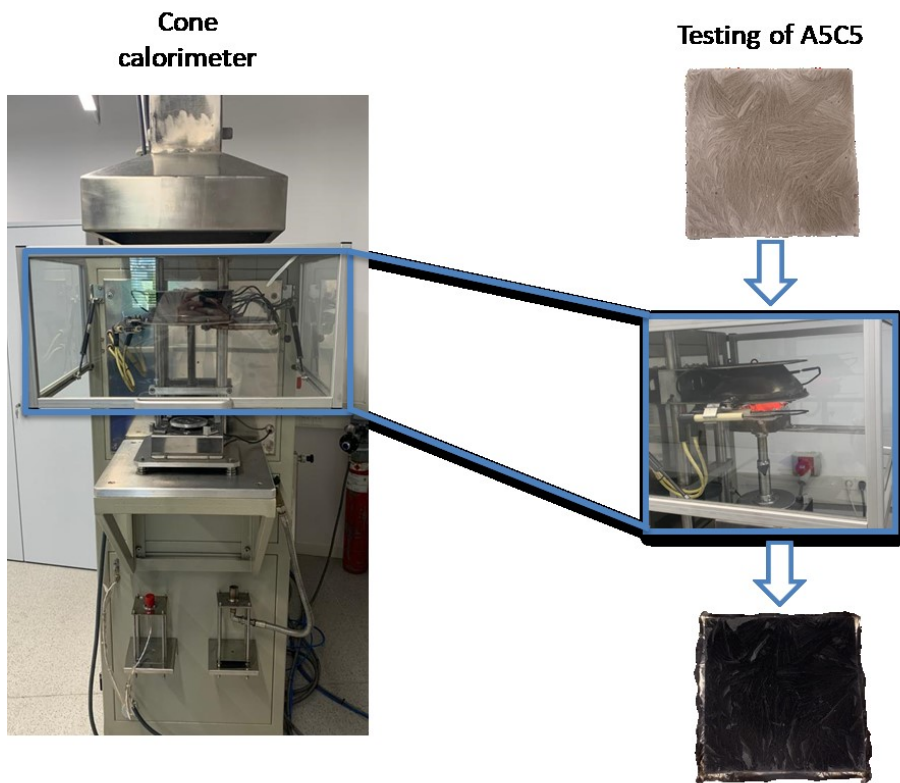
In this project, the calorimetric cone is used: A machine that burns rectangular samples and through an aspiration hood the fumes ( $CO$ ,  $CO_2$ ,  $O_2$ ) produced by the material are evaluated, from which it is possible to derive many important parameters such as [101]:

- The residue % expressed as the ratio of the residue (i.e. the amount of material present after the test) to the initial mass
- TTI: Time to ignition i.e. the time for the first flame to appear in the specimen
- PHRR: Peak heat release rate, in this project the first peak obtained was taken in each graph where it is represented the mass loss in function of temperature
- TTPHRR: Time to peak heat release rate
- THR: Total heat release i.e. the integral of HRR as a function of time so this is the area subtended by the curves in the graph where it is represented the mass loss as a function of temperature
- $THR_{eff}$ : Expressed as the ratio of THR to initial mass
- FIGRA: Fire growth rate index or the ratio of  $PHRR(t)$  to TTPHRR

The cone calorimeter that was used is the Ineltec BECC model, Tona, Spain (Figure 48); with a heat flux index of  $50 \text{ kW/m}^2$  and the ISO 5660 standard was followed.

The squared specimens used have dimensions  $100 \text{ mm} \times 100 \text{ mm} \times \sim 10 \text{ mm}$ , they were weighed and inserted into Aluminium substrates, so it was possible to evaluate the amount of residue left at the end of the process.

Three stages can be witnessed during the test: Ignition at a temperature between 600-700 K, Developing fire in which the temperature increases to 900k and finally Fully developed fire at a temperature above 900k [101].



**Figure 48.** Cone calorimeter test on A5C5 sample.

# CHAPTER 3: RESULTS

## 3.1 Intrinsic viscosity

As explained in § 2.8.1, to calculate the intrinsic viscosity, ASTM D2857 was followed by first evaluating the travel time through the capillary of the solvent, i.e. deionised water (Table 8) and then the solutions containing ammonium alginate. It is important to remember that at least four times with a standard deviation of less than 0.02 must be taken. The times obtained from the test, at a temperature of 25°C, are shown in Table 9.

**Table 8.** *Capillary travel times from solvent*

Solvent	t1	t2	t3	t4	tavg	St.Deviation
	(s)	(s)	(s)	(s)	(s)	(s)
Deionised water	18.81	18.82	18.81	18.81	18.813	0.005

**Table 9.** *Capillary travel times from solutions*

Conc.of solute (g/dL)	t1	t2	t3	t4	tavg	St.Deviation
	(s)	(s)	(s)	(s)	(s)	(s)
0.025	39.41	39.41	39.41	39.44	39.418	0.015
0.055	83.78	83.81	83.82	83.81	83.805	0.0173
0.09	150.88	150.91	150.91	150.88	150.90	0.0173

From these values, it is possible to derive the relative viscosity ( $\eta_r$ ), specific viscosity ( $\eta_{sp}$ ), inherent viscosity ( $\eta_{inh}$ ) and the reduced viscosity. Table 10 shows the calculated viscosity values.

**Table 10.** *Relative viscosity, specific viscosity, reduced viscosity, inherent viscosity*

Conc. of solute (g/dL)	$\eta_r$	$\eta_{sp}$	$\eta_{sp} / c_i$ (dL/g)	$\eta_{inh}$ (dL/g)
0.025	2.095282	1.095282	43.8113	29.58753
0.055	4.454751	3.454751	62.81365	27.16311
0.09	8.020997	7.020997	78.01107	23.13403

Following the definition of inherent viscosity defined in § 2.8.1, it is possible to derive the value from the Figure 49.

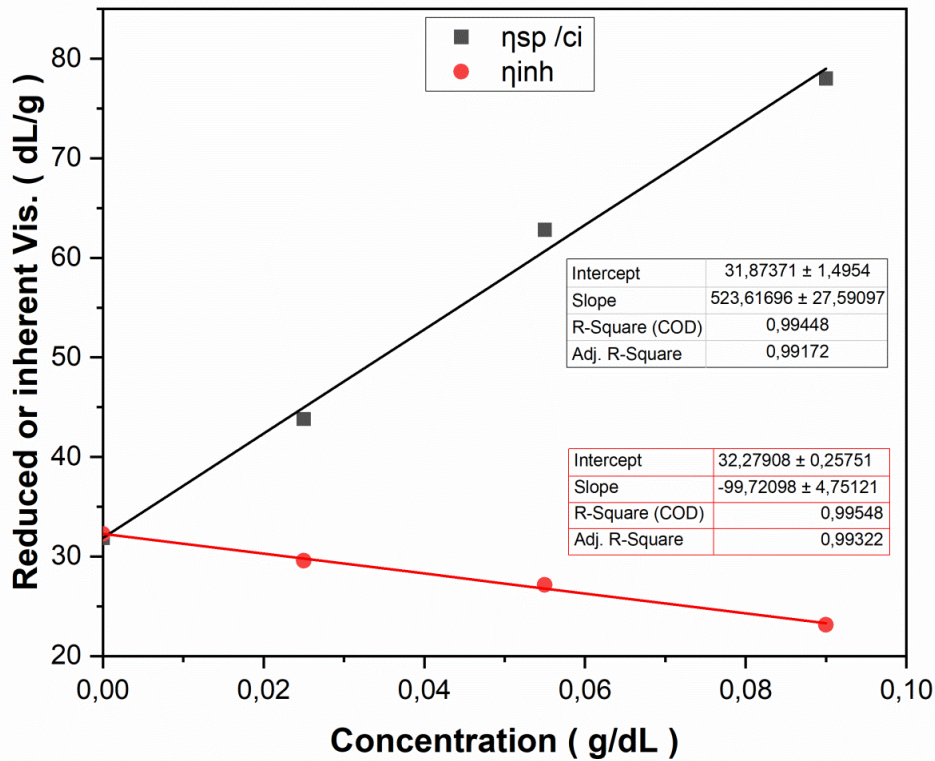


Figure 49. Reduced and inherent viscosity of ammonium alginate solutions.

The two lines interpolating the experimental data have equations:

$$\frac{\eta_{sp}}{c_i}: y = 523.61696 \cdot x + 31.87371 \quad (3.1)$$

$$\eta_{inh}: y = -99.72098 \cdot x + 32.27908 \quad (3.2)$$

Both have a very high R-Square value indicating their high accuracy.

The value of  $[\eta]$  can be calculated from the average between the ordinates at the origin of the two straight lines thus:

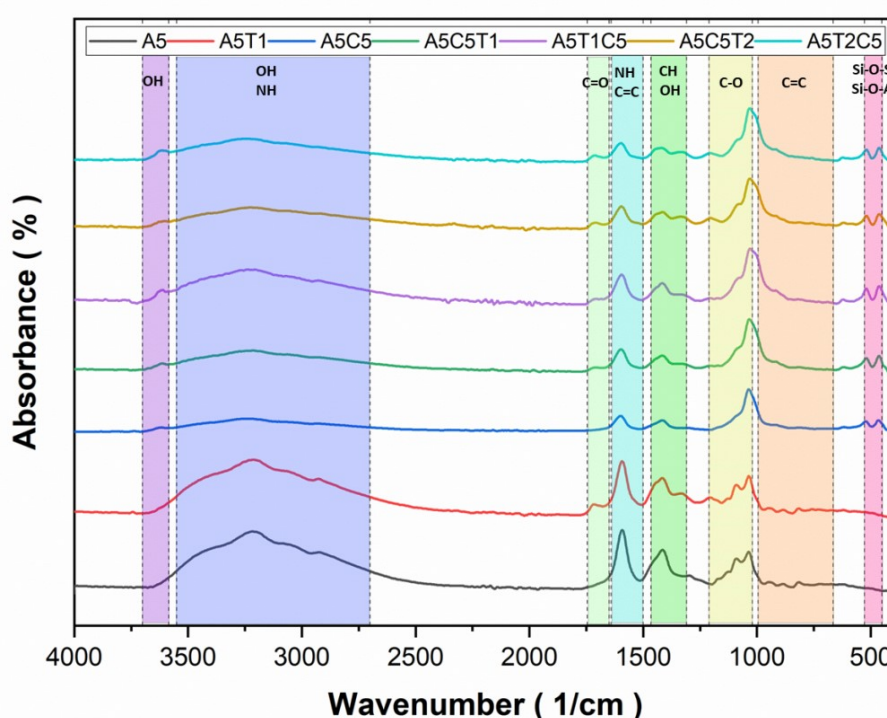
$$[\eta] = 32.076395 \frac{dL}{g} = 3207.6395 \text{ cm}^3/g \quad (3.3)$$

With this value, the average molecular weight,  $M_w$ , can be derived by following the Mark-Houwink-Sakurada equation. To the best of author's knowledge, there are no scientific articles in the literature in which the  $M_w$  of ammonium alginate is calculated, so the values of the constants  $k$  and  $a$  of sodium alginate were taken from Masuelli's work [83]:  $k =$

$0.0123\text{cm}^3/\text{g}$  and  $a = 0.960$  from which an average molecular weight is derived:  $M_w = 438489\text{ g/mol}$ . This value is not comparable, both because no studies on the intrinsic viscosity of ammonium alginate have been carried out so far and because it is strongly source-dependent.

### 3.2 FTIR

In order to be able to analyse the functional groups present in the different compositions, FTIR was used to study the spectrum with absorption as the ordinate and wave number as the abscissa (Figure 50).



**Figure 50.** Absorption spectrum obtained with FTIR.

As can be seen from the graph, the ranges of the functional groups have been entered using various tables [102][103][104] the different materials are now analysed in detail:

- A5: By studying the peaks in the spectrum, it is possible to verify the presence of the characteristic functional groups of ammonium alginate: -OH, -NH, C=C, -CH, C-O.
- A5T1: The spectrum is very similar to A5 but, compared with it, a shift of the peak in the range 3550-2700  $1/\text{cm}$  can be seen where the intermolecular bonded OH are located [102]. The maximum shifts from 3217.1 to 3210.6  $1/\text{cm}$  indicate an increase in hydrogen bonds which is consistent since tannic acid binds to ammonium alginate

thanks to these dipole-dipole interactions. A very similar deviation was observed in a study in which an ammonium alginate aerogels additivated with phytic acid was characterised [68].

- A5C5: Compared to the two above-mentioned materials, significant differences in the absorption spectrum can be noted: The presence of an additional peak at 3616.8 1/cm, this value is in the OH free range: 3700-3584 1/cm, deriving from the presence of silane groups (SiOH) in montmorillonite [105]. Two new peaks are also observed at the end of the spectrum (522.1 1/cm and 466.4 1/cm) and, also in this case, they are characteristic of clay, namely the Si-O-Al and Si-O-Si bonds [106].
- A5C5T1, A5T1C5, A5C5T2, A5T2C5: As well as in A5C5, the characteristic peaks of montmorillonite indicate the presence of silane groups, Si-O-Al and Si-O-Si. But the effect of the addition of tannic acid is substantial in that the hydrogen bonds increase: this can be observed by the deviation of the peaks in the range of the intermolecular bonded OH compared to that of A5C5 at position 3257 1/cm. In particular, in A5C5T1 and A5T1C5 it shifts to 3215.1 and 3239.1 1/cm respectively, whereas in A5C5T2 and A5T2C5 it shifts to 3227.3 and 3243.2 1/cm. From these values, it can be seen that if the tannic acid is inserted after the montmorillonite during preparation, the peaks shift to lower wavenumbers, which indicates an increase in the dipole-dipole bonds present in the material.

OMNIC<sup>TM</sup> software was used to analyse the peaks reported in Table 11.

**Table 11.** Detected peaks

Range	A5	A5T1	A5C5	A5C5T1	A5T1C5	A5C5T2	A5T2C5	Assignment	Ref.
3700-3584			3616.8	3614.2	3612.3	3603.4	3614.3	OH stretching free	[102]
3550-2700	3217.1	3210.6	3257	3215.1	3239.1	3227.3	3243.2	OH stretching intermolecular bonded NH stretching	[102]
1745-1650		1714		1709		1707.2	1711	C=O stretching	[102]
1640-1500	1592.2	1592.4	1599.1	1597.2	1594.8	1595.7	1598	NH deformation C=C vibration	[103]
1465-1310	1414.9	1416.8	1415.7	1416.3	1416.5	1415.4	1420.8	CH bending OH bending	[102]
1210-1020	1089.8 1036.3	1090.2 1035.9	1036.2	1033.7	1030.9	1031.4	1032.3	C-O stretching	[102] [104]
995-665	816.8	816.7						C=C bending	[102]
527-450			522.1 466.4	519.5 463.6	519.4 462.8	518.8 462.5	518.7 463.7	Si-O-Si Si-O-Al	[106]

### 3.3 Thermal conductivity

The thermal conductivity values,  $\lambda$ , calculated using the TCi Thermal conductivity Analyzer are shown in Table 12. It can be seen that the standard deviation is present because each specimen was tested twice in order to obtain a more accurate average value.

**Table 12.** Thermal conductivities detected

Sample	$\lambda$ (W/m·K)	St.Dev (W/m·K)
A5	0.038	0.001
A5T1	0.038	0.002
A5C5	0.043	0.002
A5C5T1	0.044	0.001
A5T1C5	0.043	0.002
A5C5T2	0.044	0.001
A5T2C5	0.044	0.001

It can be seen that the addition of tannic acid, in the quantities used, does not affect this property, as both A5 and A5T1 exhibit a thermal conductivity of  $0.038 \text{ W/ m}\cdot\text{K}$ . Furthermore, A5C5T1 A5T1C5 A5C5T2 and A5T2C5 also exhibit the same  $\lambda$  considering the standard deviation.

Montmorillonite, on the other hand, influences this property because it has a higher thermal conductivity than ammonium alginate and, in addition, the presence of it increases the amount of solid present in the aerogel. In particular, the presence of montmorillonite, at the concentrations studied, caused an increase in  $\lambda$  of 13.64% with respect to A5.

The thermal conductivity value obtained by the aerogel consisting of ammonium alginate alone is practically the same as Cao et al. reported [68], i.e.  $\lambda = 0.036 \text{ W/ m}\cdot\text{K}$ .

### 3.4 Stabilisation

Before testing the samples mechanically, they were stabilised to match the operating conditions of the specimens with the same composition. As explained in § 2.8.4, the percentage moisture absorption was calculated by referring to the weight at different times until the plateau was reached.

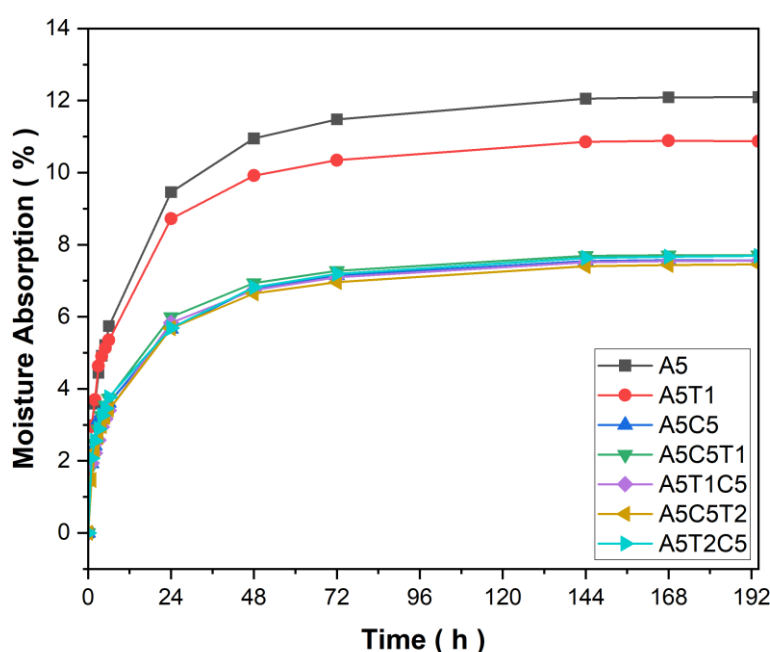


Figure 51. Moisture adsorption (%).

Graphically, in Figure 51, it can be observed that stabilisation already takes place after 144 hours. The specimens with only ammonium alginate and those with also tannic acid



increased their weight more: In fact, the percentage of absorbed moisture was about 12% and 11%, respectively. On the other hand, the presence of montmorillonite decreases the amount of moisture absorbed; in fact, independently of the amount of tannic acid, the M.% value was approximately 7%.

### 3.5 Density

As explained in § 2.8.5 in this project, the bulk density was calculated. To obtain the density values for each composition, the volumes were calculated and the masses weighed as shown in Table 13.

**Table 13.** Measurements taken to calculate bulk density

Aerogel	Samples	Weight	Apparent volume	Bulk density	Average bulk density	St.Dev
Composition	Number	(g)	(cm <sup>3</sup> )	(g/cm <sup>3</sup> )	(g/cm <sup>3</sup> )	(g/cm <sup>3</sup> )
A5	A5_1	1.1596	19.8790	0.0583	0.0591	0.0010
	A5_2	1.1108	18.4415	0.0602		
	A5_3	1.1321	19.2962	0.0587		
A5T1	A5T1_1	1.4345	20.9757	0.0684	0.0707	0.0021
	A5T1_2	1.2399	17.1100	0.0725		
	A5T1_3	1.2784	17.9719	0.0711		
A5C5	A5C5_1	2.2350	22.4144	0.0997	0.1004	0.0015
	A5C5_2	2.0775	20.9006	0.0994		
	A5C5_3	2.1196	20.7658	0.1021		
A5C5T1	A5C5T1_1	2.4626	21.5159	0.1145	0.1149	0.0008
	A5C5T1_2	2.1292	18.6103	0.1144		
	A5C5T1_3	2.4132	20.8403	0.1158		
A5T1C5	A5T1C5_1	2.4915	22.0819	0.1128	0.1123	0.0005
	A5T1C5_2	2.6379	23.5625	0.1120		
	A5T1C5_3	2.7111	24.1979	0.1120		
A5C5T2	A5C5T2_1	2.6150	22.0169	0.1188	0.1202	0.0022
	A5C5T2_2	2.6069	21.8819	0.1191		
	A5C5T2_3	2.5254	20.5652	0.1228		
A5T2C5	A5T2C5_1	2.8416	22.5484	0.1260	0.1261	0.0001
	A5T2C5_2	2.6648	21.1409	0.1260		
	A5T2C5_3	2.7246	21.6042	0.1261		

It can be seen from Table 13 that the addition of both tannic acid and montmorillonite cause an increase in bulk density because it increases the amount of solid phase in aerogels.

### 3.6 Compressive strength

The compressive mechanical behaviour of porous materials, as explained in § 2.8.6, can be divided into three zones: At the beginning the linear elastic range, then there is a more or less constant zone, and finally there is a rapid rise associated with densification [96].

In Figure 52 and Figure 53, it can be seen that clay-containing aerogels exhibit precisely this behaviour.

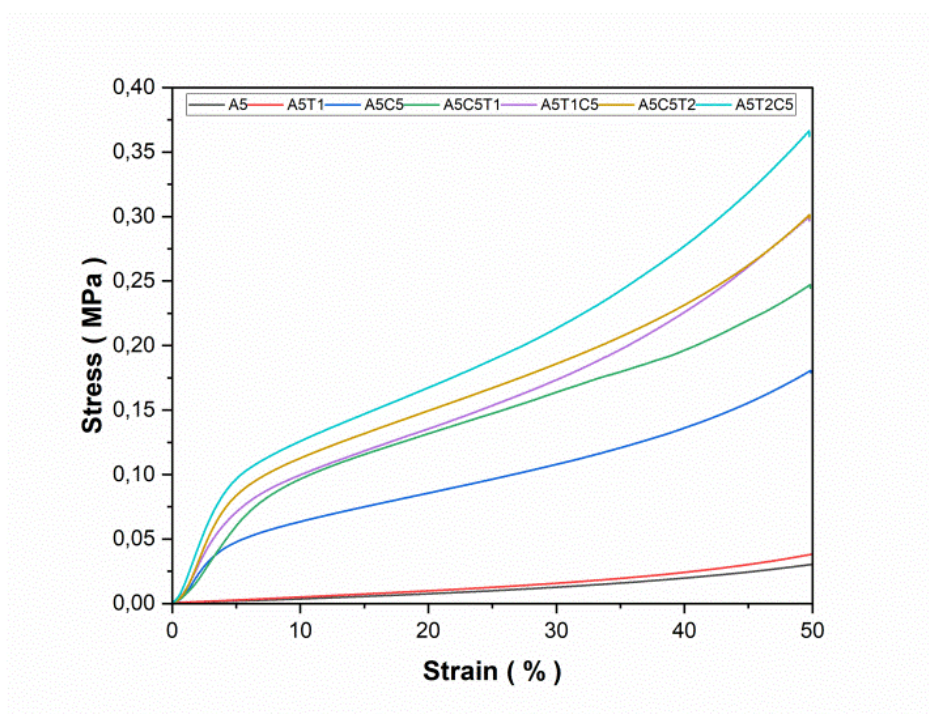


Figure 52. Stress-strain curves.

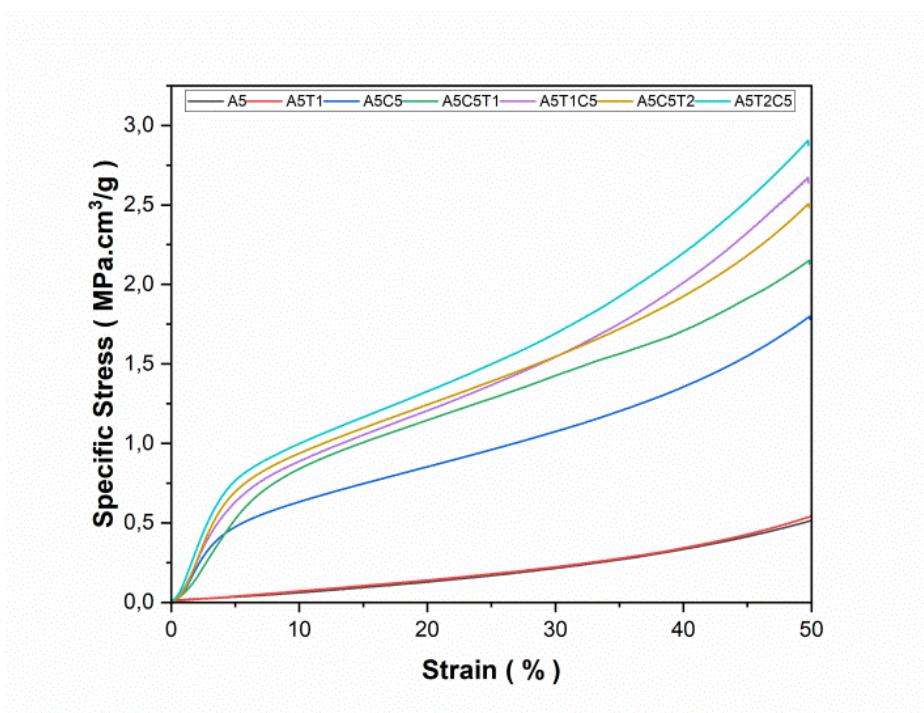


Figure 53. Specific stress-strain curves.

Young's modulus,  $E$ , was calculated by evaluating the slope of the curves in the linear elastic zone. However, it can be seen that the curves, for very low deformations, have an initial plateau related to the imperfect parallelism between the upper and lower surfaces of the samples, the calculation of  $E$  was made immediately after the initial plateau by evaluating its position for each curve.

Yield strength, on the other hand, was determined by evaluating the intersection between two straight lines: the first in the linear elastic zone, the second where the curve presents a variation in slope.

The results are shown in Table 14: Young's modulus, yield stress, specific Young's modulus and specific yield stress. It can be seen that both tannic acid and montmorillonite affect the mechanical properties, in particular the combined use of them significantly increased  $E$  and  $E_{\text{spec}}$ . Test sample A5T1 presented a Young's modulus twice as high as A5 but, the presence of montmorillonite is crucial, in fact A5C5 presents higher properties ( $E = 0.96$  MPa) than aerogels made of alginate alone ( $E = 0.03$  MPa).

The specimens containing both additives showed higher  $E$  and  $\sigma_y$ , in particular, it can be seen that as the amount of tannic acid increased, with the same amount of montmorillonite, both the slope of the line and the yield stress increased. In addition, the "step change" during preparation can also modulate the mechanical properties with the same amount of montmorillonite and tannic acid: A5T1C5 and A5T2C5 specimens exhibited better specific

properties,  $E$  and  $\sigma_y$ , than A5C5T1 and A5C5T2, respectively. This variation may be related to a different dispersion during the preparation stage, i.e.: in A5T1C5 and A5T2C5, the tannic acid was added before the montmorillonite, decreasing the viscosity and thus facilitating the dispersion of the clay, vice versa in A5C5T1 and A5C5T2, mixing the montmorillonite with the ammonium alginate first created a much more viscous mixture and thus the dispersion of the clay was more difficult.

**Table 14.** *Calculated mechanical properties*

<b>Composition</b>	<b>E (MPa)</b>	<b><math>\sigma_y</math> (Mpa)</b>	<b><math>E_{spec}</math> (MPa cm<sup>3</sup>/g)</b>	<b><math>\sigma_{yspec}</math> (MPa cm<sup>3</sup>/g)</b>
<b>A5</b>	0.03 ± 0.01	-	0.52 ± 0.12	-
<b>A5T1</b>	0.06 ± 0.04	-	0.84 ± 0.56	-
<b>A5C5</b>	0.96 ± 0.21	0.045 ± 0.004	9.53 ± 2.09	0.45 ± 0.04
<b>A5C5T1</b>	1.37 ± 0.45	0.089 ± 0.018	11.88 ± 3.94	0.77 ± 0.16
<b>A5T1C5</b>	1.58 ± 0.50	0.092 ± 0.002	14.08 ± 4.45	0.81 ± 0.02
<b>A5C5T2</b>	1.70 ± 0.60	0.095 ± 0.001	14.12 ± 4.70	0.79 ± 0.01
<b>A5T2C5</b>	1.99 ± 0.50	0.110 ± 0.010	15.79 ± 4.03	0.87 ± 0.07

The values obtained can be compared with those reported by Chen et al. [25] in which A5 had a Young's modulus of  $0.99 \pm 0.06$  MPa and A5C5 an  $E$  of  $5.8 \pm 0.7$  MPa. It can be seen that there is a significant difference, but this is related to the anisotropic structure:

- In this project, specimens with a predominantly radial direction of growth are tested, as can be seen in Figure 54. Therefore, the mechanical tests were carried out in the direction orthogonal to them, which means that the mechanical properties were evaluated in the weaker direction.
- Conversely, Chen et al. reported [25] the mechanical properties evaluated in parallel to the direction of ice-growth, thus along the stronger direction.

Figure 54 shows the two different microstructures:

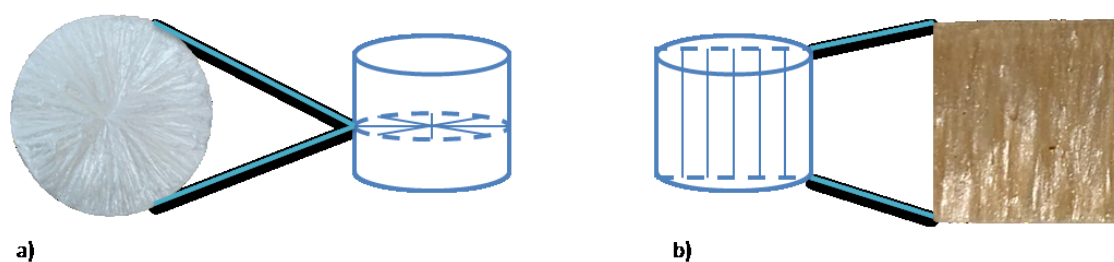


Figure 54. a) Microstructure in this project b) Microstructure in the article [25].

### 3.7 Moisture content

The values in Table 15 were obtained using Moisture Analyzer HE53, in which the change in weight with increasing temperature is evaluated.

Table 15. Humidity values in aerogels

Composition	Initial Weight (g)	Humidity (%)
A5	0.570	21.0
A5T1	0.725	22.1
A5C5	0.998	13.8
A5C5T1	1.278	14.1
A5T1C5	1.200	14.2
A5C5T2	1.238	13.9
A5T2C5	1.369	14.3

Based on the percentage values obtained, it can be seen that aerogels: A5T1 and A5 absorb more than those containing montmorillonite because ammonium alginate is hygroscopic [92] whereas tannic acid has no significant influence on humidity as A5C5T1, A5T1C5, A5C5T2 and A5T2C5 also have similar moisture content values.

Montmorillonite, on the other hand, has a high impact; in fact, compared to A5, which has a humidity content of 21.1%, A5C5 has a moisture content of 13.8%. This improvement could be related both to the barrier effect of the silica layers present in the montmorillonite and because the path of water molecules in the air inside the aerogels is hindered by the microstructure [107].

### 3.8 TGA

TGA was used to analyse the thermal stability of the aerogels produced: Figure 55 and Figure 56 show the characteristic curves obtained. The corresponding relevant values,  $T_{d5\%}$ ,  $T_{dmax}$ ,  $dW/dT_{dmax}$  and Residue, described in § 2.8.8 are shown in Table 16.

**Table 16.** Data obtained from analysis of TGA graphs

Composition	$T_{d5\%}$ (°C)	$T_{dmax}$ (°C)	$dW/dT_{dmax}$ (%/°C)	Residue (%)
A5	71.98	200.0	0.72	27.7
A5T1	95.88	222.0	0.75	32.4
A5C5	188.22	209.3	0.42	59.6
A5C5T1	100.6	210.7	0.37	58.8
A5T1C5	83.97	209.3	0.36	57.6
A5C5T2	109.12	224.0	0.36	57.1
A5T2C5	107.87	222.7	0.35	57.8

Ammonium alginate, as discussed in § 2.8.7, being strongly hydrophilic and hygroscopic absorbs a lot of water. As can be seen in the first weight loss, related to the desorption of water and volatile compounds, the amount of water was higher than in aerogels containing montmorillonite.

The effect of tannic acid can be observed in Table 16 by comparing A5 and A5T1: The rate of degradation does not change as the values of  $dW/dT_{dmax}$  were similar, however the temperature required for degradation increased as both  $T_{d5\%}$  and  $T_{dmax}$  increased from 71.98°C to 95.88°C and 200.0°C to 222.0°C respectively, the amount of residue also increased.

Montmorillonite, on the other hand, improved the following characteristics: Being an inorganic and ceramic material, it is very resistant to the test conditions (30-600°C). A high increase in the residue was noted, which increased from 27.7% (A5) to 59.6% (A5C5). In addition,  $dW/dT_{dmax}$  also dropped considerably as compared to A5, as can be seen in Figure 56. A5C5 caused a decrease of 41.7% because the silicates delay the propagation and decomposition of the organic components by acting as a protective barrier [25].

The aerogels tested that present the best characteristics are those containing both additives. The curves of A5C5T1, A5T1C5, A5C5T2 and A5T2C5 in Figure 56 are also lower than those of A5C5.  $dW/dT_{dmax}$  decreased from 0.42 %/°C to values below 0.37 %/°C which was related to the better thermal protection obtained in the aerogels. Again, the effect of tannic acid is to delay degradation. Increasing the amount of it, for the same amount of

ammonium alginate and montmorillonite, resulted in an increase of  $T_{dmax}$ . Finally, the residue was practically identical to that of A5C5 since it is a function of the amount of inorganic material in the mixture. The graphs obtained and the magnitudes studied of A5 and A5C5 were consistent with those reported by Chen et al. [25].

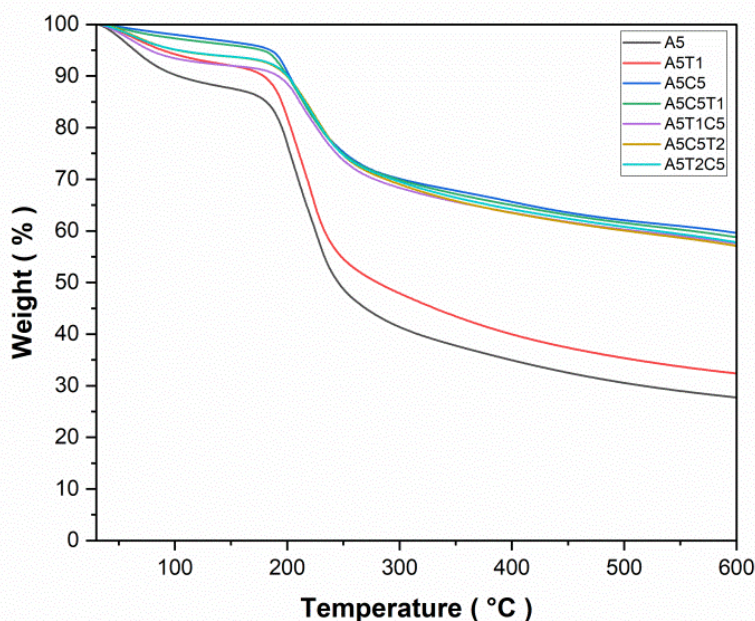


Figure 55. Mass loss as a function of temperature.

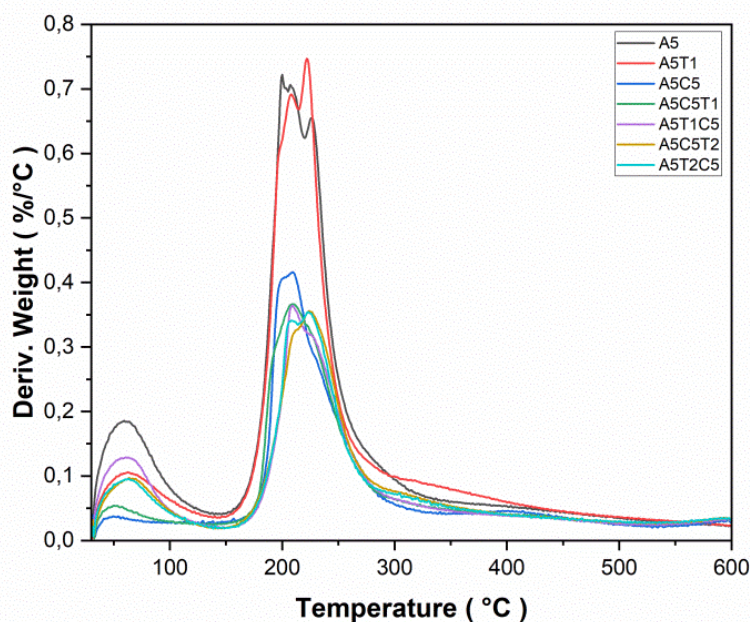


Figure 56. Derivate mass loss of aerogels as a function of temperature.

### 3.9 Cone calorimetry

The fire behaviour of the samples was tested using the calorimetric cone. Table 17 shows the quantities defined in § 2.8.9, obtained:

- The initial mass of the test specimen measured with the balance
- The mass of the residue, i.e. the amount of material present after the test
- The residue %
- TTI: Time to ignition
- PHRR: Peak heat release rate
- TTPHRR: Time to peak heat release rate
- THR: Total heat release
- $THR_{eff}$ : Expressed as the ratio of THR to initial mass
- FIGRA: Fire growth rate index

Table 17. Data obtained from the calorimetric cone test

Aerogel	Weight (g)	Residue (g)	Residue (%)	TTI (s)	PHRR (kW/m <sup>2</sup> )	TTPHRR (s)	THR (MJ/m <sup>2</sup> )	$THR_{eff}$ (MJ/m <sup>2</sup> g)	FIGRA (kW/m <sup>2</sup> s)
A5	3.774	0.056	1.48	11	84.40	33	4.08	1.08	2.56
A5T1	5.240	0.079	1.51	21	76.43	42	10.04	1.92	1.82
A5C5	6.856	2.927	42.69	-	42.27	45	5.99	0.87	0.94
A5C5T1	7.352	3.076	41.84	-	23.08	39	4.06	0.55	0.59
A5T1C5	9.901	4.283	43.26	-	21.06	42	4.09	0.41	0.50
A5C5T2	9.415	3.767	40.01	-	17.27	42	3.97	0.42	0.41
A5T2C5	8.960	3.552	39.64	-	17.73	42	3.17	0.35	0.42

Figure 57 shows the HRR of all the compositions tested as a function of time: it can be seen that compared to A5, the addition of tannic acid decreased the height of the first peak because it reduced radicals and oxidants thanks to its intumescent characteristics by decreasing the quantity of combustible solid [108]. On the other hand, A5C5 had a PHRR of 42.27 kW/m<sup>2</sup>, which was about half that of A5 (84.40 kW/m<sup>2</sup>), which is due to the clay's ability to form a protective barrier that decreases the flow of decomposition gases that feed combustion.

The presence of both montmorillonite and tannic acid further decreased the peak heat release rate: It can be seen that when the amount of tannic acid increased, there was a slight decrease in the peak, the "step change" did not affect this value significantly. FIGRA was



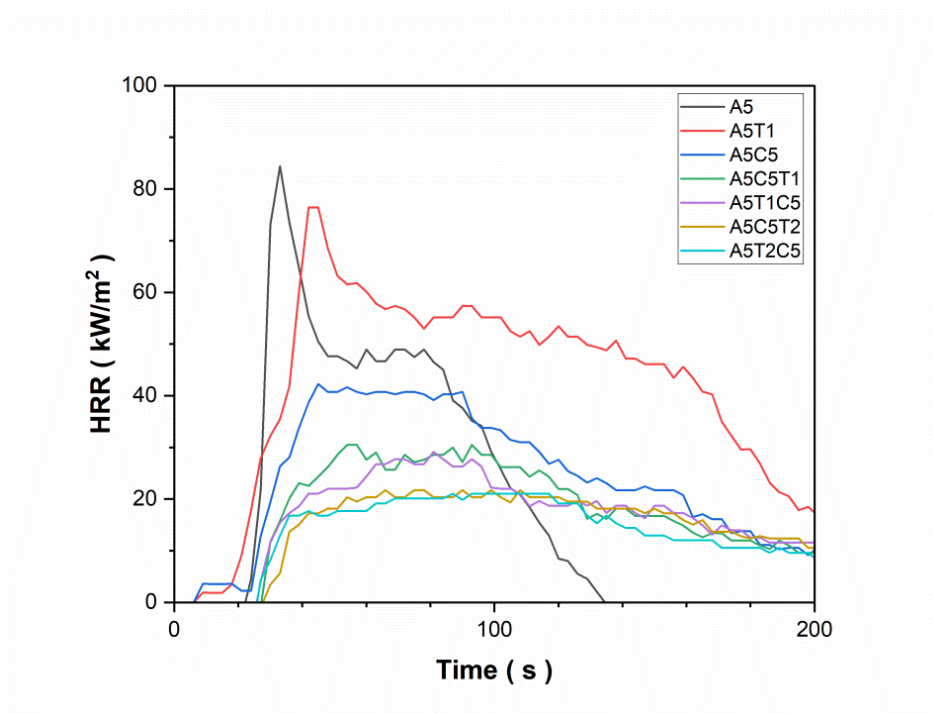
consistent with PHRR; in Table 17 it can be seen that this quantity decreased similarly to the peak heat release rate.

The TTPHRR showed an improvement if additives were added; it increased as compared to A5 (33s).

A fundamental quantity is the TTI, which for safety reasons must be as high as possible. It can be seen that tannic acid increased the time required for a flame to appear as compared with A5, from 11s to 21s. But the most surprising results were obtained in the presence of montmorillonite, because no flames appeared in the specimens for the entire duration of the test: the phenomenon of "smouldering" was observed, i.e. a thermal decomposition of the solid phase in the absence of flames in which volatiles and carbonaceous char are produced [109], which can be seen in Table 18.

The  $THR_{eff}$  represents the area subtended by the normalised curve as a function of mass and, therefore, is the total heat released with respect to the mass tested. The addition of tannic acid does not lead to an improvement over A5 but, on the contrary, the  $THR_{eff}$  value increased from 1.08 MJ/m<sup>2</sup>g to 1.92 MJ/m<sup>2</sup>g. It can be observed in Figure 57 that the curve of A5T1 enclosed a much larger area than A5, namely the THR values were 10.04 MJ/m<sup>2</sup> and 4.08 MJ/m<sup>2</sup>, respectively.






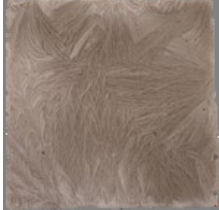


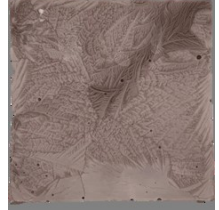







Also in the case of  $THR_{eff}$  the addition of the clay but above all the presence of both additives improved this property: As compared with the other analyses carried out in this case it was possible to note a variation with the "step change". Given the same quantity of the components, in the specimens in which the tannic acid was mixed first with ammonium alginate resulted in an improvement in  $THR_{eff}$ . A5T1C5 and A5T2C5 exhibited an effective total heat release value of 0.41 MJ/m<sup>2</sup>g and 0.35 MJ/m<sup>2</sup>g respectively, which are lower than A5C5T1 (0.55 MJ/m<sup>2</sup>g) and A5C5T2 (0.42 MJ/m<sup>2</sup>g).



**Figure 57.** Representative graph of HRR evolution as a function of time.

Montmorillonite is also essential in order to obtain a high residue quantity, as it is inorganic and allows the aerogel's structure to be maintained after the combustion process. Both the Table 17 and Table 18 show the high residue present after the calorimetric cone test; furthermore, the results obtained are congruent with the TGA analysis.

**Table 18.** *Residue and type of burning*

Composition	Samples before testing	Burned samples	Type of burning
A5			Flame 
A5T1			
A5C5			Smouldering 
A5C5T1			
A5T1C5			
A5C5T2			
A5T2C5			



# Environmental impact

Eco-friendly alternatives to traditional petroleum-based foams were sought in this project. In fact, bio-based aerogels containing ammonium alginate, tannic acid and montmorillonite were produced so the environmental impact of raw materials at the end of their life was very low. Deionised water was used as a solvent so as not to use other solvents such as ethanol which is costlier in terms of pollution.

In order to assess the environmental impact in terms of the generated CO<sub>2</sub> footprint during this work it is necessary to consider both the production process, i.e. the use of the freeze-dryer and mixers, and the machinery used for characterisation. Table 19 shows the electrical energy consumed by each technology; FTIR and TCi have been neglected as they are very fast tests.

**Table 19.** *Electrical energy consumed*

<b>Equipment</b>	<b>Use (h)</b>	<b>Power (kW)</b>	<b>Energy consumption (kW·h)</b>
<b>Lyophilizer</b>	520	2.05	1066.00
<b>Vacuum oven</b>	30	2.00	60.00
<b>Compressive testing machine</b>	7	0.60	4.18
<b>Moisture analyzer</b>	7	0.40	2.80
<b>TGA</b>	14	1.38	19.32
<b>Cone calorimeter</b>	4	7.00	28.00
<b>Ultra turrax</b>	30	0.50	15.00
<b>Propeller stirrer</b>	20	0.08	1.54
<b>Magnetic stirrer</b>	9	0.55	4.95
<b>Total</b>			1201.79

The “Comisión Nacional de los Mercados y la Competencia” (CNMC) estimated a production of 0.259 kg of CO<sub>2</sub>/kWh [110], so multiplying this value with the total energy consumption in Table 19 results in a CO<sub>2</sub> emission of 311.2 kg.

Finally, the transportation of raw materials should be considered: Deionised water and tannic acid were produced in Spain, so the environmental impact in terms of CO<sub>2</sub> emitted by lorries is negligible. The discourse is different for alginate, which is mainly obtained from the North Atlantic and the Pacific Ocean; and for montmorillonite, which was

purchased from an american producer. Hence, the amount of CO<sub>2</sub> produced by land and sea transport would have to be considered.

# Conclusion

In this research, different bio-based aerogels were produced and tested: A5, A5T1, A5C5, A5C5T1, A5T1C5, A5C5T2, A5T2C5. Thanks to the results obtained, it was possible to compare the different materials and observe the influence of montmorillonite and tannic acid in them. In particular:

- The bulk density increased with increasing components in the material, in fact it rose from  $0.0591 \text{ g/cm}^3$  in A5 to  $0.1261 \text{ g/cm}^3$  in A5T2C5.
- The thermal conductivity,  $\lambda$ , a fundamental property for thermal insulators, depends on the presence of montmorillonite. In fact, no variations were observed between A5 and A5T1 where  $\lambda$  of  $0.038 \text{ W/m}\cdot\text{K}$  was recorded. In contrast, an increase of 13.6% was observed in materials in which clay was present.
- The mechanical properties, assessed by means of a compression test, varied according to both tannic acid and montmorillonite content. Indeed, the addition of the tannic acid doubled the Young's modulus as compared to A5, the montmorillonite is also crucial because, as compared to A5 where an E of 0.03 MPa was calculated in A5C5 it amounts to 0.96 MPa. The aerogels that showed the best mechanical properties in terms of E,  $E_{\text{spec}}$ ,  $\sigma_y$  and  $\sigma_{y\text{spec}}$  were those in which all three chemical species were present: increasing the tannic acid increased both E and  $\sigma_y$  for the same amount of montmorillonite. It has also been noted that the “step change” modifies these properties: An improvement was seen if the addition of tannic acid to ammonium alginate was done before the montmorillonite in preparation. Finally, it should be remembered that the mechanical tests were carried out in the weaker direction.
- The moisture content, i.e. the amount of moisture absorbed by the aerogels, is crucial as it can influence the material's properties. Hence, the addition of montmorillonite is decisive as there is a significant decrease in the amount of moisture absorbed thanks to the barrier effect of the silica layers. For example, in A5 the moisture absorbed was 21%, whereas in A5C5 it is 14%.
- The thermal degradation, evaluated using TGA, highlights both the retarding effect of the tannic acid, the reduction of the degradation rate and the presence of a high amount of residue in the case of montmorillonite. As they increase, the thermal properties improve, as can be seen for A5C5T2 and A5T2C5 which have both the

highest maximum degradation temperatures  $T_{dmax}$  and the lowest respective degradation rates,  $dW/dT_{dmax}$ .

- Finally, the samples were tested with the calorimetric cone in order to assess the fire properties. The presence of tannic acid increased the time to ignition by about twice as much as aerogels containing only ammonium alginate. Moreover, it decreased the peak heat release rate, PHRR, because it reduces radicals and oxidants thanks to its intumescent characteristics by decreasing the quantity of combustible solid. The presence of montmorillonite was fundamental because a flame never developed on the aerogels because smouldering occurred, and the residue present at the end of the test increased considerably as compared to A5 and A5T1. The PHRR, THR, FIGRA also decreased which was ascribed to the clay's ability to form a protective barrier that decreases the flow of decomposition gases that feed combustion.

Also in this case, the presence of both additives caused a synergetic effect that improved the fire resistance characteristics, as the amount of tannic acid increased, with the same amount of montmorillonite, the properties improved. The "*step change*" modified the  $THR_{eff}$  in the specimens in which tannic acid was added first to ammonium alginate during preparation as compared to montmorillonite, a greater reduction in  $THR_{eff}$  was noted.



# Economic analysis

The economic analysis was divided into three parts in Table 20 are the costs and quantities of raw materials used, in Table 21 the costs spent on the operation of the machinery used both to produce the material and to characterise it were estimated. Finally, in Table 22, labour costs are presented.

Considering that 21 calorimetric cone specimens and 89 cylindrical specimens were produced, it is possible to evaluate the cost of raw materials:

**Table 20.** *Costs of materials*

Material	Quantity	Price	Cost
<b>Ammonium alginate</b>	260 g	23.40 €/kg	6.08 €
<b>Tannic acid</b>	55 g	130 €/kg	7.15 €
<b>Montmorillonite</b>	195 g	163.4 €/kg	31.86 €
<b>Deionized water</b>	5,2 l	0.79 €/l	4.11 €
<b>Ethanol</b>	8 l	6.28 €/l	50.24 €
<b>CO<sub>2</sub></b>	40 kg	42 €/20kg	84.00 €
<b>Total</b>			183.44 €

The running costs of the technologies are shown in Table 21, it is important to mention that the FTIR and TCi were performed in a laboratory outside the ePLASCOM research group.

**Table 21.** *Costs of the equipments*

Equipment	Use	Price	Cost
<b>Lyophilizer</b>	520 h	4 €/h	2.080 €
<b>Vacuum Oven</b>	30 h	2 €/h	60 €
<b>Cleaner</b>	2 h	20 €/h	40 €
<b>FTIR</b>	7 samples	105 €/sample	735 €
<b>TCi</b>	7 samples	10 €/sample	70 €
<b>Compressive testing machine</b>	28 samples	12 €/sample	336 €
<b>Moisture analyzer</b>	7 samples	60 €/sample	420.00 €
<b>TGA</b>	14 samples	120 €/sample	1.680 €
<b>Cone Calorimeter</b>	7 samples	150 €/sample	1.050 €
<b>Total.</b>			6.471 €

In the costs of the equipment, VAT, transport of waste and also the travel costs in the case of FTIR and TCi were not considered.

Finally, in Table 22, labour costs were estimated considering the salary of a junior engineer, a Phd student, a professor-researcher and a full-professor.

**Table 22.** *Labour costs*

<b>Profession</b>	<b>Salary (€/h)</b>	<b>Work hours (h)</b>	<b>Cost</b>
<b>Junior engineer</b>	15	750	11250€
<b>Phd student</b>	20	120	2400€
<b>Research professor</b>	30	60	1800€
<b>Full professor</b>	40	60	2400€
<b>Total</b>			17850€

Therefore, to develop this project, a total cost of 24504.44€ can be estimated considering: raw materials, equipment and personnel.

# Glossary

## Abbreviations

AlO(OH) <sub>2</sub>	Hydrated alumina oxide
CO	Carbon monoxide
CO <sub>2</sub>	Carbon dioxide
Cu	Copper
DMA	Dynamic mechanical analysis
DSC	Differential scanning calorimetry
FD	Freeze-Drying
Fe	Iron
FTIR	Fourier transform infrared spectroscopy
G-Blocks	$\alpha$ -L-guluronic blocks
H·	Hydrogen radical
H <sub>2</sub> O	Water
H <sub>3</sub> O <sup>+</sup>	Hydronium
HCl	Hydrochloric acid
HO·	Hydroxyl radical
HTSCD	High temperature supercritical drying
IUPAC	International Union of Pure and Applied Chemistry
K	Potassium
LOD	Loss on drying
LOI	Limited Oxygen Index
LTSCD	Low temperature supercritical drying

---

M-Blocks	$\beta$ -D mannuronic blocks
Mg	Magnesium
MMT	Montmorillonite
MTPS	Modified transient plane source
N <sub>2</sub> O	Nitrous Oxide
Na	Sodium
NH <sub>4</sub> OH	Ammonium hydroxide
Ni	Nickel
O	Oxygen atom
O <sub>2</sub>	Oxygen
-OH	Hydroxyl group
P <sub>c</sub>	Critical Pressure
PVA	Polyvinyl alcohol
PVOH	Polyvinyl alcohol
S.B.I.	Single Burning Item
SCD	Supercritical drying
Si	Silicon
TA	Tannic acid
T <sub>c</sub>	Critical Temperature
TCi	Thermal conductivity analyser
TGA	Thermogravimetric Analysis
TMA	Thermomechanical analysis
V	Vanadium
Xe	Xenon
Zn	Zinc

## Symbols

$M_w$	Average molecular weight	$g/mol$
$[\eta]$	Intrinsic viscosity	$cm^3/g$
$\eta_r$	Relative viscosity	
$\eta_{sp}$	Specific viscosity	
$t$	Travel time of a solution	$s$
$t_o$	Travel time of solvent	$s$
$\eta_{inh}$	Inherent viscosity	$dL/g$
$c_i$	Concentration of the $i$ -th solution	$g/dL$
$\lambda$	Thermal conductivity	$W/m \cdot K$
$\lambda_s$	Thermal conductivity of solid phase	$W/m \cdot K$
$\lambda_g$	Thermal conductivity of gas phase	$W/m \cdot K$
$\lambda_c$	Convection of the gas phase	$W/m \cdot K$
$\lambda_r$	Radiation in the foam cells	$W/m \cdot K$
$q$	Heat flow	$kW$
$M. \%$	Amount of moisture absorbed	
$W_i$	Wet mass	$g$
$W_o$	Dry mass leaving the oven	$g$
$\rho_{bulk}$	Bulk density	$g/cm^3$
$\varepsilon_c^*$	Maximum nominal deformation of the compression test	$mm/mm$
$T_{d5\%}$	Onset decomposition temperature	$^{\circ}C$
$T_{dmax}$	Maximum degradation temperature	$^{\circ}C$
$dW/dT_{dmax}$	Degradation rate at $T_{dmax}$	$\%/^{\circ}C$
$TTI$	Time to ignition	$s$

---

PHRR	Peak heat release rate	$kW/m^2$
TTPHRR	Time to peak heat release rate	$s$
THR	Total heat release	$MJ/m^2$
THR <sub>eff</sub>	Effective total heat release	$MJ/m^2$
FIGRA	Fire growth rate index	$W/s$
E	Young's modulus	$Mpa$
$\sigma_y$	Yield stress	$Mpa$
E <sub>spec</sub>	Specific Young's modulus	$MPa\ cm^3/g$
$\sigma_{spec}$	Specific yield stress	$MPa\ cm^3/g$

# References

- [1] Vareda, J. P., Lamy-Mendes, A., & Durães, L. (2018). A reconsideration on the definition of the term aerogel based on current drying trends. *Microporous and Mesoporous Materials*, 258, 211-216. <https://doi.org/10.1016/j.micromeso.2017.09.016>
- [2] IUPAC, I. (1997). Compendium of chemical terminology. *the "Gold Book."* Blackwell Scientific Publications Oxford.
- [3] Hüsing, N., & Schubert, U. (2000). Aerogels. *Ullmann's encyclopedia of industrial chemistry*. [https://doi.org/10.1002/14356007.c01\\_c01](https://doi.org/10.1002/14356007.c01_c01)
- [4] Leventis, N., Sadekar, A., Chandrasekaran, N., & Sotiriou-Leventis, C. (2010). Click synthesis of monolithic silicon carbide aerogels from polyacrylonitrile-coated 3D silica networks. *Chemistry of Materials*, 22(9), 2790-2803. <https://doi.org/10.1021/cm903662a>
- [5] Ziegler, C., Wolf, A., Liu, W., Herrmann, A. K., Gaponik, N., & Eychmüller, A. (2017). Modern inorganic aerogels. *Angewandte Chemie International Edition*, 56(43), 13200-13221. <https://doi.org/10.1002/anie.201611552>
- [6] Ing. Urciuolo F. (2017). Slides: *Gel polimerici in ingegneria dei tessuti*. Website: <https://www.docenti.unina.it/webdocenti-be/allegati/materiale-didattico/642368>
- [7] Gupta, R. A. H. U. L., Mishra, A. K., & Pathak, A. K. (2014). Supercritical Fluid technology a boon for pharmaceutical Particle Manufacturing. *Science & Technology For Human Development*. DOI:[10.13140/RG.2.1.3632.7286](https://doi.org/10.13140/RG.2.1.3632.7286)
- [8] Aegerter, M. A., Leventis, N., & Koebel, M. M. (Eds.). (2011). *Aerogels handbook*. Springer Science & Business Media.
- [9] Furlanetto L. (2007) *CAST Stardust*. Website: [https://www.castfvg.it/zzz/nasa/sonde/stardust/stardust\\_01.htm](https://www.castfvg.it/zzz/nasa/sonde/stardust/stardust_01.htm)
- [10] Bernardo E. (2016) *Dispense, chapter.14*.
- [11] Ansari, M. O., Khan, A. A. P., Ansari, M. S., Khan, A., Kulkarni, R. M., & Bhamare, V. S. (2021). Aerogel and its composites: Fabrication and properties. In *Advances in Aerogel Composites for Environmental Remediation* (pp. 1-17). Elsevier.
- [12] Woignier, T., Hafidi Alaoui, A., Primera, J., & Phalippou, J. (2009). Mechanical Properties of Aerogels: Brittle or Plastic Solids?. In *Key Engineering Materials* (Vol. 391, pp. 27-44). Trans Tech Publications Ltd. <https://doi.org/10.4028/www.scientific.net/KEM.391.27>
- [13] Pillai, S. C., & Hehir, S. (Eds.). (2017). *Sol-gel materials for energy, environment and electronic applications*. New York: Springer.

- [14] Melde, B. J., Johnson, B. J., & Charles, P. T. (2008). Mesoporous silicate materials in sensing. *Sensors*, 8(8), 5202-5228. <https://doi.org/10.3390/s8085202>
- [15] Zhao, S., Malfait, W. J., Guerrero-Albuquerque, N., Koebel, M. M., & Nyström, G. (2018). Biopolymer aerogels and foams: Chemistry, properties, and applications. *Angewandte Chemie International Edition*, 57(26), 7580-7608. <https://doi.org/10.1002/anie.201709014>
- [16] Fricke, J., & Emmerling, A. (1998). Aerogels—recent progress in production techniques and novel applications. *Journal of Sol-Gel Science and Technology*, 13(1), 299-303. <https://doi.org/10.1023/A%3A1008663908431>
- [17] Lamy-Mendes, A., Pontinha, A. D. R., Alves, P., Santos, P., & Durães, L. (2021). Progress in silica aerogel-containing materials for buildings' thermal insulation. *Construction and Building Materials*, 286, 122815. <https://doi.org/10.1016/j.conbuildmat.2021.122815>
- [18] Deville, S., Meille, S., & Seuba, J. (2015). A meta-analysis of the mechanical properties of ice-templated ceramics and metals. *Science and Technology of Advanced Materials*. <https://doi.org/10.1088/1468-6996/16/4/043501>
- [19] Akhter, F., Soomro, S. A., & Inglezakis, V. J. (2021). Silica aerogels; a review of synthesis, applications and fabrication of hybrid composites. *Journal of Porous Materials*, 28(5), 1387-1400. <https://doi.org/10.1007/s10934-021-01091-3>
- [20] Nita, L. E., Ghilan, A., Rusu, A. G., Neamtu, I., & Chiriac, A. P. (2020). New trends in bio-based aerogels. *Pharmaceutics*, 12(5), 449. <https://doi.org/10.3390/pharmaceutics12050449>
- [21] Walker, S., & Rothman, R. (2020). Life cycle assessment of bio-based and fossil-based plastic: A review. *Journal of Cleaner Production*, 261, 121158. <https://doi.org/10.1016/j.jclepro.2020.121158>
- [22] Cheng, Z., DeGracia, K., & Schiraldi, D. A. (2018). Sustainable, low flammability, mechanically-strong poly (vinyl alcohol) aerogels. *Polymers*, 10(10), 1102. <https://doi.org/10.3390/polym10101102>
- [23] Madyan, O. A., Fan, M., Feo, L., & Hui, D. (2016). Physical properties of clay aerogel composites: An overview. *Composites Part B: Engineering*, 102, 29-37. <https://doi.org/10.1016/j.compositesb.2016.06.057>
- [24] Long, L. Y., Weng, Y. X., & Wang, Y. Z. (2018). Cellulose aerogels: Synthesis, applications, and prospects. *Polymers*, 10(6), 623. <https://doi.org/10.3390/polym10060623>
- [25] Chen, H. B., Wang, Y. Z., Sánchez-Soto, M., & Schiraldi, D. A. (2012). Low flammability, foam-like materials based on ammonium alginate and sodium



- montmorillonite clay. *Polymer*, 53(25), 5825-5831.  
<https://doi.org/10.1016/j.polymer.2012.10.029>
- [26] Borges-Vilches, J., Figueroa, T., Guajardo, S., Meléndrez, M., & Fernández, K. (2020). Development of gelatin aerogels reinforced with graphene oxide by microwave-assisted synthesis: Influence of the synthesis conditions on their physicochemical properties. *Polymer*, 208, 122951. <https://doi.org/10.1016/j.polymer.2020.122951>
- [27] Otani, L. B., Pereira, A. H. A., Melo, J. D. D., & Amico, S. C. (2014). Elastic Moduli characterization of composites using the Impulse Excitation. *Technical-Scientific Informative ATCP Physical Engineering: White Paper*.  
<http://dx.doi.org/10.13140/RG.2.1.1551.2481>
- [28] Gao, S. L., & Mäder, E. (2015). Multifunctional interphases in polymer composites. *Multifunctionality of polymer composites: challenges and new solutions*. William Andrew Applied Science Publishers, Oxford, 338-362.
- [29] Shi, C., Tu, Q., Fan, H., Rios, C. A., & Li, S. (2016). Interphase models for nanoparticle-polymer composites. *Journal of Nanomechanics and Micromechanics*, 6(2), 04016003. [https://doi.org/10.1061/\(ASCE\)NM.2153-5477.0000107](https://doi.org/10.1061/(ASCE)NM.2153-5477.0000107)
- [30] Wang, Y., Zhang, Y., Zhao, H., Li, X., Huang, Y., Schadler, L. S., ... & Brinson, L. C. (2018). Identifying interphase properties in polymer nanocomposites using adaptive optimization. *Composites Science and Technology*, 162, 146-155.  
<https://doi.org/10.1016/j.compscitech.2018.04.017>
- [31] Hüsing, N., & Schubert, U. (1998). Aerogels—airy materials: chemistry, structure, and properties. *Angewandte Chemie International Edition*, 37(1-2), 22-45.  
[https://doi.org/10.1002/\(SICI\)1521-3773\(19980202\)37:1/2%3C22::AID-ANIE22%3E3.0.CO;2-I](https://doi.org/10.1002/(SICI)1521-3773(19980202)37:1/2%3C22::AID-ANIE22%3E3.0.CO;2-I)
- [32] Kutz, M. (2013). *Handbook of environmental degradation of materials*. William Andrew. <https://doi.org/10.1016/C2010-0-66227-4>
- [33] Dasari, A., Yu, Z. Z., Cai, G. P., & Mai, Y. W. (2013). Recent developments in the fire retardancy of polymeric materials. *Progress in Polymer Science*, 38(9), 1357-1387.  
<https://doi.org/10.1016/j.progpolymsci.2013.06.006>
- [34] Sánchez-Soto, M., Wang, L., Abt, T., Lucía, G., & Schiraldi, D. A. (2018). Thermal, electrical, insulation and fire resistance properties of polysaccharide and protein-based aerogels. In *Biobased Aerogels* (pp. 158-176). <https://doi.org/10.1039/9781782629979-00158>
- [35] Wang, L., & Sánchez-Soto, M. (2015). Green bio-based aerogels prepared from recycled cellulose fiber suspensions. *RSC Advances*, 5(40), 31384-31391.  
<https://doi.org/10.1039/C5RA02981C>

- [36] L. G. De la Cruz, T. Abt, N. León, M. Sánchez-Soto (2021). *Flame Retardant Crosslinked Aerogels based on Poly(vinyl alcohol) modified with Alginate and Tannic Acid*
- [37] Segato, M., & Cavalheiro, É. (2007). Thermal analysis of ammonium, mono-, di- and triethanolammonium alginates. *Journal of thermal analysis and calorimetry*, 87(3), 737-741. <https://doi.org/10.1007/s10973-006-7753-5>
- [38] Kabir, I. I., Sorrell, C. C., Mofarah, S. S., Yang, W., Yuen, A. C. Y., Nazir, M. T., & Yeoh, G. H. (2021). Alginate/polymer-based materials for fire retardancy: Synthesis, structure, properties, and applications. *Polymer Reviews*, 61(2), 357-414. <https://doi.org/10.1080/15583724.2020.1801726>
- [39] Pawar, S. N., & Edgar, K. J. (2012). Alginate derivatization: A review of chemistry, properties and applications. *Biomaterials*, 33(11), 3279-3305. <https://doi.org/10.1016/j.biomaterials.2012.01.007>
- [40] Wang, Y., He, Y., Fan, Y., Li, H., Yu, H., Yu, J., ... & Wang, S. (2021). A robust anti-fouling multifunctional aerogel inspired by seaweed for efficient water purification. *Separation and Purification Technology*, 259, 118153. <https://doi.org/10.1016/j.seppur.2020.118153>
- [41] Samyn, P. (2021). A platform for functionalization of cellulose, chitin/chitosan, alginate with polydopamine: A review on fundamentals and technical applications. *International Journal of Biological Macromolecules*, 178, 71-93. <https://doi.org/10.1016/j.ijbiomac.2021.02.091>
- [42] Ahmad, N., Alam, M., Naushad, M., Ansari, A. A., Alrayes, B. F., & Alotaibe, M. A. (2018). Thermal decomposition and kinetic studies of tannic acid using model free-methods. *Journal of the Chilean Chemical Society*, 63(1), 3824-3828. <http://dx.doi.org/10.4067/s0717-97072018000103824>
- [43] Sigma-Aldrich, *SAFETY DATA SHEET*. Website: <https://www.sigmaaldrich.com/ES/en/sds/sial/403040>
- [44] Pasquali M. *MATERIALI CERAMICI Classificazione e caratteristiche generali*. Website: <http://www.sbai.uniroma1.it/~mauro.pasquali/page2/page9/page10/files/06-01.pdf>
- [45] Guglielmi M. (2016). *Scienza e Tecnologia dei Materiali Ceramici*
- [46] *Silicati e minerali argillosi*. Website: [https://www.unirc.it/documentazione/materiale\\_didattico/598\\_2011\\_280\\_13296.pdf](https://www.unirc.it/documentazione/materiale_didattico/598_2011_280_13296.pdf)
- [47] Massaro, M., Cavallaro, G., Lazzara, G., & Riela, S. (2020). Covalently modified nanoclays: synthesis, properties and applications. In *Clay Nanoparticles* (pp. 305-333). Elsevier. <https://doi.org/10.1016/B978-0-12-816783-0.00013-X>

- [48] Król-Morkisz, K., & Pielichowska, K. (2019). Thermal decomposition of polymer nanocomposites with functionalized nanoparticles. In *Polymer composites with functionalized nanoparticles* (pp. 405-435). Elsevier. <https://doi.org/10.1016/B978-0-12-814064-2.00013-5>
- [49] Zhou, C., Tong, D., & Yu, W. (2019). Smectite Nanomaterials: Preparation, Properties, and Functional Applications. In *Nanomaterials from Clay Minerals* (pp. 335-364). Elsevier. <https://doi.org/10.1016/B978-0-12-814533-3.00007-7>
- [50] *Differenza tra acqua distillata e demineralizzata*. Website: <https://www.chimica-online.it/come-quando-perche/differenza-tra-acqua-distillata-e-demineralizzata.htm>
- [51] *Acqua deionizzata/demineralizzata*. Website: <https://www.lenntech.it/applicazioni/processo/demineralizzata/acqua-deionizzata-demineralizzata.htm>
- [52] SINERGICA. (2018). *Cosa sono e come funzionano gli Agitatori da Laboratorio*. Website: <https://www.sinergica-soluzioni.it/blog/cosa-sono-e-come-funzionano-gli-agitatori-da-laboratorio-n124>
- [53] GEMINI LAB. *Heidolph RZR1 overhead stirrer*. Website: <https://www.geminibv.com/labware/heidolph-rzr1-overhead-stirrer/>
- [54] Hemrajani, R. R., & Tatterson, G. B. (2004). Mechanically stirred vessels. *Handbook of industrial mixing: science and practice*, 345-390.
- [55] James B. (2013). *Mixing 101: Flow Patterns & Impellers*. Website: <https://dynamixinc.com/mixing-101-the-basic-principles-of-mixing-and-impellers/>
- [56] KEWLAB. (2021). *Magnetic Stirrer: Working Principle and Uses*. Website: <https://www.kewlab.com/blog/post/magnetic-stirrer-working-principle-and-uses>
- [57] BQ s.r.l. *Agitador Magnético "Agimatic-E"*. Website: [http://www.bioquimicasrl.com/archivos\\_productos/Descripcion%20completa%207002431.pdf](http://www.bioquimicasrl.com/archivos_productos/Descripcion%20completa%207002431.pdf)
- [58] Halász, G., Gyüre, B., Jánosi, I. M., Szabó, K. G., & Tél, T. (2007). Vortex flow generated by a magnetic stirrer. *American Journal of Physics*, 75(12), 1092-1098. <https://doi.org/10.1119/1.2772287>
- [59] Fisher scientific. *JP Selecta™ Magnetic Stirrers*. Website: <https://www.fishersci.es/shop/products/magnetic-stirrers-2/12048373>
- [60] Schmidt, J., Mirzaie Yegane, M., Dugonjic-Bilic, F., Gerlach, B., & Zitha, P. (2019, June). Novel method for mitigating injectivity issues during polymer flooding at high salinity conditions. In *SPE Europec featured at 81st EAGE Conference and Exhibition*. OnePetro. <https://doi.org/10.2118/195454-MS>

- [61] Farmaci Leva (2014). *Ultra-Turrax T 18 Basic*. Website: <https://www.farmacialeva.it/2014/07/20/ultra-turrax-t-18-basic/#:~:text=FUNCTION%3A%20the%20C3%A8%20device%20conceived%20the%20crevices%20of%20the%20rotor%2Dstator>
- [62] IKA. *T 25 digital ULTRA-TURRAX®*. Website: <https://www.ika.com/en/Products-Lab-Eq/Dispersers-Homogenizer-csp-177/T-25-digital-ULTRA-TURRAX-cpdt-3725000/>
- [63] ATS. *IKA T 25 digital ULTRA-TURRAX, Dispersing and Homogenising Drive with tool- S25N 18G*. Website: <https://webshop.ats-net.com/155701025/en>
- [64] RAYGER ST. *The Easy Solution to Measure Temperature*. Website: <https://docs.rs-online.com/b5b1/0900766b8002db79.pdf>
- [65] Hou, L., & Wu, P. (2019). Exploring the hydrogen-bond structures in sodium alginate through two-dimensional correlation infrared spectroscopy. *Carbohydrate polymers*, 205, 420-426. <https://doi.org/10.1016/j.carbpol.2018.10.091>
- [66] Chen, C., Yang, H., Yang, X., & Ma, Q. (2022). Tannic acid: A crosslinker leading to versatile functional polymeric networks: A review. *RSC advances*, 12(13), 7689-7711. <https://doi.org/10.1039/D1RA07657D>
- [67] Meyers, R. A. (2002). *Encyclopedia of physical science and technology*. Academic.
- [68] Cao, M., Liu, B. W., Zhang, L., Peng, Z. C., Zhang, Y. Y., Wang, H., ... & Wang, Y. Z. (2021). Fully biomass-based aerogels with ultrahigh mechanical modulus, enhanced flame retardancy, and great thermal insulation applications. *Composites Part B: Engineering*, 225, 109309. <https://doi.org/10.1016/j.compositesb.2021.109309>
- [69] Zlopasa, J., Norder, B., Koenders, E. A., & Picken, S. J. (2016). Rheological investigation of specific interactions in Na Alginate and Na MMT suspension. *Carbohydrate polymers*, 151, 144-149. <https://doi.org/10.1016/j.carbpol.2016.05.055>
- [70] Su, X., & Chen, B. (2018). Transparent, UV-proof and mechanically strong montmorillonite/alginate/Ca<sup>2+</sup> nanocomposite hydrogel films with solvent sensitivity. *Applied Clay Science*, 165, 223-233. <https://doi.org/10.1016/j.clay.2018.07.044>
- [71] Yin, K., Divakar, P., & Wegst, U. G. (2019). Freeze-casting porous chitosan ureteral stents for improved drainage. *Acta biomaterialia*, 84, 231-241. <https://doi.org/10.1016/j.actbio.2018.11.005>
- [72] Fan, L., Li, J. L., Cai, Z., & Wang, X. (2018). Creating biomimetic anisotropic architectures with co-aligned nanofibers and macrochannels by manipulating ice crystallization. *ACS nano*, 12(6), 5780-5790. <https://doi.org/10.1021/acs.nano.8b01648>
- [73] Wang, C., Chen, X., Wang, B., Huang, M., Wang, B., Jiang, Y., & Ruoff, R. S. (2018). Freeze-casting produces a graphene oxide aerogel with a radial and

- centrosymmetric structure. *ACS nano*, 12(6), 5816-5825.  
<https://doi.org/10.1021/acsnano.8b01747>
- [74] Su, F. Y., Mok, J. R., & McKittrick, J. (2019). Radial-concentric freeze casting inspired by porcupine fish spines. *Ceramics*, 2(1), 161-179.  
<https://doi.org/10.3390/ceramics2010015>
- [75] Bouville, F., Maire, E., Meille, S., Van de Moortèle, B., Stevenson, A. J., & Deville, S. (2014). Strong, tough and stiff bioinspired ceramics from brittle constituents. *Nature materials*, 13(5), 508-514. <https://doi.org/10.1038/nmat3915>
- [76] Jung, H. D., Yook, S. W., Jang, T. S., Li, Y., Kim, H. E., & Koh, Y. H. (2013). Dynamic freeze casting for the production of porous titanium (Ti) scaffolds. *Materials Science and Engineering: C*, 33(1), 59-63. <https://doi.org/10.1016/j.msec.2012.08.004>
- [77] Tang, Y., Yeo, K. L., Chen, Y., Yap, L. W., Xiong, W., & Cheng, W. (2013). Ultralow-density copper nanowire aerogel monoliths with tunable mechanical and electrical properties. *Journal of Materials Chemistry A*, 1(23), 6723-6726.  
<https://doi.org/10.1039/C3TA10969K>
- [78] Lewis, L., Hatzikiriakos, S. G., Hamad, W. Y., & MacLachlan, M. J. (2019). Freeze-thaw gelation of cellulose nanocrystals. *ACS Macro Letters*, 8(5), 486-491.  
<https://doi.org/10.1021/acsmacrolett.9b00140>
- [79] Shao, G., Hanaor, D. A., Shen, X., & Gurlo, A. (2020). Freeze casting: from low-dimensional building blocks to aligned porous structures—a review of novel materials, methods, and applications. *Advanced Materials*, 32(17), 1907176.  
<https://doi.org/10.1002/adma.201907176>
- [80] Aschenbrenner, M., Foerst, P., & Kulozik, U. (2015). *Freeze-drying of Probiotics* (pp. 213-241). Boca Raton, FL, USA: CRC Press.
- [81] Telstar. USER'S MANUAL: *Laboratory Freeze Dryer CRYODOS*
- [82] Barley, J. (2009). Basic principles of freeze drying. *SP Scientific*. Available online at: <https://www.spscientific.com/freeze-drying-lyophilization-basics>. Website: [https://sp-lineofsight.com/uploads/PDF\\_Files/Tech%20Note%20-%20Basic%20Principles%20of%20Freeze-Drying.pdf](https://sp-lineofsight.com/uploads/PDF_Files/Tech%20Note%20-%20Basic%20Principles%20of%20Freeze-Drying.pdf)
- [83] Masuelli, M. A., & Illanes, C. O. (2014). Review of the characterization of sodium alginate by intrinsic viscosity measurements: Comparative analysis between conventional and single point methods. <http://hdl.handle.net/11336/69467>
- [84] Rudin, A. (2013). *Solution manual for the elements of polymer science and engineering*. Elsevier.
- [85] Wilke J., Kryk H., Hartmann J., Wagner D. (2011). *Visco handbook*

- [86] Letslab®. *VISCOSIMETER PRECISION BATH VB-1423*. Website: <https://www.letslab.co.uk/viscosimeter-precision-bath-vb-1423.lab>
- [87] Chee, S. Y., Wong, P. K., & Wong, C. L. (2011). Extraction and characterisation of alginate from brown seaweeds (Fucales, Phaeophyceae) collected from Port Dickson, Peninsular Malaysia. *Journal of Applied Phycology*, 23(2), 191-196. <https://doi.org/10.1007/s10811-010-9533-7>
- [88] Sindhu, R., Binod, P., & Pandey, A. (2015). Microbial poly-3-hydroxybutyrate and related copolymers. In *Industrial Biorefineries & White Biotechnology* (pp. 575-605). Elsevier. <https://doi.org/10.1016/B978-0-444-63453-5.00019-7>
- [89] Clayborne A., Morris V. (2017). *Fourier Transform Infrared Spectroscopy (FTIR) How a Fourier Transform Infrared Spectrometer Work*. Website: [https://chem.libretexts.org/Courses/Howard\\_University/Howard%3A\\_Physical\\_Chemistry\\_Laboratory/14\\_Fourier\\_Transform\\_Infrared\\_Spectroscopy\\_\(FTIR\)](https://chem.libretexts.org/Courses/Howard_University/Howard%3A_Physical_Chemistry_Laboratory/14_Fourier_Transform_Infrared_Spectroscopy_(FTIR))
- [90] Hrubesh, L. W., & Pekala, R. W. (1994). Thermal properties of organic and inorganic aerogels. *Journal of Materials Research*, 9(3), 731-738. <https://doi.org/10.1557/JMR.1994.0731>
- [91] Wang, H., Lu, G., Feng, S., Wen, X., & Yang, J. (2019). Characterization of bitumen modified with pyrolytic carbon black from scrap tires. *Sustainability*, 11(6), 1631. <https://doi.org/10.3390/su11061631>
- [92] Berglund, L., Nissila, T., Sivaraman, D., Komulainen, S., Telkki, V. V., & Oksman, K. (2021). Seaweed-Derived Alginate–Cellulose Nanofiber Aerogel for Insulation Applications. *ACS Applied Materials & Interfaces*, 13(29), 34899-34909. <https://doi.org/10.1021/acsami.1c07954>
- [93] PSELECTA, (2019). *INSTRUCTION MANUAL CODE 80152 REV E*. Website: <https://grupo-selecta.com/wp-content/uploads/M.80152.00-E.pdf>
- [94] Basu, P. (2018). *Biomass gasification, pyrolysis and torrefaction: practical design and theory*. Academic press.
- [95] Priyadarshini, A., Kiran, C. P., & Suresh, K. (2018, March). Effect of Friction on Barreling during cold Upset Forging of Aluminium 6082 Alloy Solid cylinders. In *IOP Conference Series: Materials Science and Engineering* (Vol. 330, No. 1, p. 012072). IOP Publishing. <http://dx.doi.org/10.1088/1757-899X/330/1/012072>
- [96] Gibson, L. J. (2003). Cellular solids. *Mrs Bulletin*, 28(4), 270-274. <https://doi.org/10.1557/mrs2003.79>
- [97] Zwick Roel. *10 kN RetroLine*. Website: <https://www.zwickroell.com/products/pre-owned-market/pre-owned-z010-allroundline-10-kn/>

- [98] Precisa. *What is a Moisture Analyser and how can it be used for Moisture Analysis?* Website: <https://www.precisa.co.uk/what-is-a-moisture-analyser/>
- [99] Ebnesajjad, S. (2011). Surface and material characterization techniques. In *Handbook of Adhesives and Surface Preparation* (pp. 31-48). William Andrew Publishing. <https://doi.org/10.1016/B978-1-4377-4461-3.10004-5>
- [100] Maggiore, S., Pedemonte, M., Bazurro, A., Stagnaro, P., Utzeri, R., & Luciano, G. (2020). Characterization of the effect of an epoxy adhesive in hybrid FSW-bonding aluminium-steel joints for naval application. *International Journal of Adhesion and Adhesives*, 103, 102702. <https://doi.org/10.1016/j.ijadhadh.2020.102702>
- [101] Schartel, B., & Hull, T. R. (2007). Development of fire-retarded materials—interpretation of cone calorimeter data. *Fire and Materials: An International Journal*, 31(5), 327-354. <https://doi.org/10.1002/fam.949>
- [102] MERCK, (2022). *IR SPECTRUM TABLE BY FREQUENCY RANGE*. Website: <https://www.sigmaaldrich.com/ES/es/technical-documents/technical-article/analytical-chemistry/photometry-and-reflectometry/ir-spectrum-table>
- [103] QUIRED, (2002). *Recursos Educativos de Química Orgánica Tablas de Espectroscopía*. Website: [https://www.ugr.es/~quired/lab/tablas\\_espec/ir.htm](https://www.ugr.es/~quired/lab/tablas_espec/ir.htm)
- [104] Jones, R. N. (1979). Group frequencies and the chemical bond. In *Infrared and Raman Spectroscopy of Biological Molecules* (pp. 81-93). Springer, Dordrecht.
- [105] Kevadiya, B. D., Joshi, G. V., Patel, H. A., Ingole, P. G., Mody, H. M., & Bajaj, H. C. (2010). Montmorillonite-alginate nanocomposites as a drug delivery system: intercalation and in vitro release of vitamin B1 and vitamin B6. *Journal of biomaterials applications*, 25(2), 161-177. <https://doi.org/10.1177%2F0885328209344003>
- [106] Ferfera-Harrar, H., & Dairi, N. (2013). Elaboration of cellulose acetate nanobiocomposites using acidified gelatin-montmorillonite as nanofiller: Morphology, properties, and biodegradation studies. *Polymer composites*, 34(9), 1515-1524. <https://doi.org/10.1002/pc.22440>
- [107] Ortiz-Zarama, M. A., Jiménez-Aparicio, A. R., & Solorza-Feria, J. (2016). Obtainment and partial characterization of biodegradable gelatin films with tannic acid, bentonite and glycerol. *Journal of the Science of Food and Agriculture*, 96(10), 3424-3431. <https://doi.org/10.1002/jsfa.7524>
- [108] Li, L., Liu, X., Shao, X., Jiang, L., Huang, K., & Zhao, S. (2020). Synergistic effects of a highly effective intumescent flame retardant based on tannic acid functionalized graphene on the flame retardancy and smoke suppression properties of natural rubber. *Composites Part A: Applied Science and Manufacturing*, 129, 105715. <https://doi.org/10.1016/j.compositesa.2019.105715>

[109] Gutsell, S. L., & Johnson, E. A. (2007). Wildfire and tree population processes. *Plant disturbance ecology: the process and the response*, 441-477.

[110] Gencat, (2022). *Factor de emisi3n de la energ3a el3ctrica: el mix el3ctrico*. Website: [https://canvclimatic.gencat.cat/es/actua/factors\\_demissio\\_associats\\_a\\_lenergia/#:~:text=El%20mix%20de%20la%20red%20el%C3%A9ctrica%20espa%C3%B1ola%20publicado%20por%20la,259%20g%20CO2eq%2FkWh](https://canvclimatic.gencat.cat/es/actua/factors_demissio_associats_a_lenergia/#:~:text=El%20mix%20de%20la%20red%20el%C3%A9ctrica%20espa%C3%B1ola%20publicado%20por%20la,259%20g%20CO2eq%2FkWh)